An Overview of the Recent Progress in Polymeric CarbonNitrideBased Photocatalysis

Muhammad Humayun,[a,b] Habib Ullah,[c] Asif AliTahir,[c]Abd. Rashid bin Mohd Yusoff,[d]Mohd Asri Mat Teridi,[e]Mohammad Khaja Nazeeruddin,[f]Wei Luo,*[a,b]

Abstract: Recently, polymeric carbon nitride (g-C_3N_4) as a proficient photo-catalyst has been effectively employed in photocatalysis for energy conversion, storage, and pollutants degradationdue to its low cost, robustness, and environmentally friendly nature. The critical review summarized the recent development, fundamentals, nanostructures design, advantages, and challenges of g-C_3N_4 (CN), as potential future photoactive material. The review also discusses the latest information on the improvement of CN-based heterojunctions including Type-II, Z-scheme, metal/CN Schottky junctions, noble metal@CN, graphene@CN, carbon nanotubes (CNTs)@CN, metal-organic frameworks (MOFs)/CN, layered double hydroxides (LDH)/CN heterojunctions and CN-based heterostructures for H_2 production from H_2O, CO_2conversion and pollutants degradation in detail. The optical absorption,electronic behavior, charge separation and transfer, and bandgap alignment of CN-based heterojunctions are discussed elaborately. The correlations between CN-based heterostructures and photocatalytic activities are described excessively. Besides, the prospects of CN-based heterostructures for energy production, storage, and pollutants degradation are discussed.

1. Introduction

Due to rapid population growth, urbanization and improvement of living standards, clean energy production, environmental purification,and controlling greenhouse gasses became key challenges.[1]It is estimated that the globe will need 2-time of its current energy supply by the mid of 21st century and the world is committed to reduce CO_2 emission [2]. At the same time, rapid industrialization has increased environmental pollution including water pollution to its highest level which also needs to address on a priority basis. Development and discovery of semiconductor materials with high solar energy transformation efficiency and environmental redress properties is the way forward to overcome energy and environment-related global issues. In this regard, new discoveries in nanoscience and nanoengineering have been chased to prevail the barrier for energy transferring and environmental remediation.[3]Among the diverse opportunities for exploring sustainable zero-emission energy generation technologies, heterogeneous photocatalytic technology has been deemed as a proficient technique to meet the current energy and environmental issues.[4] However, photocatalysis requires a stable and suitable semiconductor that can effectively convert solar energy through photocatalytic processes such as H_2 from H_2O splitting,[5] photoreduction of CO_2 hydrocarbon fuels and photodegradation of waste plastic to fuel.[6]

Since Fujishima and Honda's discovery of H_2O splitting in 1972,[7] followed by Inoue *et al*.[8]investigation of the photocatalytic CO_2 conversion to hydrocarbon fuels utilizing TiO_2, ZnO, GaP, SiC, and CdS semiconductors trigger extensive research on the synthesis of numerous semiconductor photo-catalysts.[9]The common examples of UV and visible-light responsive semiconductor photocatalysts includes TiO_2,[10] SnO_2,[11] BiOCl,[12]ZnO,[13]$SrTiO_3$,[14] Cds,[15] $BiVO_4$,[16]Fe_2O_3,[17] $LaFeO_3$,[18] $BiFeO_3$,[19] WO_3,[20] Bi_2WO_6,[21] Ta_2O_5,[22] TaON,[23] Cu_2O,[24] Ta_3N_5,[25] and so on. So far, the construction of high-efficiency photocatalysts for overcoming energy and environmental problems has received marvelous attention in photocatalysis. The research scientists have devoted great efforts to fabricate visible-light responsive novel photocatalysts to effectively utilize solar energy as solar spectrum comprises of ca. 46% of visiblelight.[26] TiO_2 (Eg=3.2 eV) is among the widely investigated semiconductor photocatalysts, however, it is active only under UV light (ca. 4%).[27]

The CN has become an emerging star of scientific studies, due to its unique optical and electronic structure, ease of preparation, high chemical and thermal stability, cost-effectiveness, and "earth-rich" environment.[15b, 28] Wang *et al*.[29] utilized CN in photocatalysis in 2006, which prompt the utilization of CN as a potential catalyst with proper energy band gap (i.e. 2.7 eV). The valence band (VB) and conduction band (CB) potentialsof CNare about +1.4 V and -1.3 V, respectively relative to the Normal H_2 electrode (NHE) reduction potential.[30] Since, CN has an aromatic C-N heterocyclic ring with stability up to 600 °C in air environment. It exhibits high chemical stability in numerous solvents such as H_2O, alcohols, diethyl ether, glacial acetic acid, toluene, *N*, *N*-dimethyl-formamide (DMF), tetra-hydrofuran (THF), and in 0.1 M aqueous NaOH because strong van der Waal's forces exist in the structure layers of CN.[31] It is easy to synthesize CN via the thermal polymerization of N-rich compounds like melamine,[32] cyanamide,[33] dicyandiamide,[18a, 34] urea,[35] thiourea,[36] and ammonium thiocyanate.[37] Generally, there exist seven different phases of CN, such as alpha, beta, cubic, pseudocubic, g-otriazine, g-h-triazine, and g-h-

[a] *Dr. M. Humayun,Prof. W. Luo*
Engineering Research Center for Functional Ceramics of theMinistry of Education, School of Optical and Electronic Information, Huazhong University of Science and Technology, Wuhan 430074, PR China
E-mail: luowei@mail.hust.edu.cn
[b] *Dr. H. Ullah, Dr. A. A.Tahir*
Environment and SustainabilityInstitute, University of Exeter, Penryn, TR10 9FE, Cornwall, United Kingdom
[c] *Dr. A. R. B. M. Yusoff*
Department of Physics, Swansea University, Vivian Tower, Singleton Park, SA2 8PP, Swansea, United Kingdom.
[d] *Prof. M. A. M. Teridi*
Solar Energy Research Institute (SERI), UniversitiKebangsaan Malaysia, 43600 UKM Bangi, Selangor, Malaysia
[d] *Prof. M. K. Nazeeruddin*
Institute of Chemical Sciences and Engineering, École Polytechnique Fédérale de Lausanne (EPFL), Rue de l'Industrie 17, CH-1951 Sion, Switzerland

heptazine, with proper band gap energies of 5.49, 4.85, 4.3, 4.13, 0.93, 2.97, and 2.88 eV, respectively.[38] It is confirmed that triazine-(C_3N_3), and tri-s-triazine-(C_6N_7) are the basic units constituting CN allotrope (Fig. 1).[39] Among the seven existing types, (C_6N_7)-based CN is more favorable and the highly stable form.[40] Generally, the tri-s-triazine rings are considered the basic units of CN.

Muhammad Humayunwas born in Charsadda, Pakistan. He obtained his PhD degree in Chemistry & Materials Science from Heilongjiang University China in 2017. From Aug 2017-Dec 2020, he worked as a postdoc in Prof. Wei Luo group at Huazhong University of Science & Technology (HUST) China. Currently, he is working as a research fellow in the same group. He is the author, co-author of more than 50 peer-reviewed publications with citations more than 1650.His current research interests include the design of functional photo and electrocatalysts for energy and environmental applications.

Habib Ullah got his MS in Physical Chemistry in 2014, from the University of Peshawar, Pakistan. He completed his Ph.D in Renewable Energy from CEMPS, University of Exeter, United Kingdom, in 2018. Currently, he is working as a Research Fellow at the same University. Habib has published 40 peer-reviewed papers with total citations of more than 1350. He is also a guest editor of *Energies* – MDPI. His research involves DFT& Experimental study of *Energy Materials, i.e.,* Conjugated Polymers, Metal Oxides, Perovskite, and Phase Change Materials.

Asif A. Tahir graduated from the Department of Inorganic Chemistry at Quaid-i-Azam University, Pakistan, in 2009. He worked as a research associate at Loughborough University for three years and then moved to the University of Liverpool before joining the College of Engineering, Mathematics and Physical Sciences (CEMPS) at the University of Exeter as a Senior Lecturer in Renewable Energy. He specializes in the fabrication of nanomaterials using state-of-the-art techniques for solar energy conversion and photocatalysis. His research focus includes the design, synthesis, and characterization of new materials using soft chemistry approaches and the optimization of nanomaterials for high performance.

Abd. Rashid Mohd Yusoff obtained his BSc in Physics from Universiti Putra Malaysia in 2002. In 2011, he completed his PhD working with the late Prof. Ivo Hümmelgen's group in the Departamento de Física at Universidade Federal do Paraná, Brazil. Mohd Yusoff's doctoral research focused on magnetic-field effects in semiconducting materials and devices. From 2011-2013, he worked as a Postdoc Fellow in Prof. Jin Jang group at the Department of Information Display, Kyung Hee University. He then worked as a Research Professor in the same group until 2018, later he joined the Sêr SAM group at Swansea University. Mohd Yusoff is a Senior Research Fellow with Sêr SAM with a focus on perovskite photovoltaics. His research interests include photovoltaics, light emitting diodes, transistors, photochemical water splitting, and bifunctional electrocatalysts.

Mohd Asri Mat Teridi graduated from Loughborough University, UK, in 2012. He joined the Solar Energy Research Institute, National University of Malaysia in 2007, as a Junior Research Fellow/Lecturer. After he received his PhD, he was appointed as a Research Fellow/Senior Lecturer in 2013 at the same university. He has authored over 100 papers, 5 books chapters and own 8 patents. Recent research activity has focused on the development of nanostructured electrode for photocatalysis, perovskite solar cells and polymer solar cells.

Prof. Mohammad K. Nazeeruddin's current research at EPFL focuses on perovskites and light-emitting diodes. He has published more than 700 peer-reviewed papers, and ten book chapters, and is an inventor/co-inventor of over 75 patents. He has been named a Thomson Reuters "Highly Cited Researcher" since 2014, and one of the 19 scientists identified by Thomson Reuters as The World's Most Influential Scientific Minds from all scientific domains. He has been identified by the Times Higher Education as one of "the top 10 researchers in the world working on high impact perovskite materials & devices".(https://www.timeshighereducation.com/data-bites/top-universities-and-researchers-perovskite-solar-cell-research#survey-answer). He was appointed as a World Class University (WCU) professor and Adjunct Professor at King Abdulaziz University, Jeddah, and elected to the European Academy of Sciences (EURASC), and is a Fellow of The Royal Society of Chemistry. http://gmf.epfl.ch/.

Wei Luo was born in Hubei, China. He received his PhD degreein 2009 from Huazhong University of Science & Technology (HUST) China. From 2009-2012, he worked as a postdoc in HUST. From 2014-2016, he worked as a postdocin the United States University of Michigan (ANA). Since 2016, he has been working as an Associate Professor at Wuhan National Laboratory for Optoelectronics (HUST). His current research interests include the design of SAW sensors, low-dimensional semiconductor sensing materials, and energy materials.

In fact, CN consists of only C and N atoms, and its characteristics could be adjusted by easy tailoring methods, without altering its structure and chemicalcomposition.[41]Similarly, due to its polymerization properties, the CN chemical structure could easily be changed by surface engineering. Additionally, the (sp^2)-hybridized C,N bonding in CN forms a π-conjugated structure.[42]Therefore, the aforementioned unique characteristics of CN made it a promising material in photocatalysis[43]However, bare CN has a small surface area, low electrical conductivity, and rapid charge recombination rate, so its practical application is still

limited.[21b]Numerous modification approaches, including manufacturing technology, structural design, changing the electronic structure by introducing non-metallic elements, introducing point defects via vacancy generation, depositing precious metal nanoparticles, and fabricating composites, are commonly used for upgrading the CN efficiency.[44] The modification routes are toan aligned band at the interface in the designed nanocomposites is the most effective to improve photo-generated charge carrier's separation of CN for potential photocatalysis.[45] Thus, due to the copious applications of CN in photocatalysis, the fabrication of novel CN-based catalysts attracted worldwide attention from scientific research for efficient solar energy utilization. In other words, the construction of gC_3N_4-based heterostructures will enable CN to turn into a new family of the nextgeneration visible-light responsive photocatalyst.

To date, some inspiring reviews on the synthesis, textural features, and applications of CN are reported.[46] However, there has been no review article that significantly presents the developmental history, fundamentals, nanostructures design, heterostructures construction, and the CN-based heterostructures applications in photocatalysis from scientific and engineering points of view. Hence, it is of great significance to provide a broad and up-to-date review article on CN-based materials from an open perception.

2. History and Development of CN

The history and precursor materials of CN can be traced back to the emergent structure, "melamine, melam, melem, and melon", discovered by the scientists Berzelius and Liebig in 1834 (Figure 1).[47]

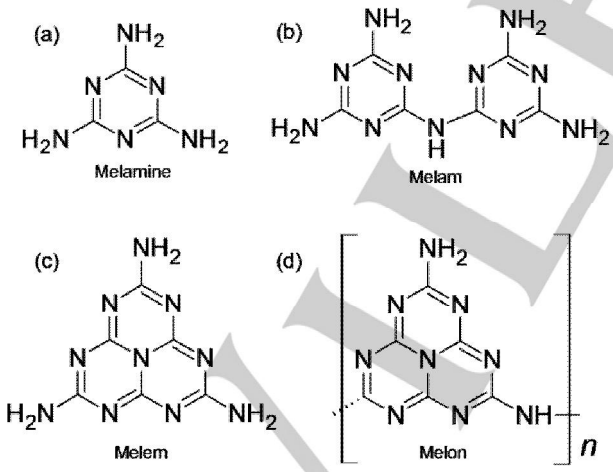

Figure1. The C and N rich compounds melamine (a), melam (b), melem (c), and melon (d), used for CN synthesis.

Further approaches toward these compound structures were demonstrated by Franklin in 1922 and proposed the concept of carbon nitride and described that it can be achieved as the final de-amination product of ammonocarbonic acids by high-temperature treatment of melon.[48] In 1937, Pauling and Sturdivant described co-planar tri-s-triazine as the fundamental structural pattern of these polymer derivatives.[49]

Redemann and Lucas suggested that appropriate similarities exist among the melon and graphite and molecules are planar and considerably large. They further concluded that Franklin's carbon nitride is a dense condensation product of twenty-one 2,5,8−triamino−tri−s−triazine ($C_{126}H_{21}N_{175}$) molecules.[50] They confirmed that a mono-structure cannot be accredited to melon, as expected it can be a collection of polymers of various sizes and structures. Later, these compounds have received worldwide scientific attention by the theoretical prediction in the 1990s. It was found that opaque C_3N_4 (*b*-C_3N_4) with sp^3 bonding has extremely high bulk modulus and hardness value compared to diamond.[38, 51] Hence, the researchers were greatly motivated toward the experimental synthesis and characterization of b-C_3N_4.[52] However, due to their low thermodynamic stability, it's very hard to synthesize single-phase sp^3-hybridized carbon nitride[53] and confirmed from the theoretical predictions that CN is the highly stable form at ambient conditions.[54]

Inspired by the graphite crystal structure, these compounds were categorized as heptazine and triazine-based compounds.[55] In polymer melon, the tri-s-triazines are interconnected by secondary nitrogen, while CN exists as 2D sheets in which the tri-s-triazines are inter-connected by tertiary amines (Figure 2).[56]

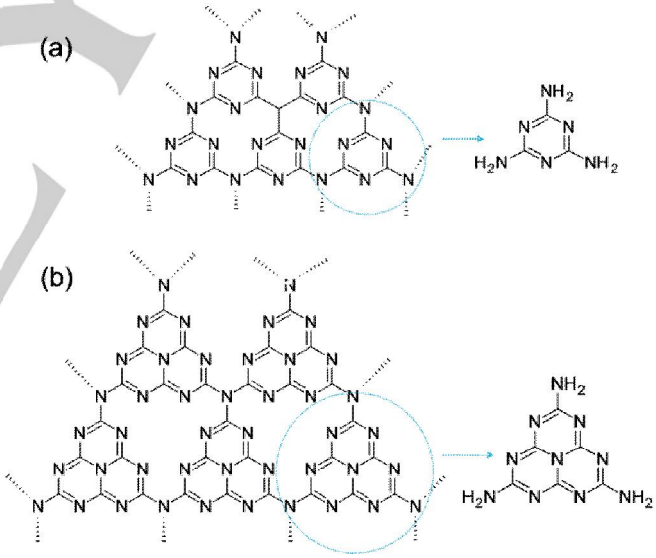

Figure 2. The s-triazine (a), and tri-s-triazine tecton (b), of CN.

According to recent reports, the pyrolysis of precursors like cyan-amide, dicyan-diamide and melamine produce a melon polymer made up of melem components[57] suggesting that tecton is the most stable configuration. Currently, the cyanamide condensation to dicyandiamide and then to melamine as illustrated by Liebig were found excellent synthetic routes to produce polymeric species with slight defect (Figure 3).

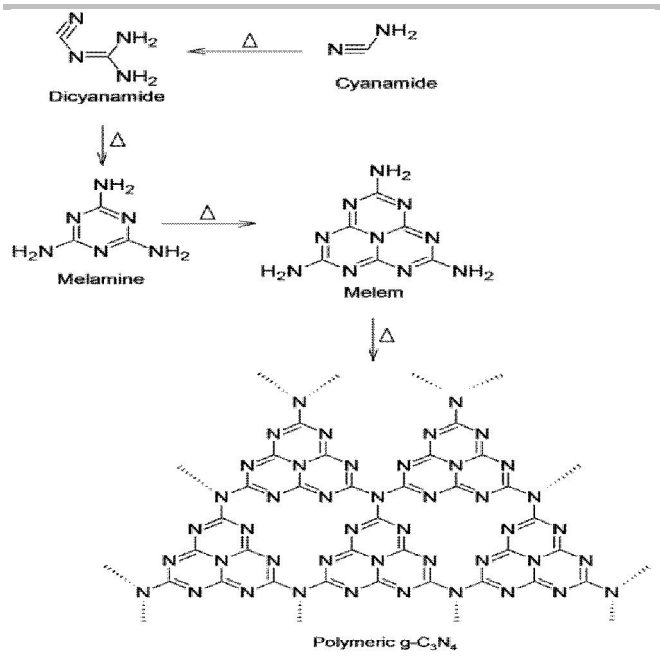

Figure 3. Condensation reaction paths of the cyanamide precursor to produce polymeric CN.

Similarly, Komatsu has prepared high molecular weight melon[58]while Schnick *et al*.[59] isolated and identified the derivatives of heptazine crystal structures melem $C_6N_7(NH_2)_3$and melam $[(H_2N)_2(C_3N_3)]_2NH$. Afterward, Bordon *et al*.[60] reported that under high pressure and temperature, the conversion of dicyandiamide definitely yields a crystalline imide phase carbon nitride, $C_2N_2(NH)$. Recently, highly crystalline carbon nitride was produced by the self-reduction of dicyandiamide precursor in a melted salt of LiCl and KCl.[61] These reports inspired huge efforts toward more improvement of CN for potential applications in photocatalysis.

3. Photocatalysis by CN

3.1. Physicochemical Properties

Among various allotropes of carbon nitride, g-C_3N_4(CN) is themost stable one.According to the broad investigations by thermo gravimetric analysis, the stability of CN could be retained up to 600 ^oC or a little above.[62] A strong endo-thermal peak related to the degradation of CN arouse at 630 ^oC, which is approximately 30 ^oC higher than the starting point of degradation (i.e. 600 ^oC). The complete degradation of CN occurs at 750 ^oC, reflecting that it exhibits high thermal stability. Further, no reactivity or solubility of CN could be observed in conventional solvents like water, toluene, ethanol, dimethyl formamide, diethyl ether, and tetrahydrofuran. The CN exhibits high chemical stability and durability in various solvents such as water, acetonitrile, ethanol, pyridine, dimethyl formamide, acetic acid, acetone, methylene chloride, and 0.1 M sodium hydroxide aqueous solution.[63] It is very important to describe the optical properties of CN, which are usually investigated by the UV-vis absorption and photoluminescence techniques. Based on the theoretical calculations, it was confirmed that the semiconductor CN exhibits a band gap larger than 5 eV, mainly relying on the structural diversities. Generally, the traditional CN exhibits absorption up to 470 nm. While introducing a mesoporous structure, its light absorption ability could be improved due to its large specific surface-area and numerous scattering assets. As investigated by the photoluminescence technique, charge recombination in mesoporous CN could be greatly suppressed. This phenomenon could be due to the electron relocalization on the surface terminal sites that promote the catalytic redox function of the CN.[64] From above all, it could be stated that CN display high stability, good durability suggesting that it could be utilized as a promising photocatalyst even under harsh and dreadful conditions.

3.2. Heterogeneous Photocatalytic Mechanism

The heterogeneous photocatalyticsystems have been designed and developed for applications in photocatalysis.[65] Photocatalysis is an interesting advanced techniqueused for energy conversion and mineralizationof various hazardous pollutants and inactivation of the bio-hazards. In particular,heterogeneous photocatalysis has broad applications in waste watertreatment owing to its prospective features like feasible temperature and pressure, complete mineralization of pollutants without producingany secondary pollutants,and reliable cost-effectively.[66] So far, the traditional biological and electrocatalytic techniques have been widely investigated but they frequently exhibited low stability, low mechanical strength, poisoning of catalyst, and electrode corrosion. Heterogeneous photocatalysis has an advantage over these techniques because of its low cost, high thermal and chemical stability, high efficiency, and no toxicity.[67] Photocatalysis produces reactive oxygen species(ROS) such asthe $\bullet O^{2-}$, H_2O_2, $\bullet OH$,$^1O_2$, and h^+under suitableconditionsby reacting with the dissolvedO_2molecules or H_2O/OH^-, which facilitate oxidationof various pollutants. In contrast, for the most favorable energy conversion, the $H^+$and CO_2could be reduced to $H_2$and hydrocarbons, while the H_2O/OH^- could be transformed to O_2 by an oxidation process.[68]

The fundamental mechanism of heterogeneous photocatalytic process has been depicted in Figure 4. The mechanism of heterogeneous photocatalytic process comprises seven important key steps including (i) solar light absorption; (ii) generationof charge carriers; (ii) separation and transfer of charge carrier's; (iv) charge carrier's recombination; (v) recombination of surface charge carrier's; (vi) surface reduction reactions; and (vii) surface oxidation reactions. In general, by constructing a layered macropore/mesoporous structure that directly affects the photocatalytic steps, the efficiency of a catalyst could be significantly improved.[69]When a semiconductor is irradiated by sunlight, and energy of a photon is equal to or higher than its energy band gap, the transition of electrons occurs from VB to the CB, while leaving holes in its VB. The CB bottom of CN is highly negative (i.e. −1.3 V vs. the NHE)[29b, 70] that facilitates its broad applications in visible-light photocatalysis.[71]

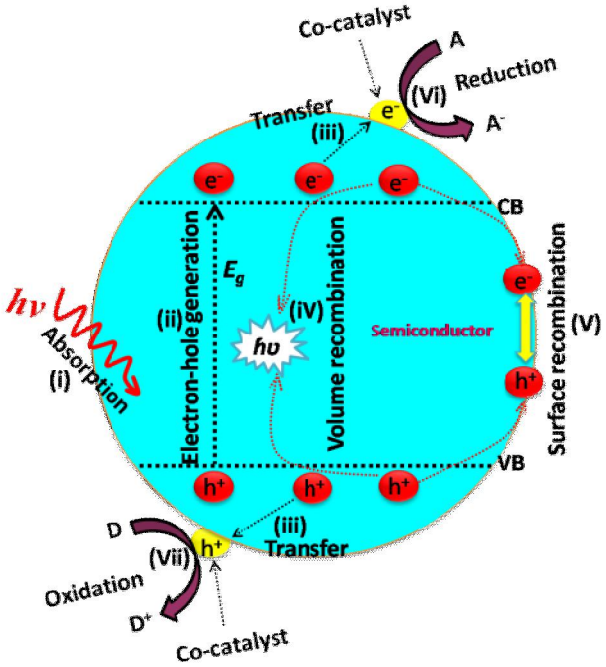

Figure 4. The fundamental mechanism and typical steps in heterogeneous photocatalysis: (i) solar light absorption; (ii) generation of charge carriers; (iii) charge carriers transfer and separation; (iv) charge recombination; (v) charge recombination on the surface; (vi) surface reduction and (vii) oxidation reactions.

The construction of interfacial heterojunctions is one of the best ways to overcome the problem of charge recombination and to enhance its separation and transfer to activesites for faster redox reactions that drastically enhance photocatalytic efficiency.[72] The surface redox reactions probably take place only if the redox potential values are enough positive or negative relative to the CB and VB potential of semiconductor photocatalysts. Various standard reduction and oxidation potentials are enlisted in Table 1 and all the enlisted reactions in Table 1 display identical linear pH reliance having a slope of −0.059 V, except for E^0 (O_2/O_2^-) which do not depend on pH.[73]

Table 1. Standard reduction and oxidation potentials of some typical species.

Reactions	E^0Vs. NHE (pH= 0)
$2e^- + 2H^+ \rightarrow H_2(g)$	0
$e^- + O_2(g) \rightarrow O_2^-(aq)$	−0.330
$H^+ + e^- + O_2(g) \rightarrow HO_2•(aq)$	−0.0460
$2H^+ + 2e^- + O_2(g) \rightarrow H_2O_2(aq)$	0.6950
$4h^+ + 2H_2O(aq) \rightarrow 4H^+ + O_2(g)$	1.2290
$2H^+ + 2e^- + O_3(g) \rightarrow H_2O + O_2(g)$	2.0750
$h^+ + OH^- \rightarrow •OH$	2.690
$e^- + CO_2 \rightarrow CO_2^-$	−1.90
$2H^+ + 2e^- + CO_2(g) \rightarrow HCOOH(aq)$	−0.1990
$2H^+ + 2e^- + 2CO_2(g) \rightarrow HOOCCOOH(aq)$	−0.4810
$2H^+ + 2e^- + CO_2(g) \rightarrow H_2O + CO(g)$	−0.110
$4H^+ + 4e^- + CO_2(g) \rightarrow H_2O + HCHO(aq)$	−0.070
$4H^+ + 4e^- + CO_2(g) \rightarrow C(s) + 2H_2O$	0.2060
$6H^+ + 6e^- + CO_2(g) \rightarrow H_2O + CH_3OH(aq)$	0.030
$8H^+ + 8e^- + CO_2(g) \rightarrow 2H_2O + CH_4(g)$	0.1690
$8H_2O + 12e^- + 2CO_2(g) \rightarrow 12OH^- + C_2H_4(g)$	0.070
$9H_2O + 12e^- + 2CO_2(g) \rightarrow 12OH^- + C_2H_5OH(aq)$	0.080
$13H_2O + 18e^- + 3CO_2(g) \rightarrow 18OH^- + C_3H_7OH(aq)$	0.090
$H^+ + e^- + H_2O_2(aq) \rightarrow OH^- + H_2O$	1.140
$H^+ + e^- + HO_2• \rightarrow H_2O_2(aq)$	1.440
$2H^+ + 2e^- + H_2O_2(aq) \rightarrow 2H_2O$	1.7630

To solve these critical issues, various modification approaches like the tuning of band gap and nano-micro structures, addition of co-catalysts, surfaces and interfaces engineering, etc. are projected and used to boost up the visible light catalytic efficiency of photocatalysts.[74]The detail about the design and modification strategies of CN for heterostructures formation will be systematically presented in section 5.

3.3. The CN Photocatalyst Advantages and Challenges

The polymer CN exhibits a 2.7 eV band gap,[75] corresponding to the approximately 460 nm absorption wavelength. Accordingly, CN is considered to be a potential visible-light catalyst. Some typical standard redox potentials at pH 7 versusNHE with respect to CN are shown in Figure 5.

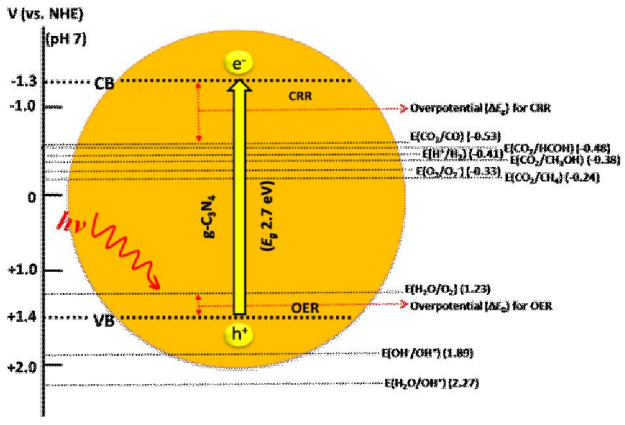

Figure 5. The redox potentials of some typical reactions versus the CN valence and CB edges at pH = 7.

Taking into consideration the over-potentials and thermodynamic losses during the photocatalytic reactions, the CNband gap by chance is located in between 2.0 eV and 3.1 eV. Thus, CN can accomplish photocatalytic water splitting reactions with adequate endothermic driving forces

(> 1.23 V) and utilize enough visible-light (< 3.1 eV).[46c, 76]Notably, the CB edge of CN is set at -1.3 V vs. NHE, which is favorable for many important reduction reactions, such as CO_2 conversion, H_2 evolution, O_2 reduction, and environment remediation by degradation of pollutants.[77]In CN photocatalyst, the C and N atoms exist with a C/N molar ratio of 0.75, signifying that it can be synthesized by cost-effective methods such as thermal condensation of nitrogen-rich precursors like cyan-amide, dicyan-diamide, thiourea, urea, melamine, guanidine hydrochloride at 450-600 ^{o}C in air/inert environments[78] while the highly crystalline well ordered and condensed CN structures could be prepared by ionic liquids,[79] molecular self-assembly,[80] ionothermal strategy,[81]and microwave irradiation,[82] as depicted in Figure 6.

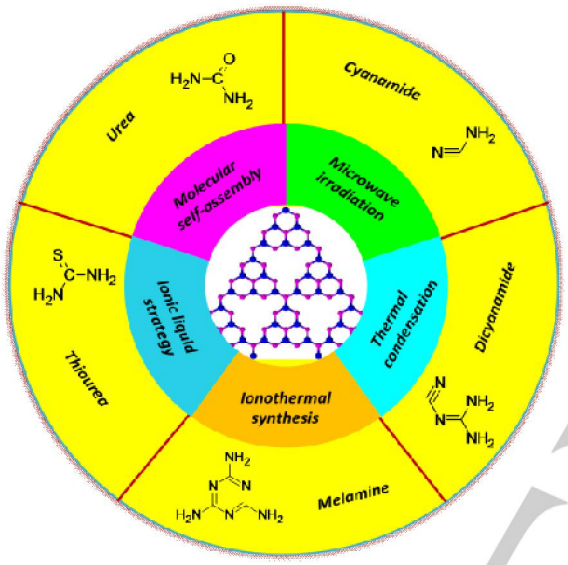

Figure 6. Various synthetic routes of CN by utilizing nitrogen-rich precursors.

Thus, the natural abundance, high stability, non-toxicity, and surface-rich features allow the use of polymeric CN as a multi-functional heterogeneous photocatalyst. Though, the activity of CN (bulk) is still low which can be attributed to some serious shortfalls such as small surface area, inadequate active sites for interfacial reactions, high charge recombination rate, low mobility of charges, moderate oxidation ability, and inadequate solar light consumption (λ < 460 nm).[83] Although, the very few drawbacks of CN greatly limit its practical applications as a potential photocatalyst, however, it still provides more opportunities to design and construct CN-based highly efficient photocatalysts for future studies.

4. Synthesis of CN Nanostructures

The nanostructure design has received considerable attention in past few years owing to the diverse applications in the improved photocatalytic efficiency of semiconductor photocatalysts.[84] Remarkable progress has been accomplished to design and develop controlled-shape CN and to investigate the correlation between morphological textures and photocatalytic activities. To synthesize CN nanostructures, two approaches such as “top-down” and “bottom-up” can be applied.[85] In the CN nanostructures design, the top-down approach comprises the liquid or thermal exfoliation techniques, while the bottom-up approach comprises solvothermal process, supra-molecular pre-organization, and template methods.

4.1. Top-down Approach

The two-dimensional (2D) CN nanosheet structure with large specific surface area, atomic and/or molecular thickness, and infinite planar lengths display exceptional optical, thermal, electrical, and mechanical characteristics and potentially exhibit broad applications in photocatalysis for solar energy conversion.[86] The top-down approach is applied to split the block system of CN into subunits, so-called CN nanosheets. The top-down approaches like liquid ammonia assisted lithiation, liquid, liquid-exfoliation technique, and thermal exfoliation, single or few-layered nanosheets of CN can be obtained.

4.1.1 Liquid Exfoliation Technique

Using liquid exfoliation technique, different sorts of mono-layer and multi-layer sheets have been extracted from CN powder in different solvents like H_2O,[81c, 87] 2-propanol,[88] 1,3-butanediol,[89] H_2O/2-propanol,[90] methanol,[91] and H_2O/2-propanol/dimethyl formamide[92] by sonication process. Xie *et al.*[93] obtained the CN nanosheets via the liquid-exfoliation of bulk CN in H_2O. The obtained nanosheets were in the range of 70-160 nm and their thickness was about 2.5 nm, suggesting that there exist approximately seven atomic layers as depicted in Figure 7(a).

The CN nanosheets showed superior light absorption and significant photocurrent response and photoactivity in comparison to the bulk and induced photo-luminescence quantum efficiency up to 19.6 %, superior to the efficiency of bulk CN. They demonstrated that nanosheets of CN soluble in H_2O having improved stability, non-toxicity and high quantum yield are promising for potential photocatalytic applications.

4.1.2 Chemical Exfoliation Technique

Zhu *et al.*[46b] synthesized ultrathin single atomic-layer (0.4 nm) CN nanosheets via a chemical exfoliation technique simply by mixing the CN (bulk) in sulphuric acid (H_2SO_4, %age purity 98%) before sonication in H_2O. The as-prepared mono atomic-layered nanosheets of CN exhibited superior charge separation and transfer and excellent activity for H_2 generation and pollutant degradation relative to the bulk one. This indicates that the single-layer nanosheets of CN exhibit broad potential applications in photocatalysis. Zhao *et al.*[94]followed the monolayer strategy of bulk nanosheets, and obtained thin-layer atomic CN nanosheets having 0.4–0.5 nm thickness by the ultrasonicexfoliation. The visible-light activity of resultant atomic single layer CN nanosheets was appraised for rhodamine B degradation. The mono-layered CN nanosheets exhibited about 3.0-folds and 10.2-folds improved activity for RhB degradation compared to the few-layer nanosheets of CN and the bulk one, respectively. The

enhanced activity has been accredited to the atomic single-layer CN nanosheets structure, which greatly prolonged the charge carrier's lifetime and served as an excellent electron transporter.

4.1.3 Mixed Solvent Approach

Lin *et al*.[92] proposed a flexible and scalable-mixed solvent approach to obtain single layer nanosheets of CN from the bulk one via a liquid exfoliation technique. In this technique, the CN nanosheets concentration can be simply tuned from 0.1 to 3 mg mL^{-1} by varying the volume-ratios of the used solvents. The nanosheets exhibit high stability, can be stored for six months without any aggregation, and have excellent photoactivity for degradation of rhodamine B and the benzyl alcohol selective oxidation, compared to the corresponding layered parts.

4.1.4 Liquid-ammonia Assisted Lithiation Method

The liquid ammonia-assisted lithiation approach has also been used efficiently to exfoliate nanosheets of CN from the bulk one. Yin *et al*.[95] prepared few layered CN via the liquid-ammonia assisted lithiation technique and the resultant few-layer thick nanosheets of CN exhibited different surface structures as well as absorption and electronic properties compared to those of the bulk one. The nanosheets exhibited improved photoactivities for H_2 production and hydroxyl radical's generation in comparison to the bulk one.

4.1.5 Thermal Exfoliation Approach

The thermal exfoliation approach is also an efficient, low cost, non-toxic, high yielding, fast, and environmental friendly technique for fabricating nanosheets of CN. Niu *et al*.[96]proposed a thermal-oxidation-etching method to obtain six to seven layered CN nanosheets (thickness about 2 nm) from the bulk one, as shown in Figure 7(b).The CN nanosheets showed a massive specific surface area, larger band gap, smaller nanosheets thickness, enhanced capability of electron transmission in-plane direction, and a longer charge carrier's lifetime due to quantum-confinement effect. Notably, the resultant CN nanosheets exhibited enhanced photo-activity for H_2O reduction to generate H_2 under UV-vis and visible irradiations, in comparison to the bulk one.

Ong *et al*.[97]synthesized graphene-like carbon nitride from the intercalation compound based on CN (CN/NH_4Cl) by thermal exfoliation. The resultant material exhibited 2D thin layered structures with 2–3 nm thickness and six to nine atomic layers. The material showed excellent photoactivity in degrading methylene blue, which was accredited to large surfacearea (30 m^2 g^{-1}), enhanced photocurrent response and electronic conductivity. Based on the above studies, it is suggested that 2D nanomaterials with single or few atomic layered structures exhibit prospective applications in catalysis, sensors, electronics, supercapacitors, and energy storage.[98]

4.2. Bottom-up Approach

4.2.1. Template Method

The template-technique is an efficient approach used for fabrication of porous architecture materials. In this method, organic and inorganic nanostructures are employed as templates.[99] The morphology, size, and porous texture can be simply altered by using various templates. Porous nanosized CN can be obtained via both the soft and hard template techniques as depicted in Figure 7(c,d).

4.2.1.1 Hard Template Method

This method is flexible, controllable, and accurate for the synthesis of nano-textured materials. In hard template strategy, the used templates are very flexible and accessible for the construction of various geometrical shapes that falls in the range of nano-scale, micro-scale, and macro-scale. This method is also effective for the synthesis of hierarchical porous structures. It is noteworthy that the well ordered mesoporous structures can be obtained using hard templates as illustrated in Figure 7(e). The CN with diverse structural morphologies can be prepared using proper templates.[100] Jun *et al*.[101] reported synthesis of large surface-area (239 m^2 g^{-1}) 2D CN with mean pore size of 4.89 nm using ordered meso-porous SBA-15 as hard template, as shown in Figure 7(f). The porous structures are much significant for improving the activity and selectivity in photocatalysis. The porous architecture allows the orientation of guest molecules and assembly of catalytic co-factors into the materials structure.

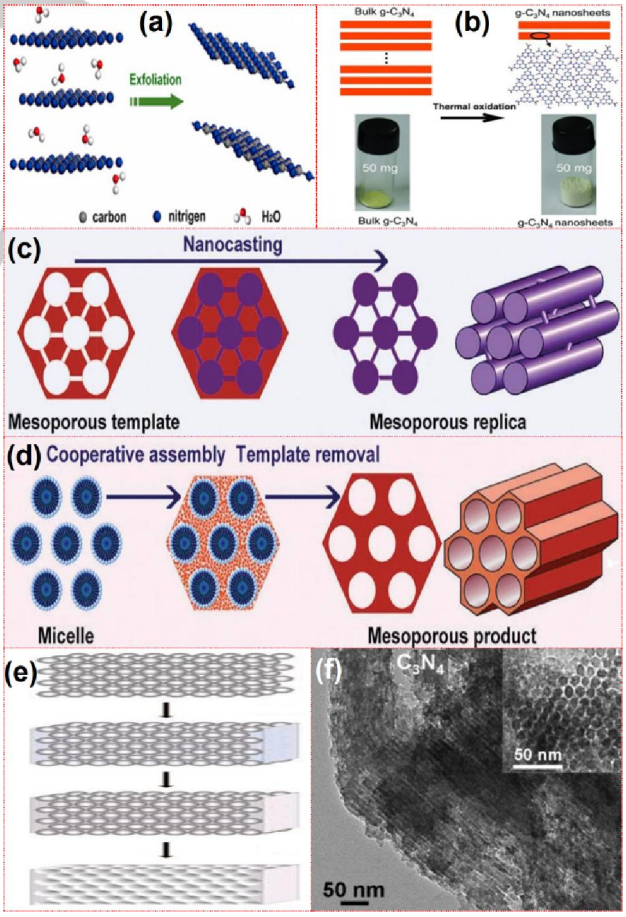

Figure 7. The liquid-exfoliation of bulk CN to nanosheets (a). Adapted with permission from ref.[93] Copyright-2013, The American Chemical Society. Thermal exfoliation of the bulk CN to nanosheets (b). Adapted with permission from ref.[96]. Copyright-2012, Wiley-VCH.Schematic

representation for fabrication of porous CN by hard-templating approach (c), and soft-templating approach (d). Adapted with permission from ref.[102] Copyright 2011, The Royal Society of Chemistry. Design for obtaining 2D porous CN via a hard template-method (e). Reproduced with permission from ref.[100a]. Copyright-2008, The American Chemical Society. The TEM micrograph of 2D CN (porous) obtained via a hard template (SBA-15 silica sieve) (f). Adapted with permission from ref.[101] Copyright-2009, Wiley-VCH.

Vinu[103] synthesized well-ordered meso-porous 2D CN (meso-CN) by nanocasting technique using ethylene-diamine ($(CH_2–NH_2)_2$) and carbon tetra-chloride (CCl_4) as the precursor materials and SBA-15 as a hard template for pores introduction as shown in Figure 8(a). The resultant TEM images are shown in Figure 8(b, c). The material exhibited 2D hexagonal ordered meso-structures with pore size about 2.9 nm, and surface area of ~ 140 m^2 g^{-1}. It was noted that by varying the weight ratio of $(CH_2–NH_2)_2$ to CCl_4 from 0.3 to 0.9, the C/N ratio could be tuned from 4.5 to 3.5.

Wang *et al*.[104] prepared ordered meso-porous CN (ompCN) via SBA-15 template assisted nano-casting method. In the resultant material, the C/N ratio was 0.73:1, and its semiconducting properties were analogous to the bulk one. The resultant ompCN material exhibited 2D framework, uniform pore sizes and large surface area leading to the superior H_2 generation with the aid of Pt as a co-catalyst and electron acceptor. Zhang *et al*.[105] combined the properties of both nanospheres and nanosheets, and fabricated nano-spherical CN photocatalyst comprised of CN nanosheets with 3D-layered framework build up from the 2D nanosheets having pointed edge-tips by hard template method using spherical silica. The open surface of 3D nanosheets with pointed edges induced an analogous promotion like “lightning rod effect” and the material showed rapid charges collection and separation at the sharp tip, and H_2 production activity for the optimized 3 wt% Pt/NS-CN catalyst was much significant with appreciable quantum efficiency of 9.6 % at wavelength 420 nm. Thus, by selecting various templates with different nanoarchitectures, CN with various porous architectures can be obtained. Similarly, the properties and photocatalytic activities can also be tuned.

4.2.1.2 Soft Template Method

Yan [106] reported the fabrication of mesoporous CN from melamine via the soft template (Pluronic-P123) that exhibited worm-like porous morphology with large surface area and broad visible-light response. The catalytic activity of the as-prepared meso-porous CN for H_2 evolution was considerably enhanced and the material even exhibited activity at wavelength greater than 700 nm.

According to Wang *et al*.,[107] porous CN can be prepared from the dicyandiamide (DCDA) precursor via different varieties of non ionic surfactant and polymers (amphiphilic block i.e. P123, F127, Triton(X-100), Brij-30, Brij-58, and Brij-76) working as a soft template. The TEM micrograph of porous CN prepared by using P123 template is shown in Figure 8(d), which reflects the pore structures within the Pluronic-based CN-material. The surface areas of the porous CN obtained via using different amount of P123 were in the range of 10.0-299 m^2 g^{-1} and exhibited microporous texture. They investigated that Triton X-100 is a good exception (soft template) for fabrication of porous CN nanomaterials. TEM micrographs of the nanostructured CN prepared by using Triton X-100 template are shown in Figure 8(e,f). The TEM images reflect the well developed porous texture and the geometric properties of original surfactants supramolecular aggregates. The corresponding pore-size diameters of nanoporous CN were of 3.8-15 nm. The specific surface area was about 76 m^2 g^{-1}, and micropores were absent. Using ionic liquids as soft templates, much better nanoporous textures were obtained especially for the used $BmimPF_6$ as shown in the TEM micrograph (Figure 8(g)).

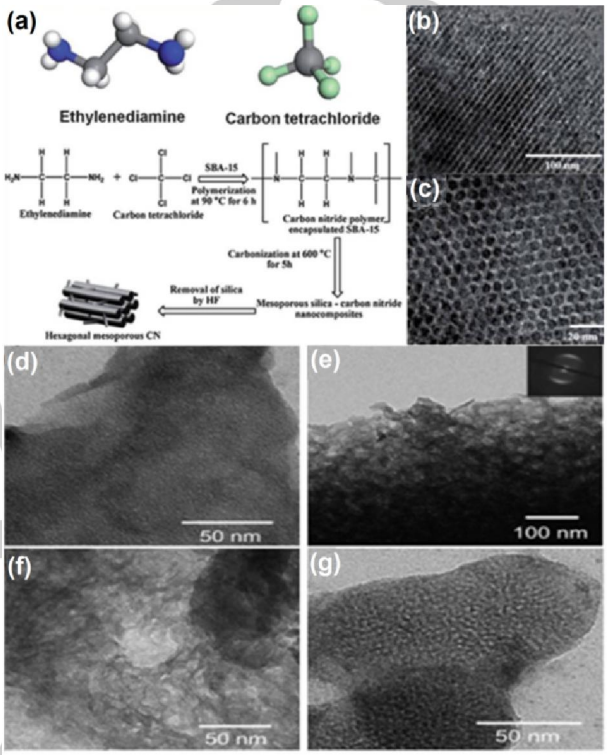

Figure 8. Design for mesoporous CN fabrication by nanocasting technique (a), the TEM micrographs of the resultant porous CN (b, c). Reproduced with permission from ref.[103] TEM micrographs of nano-porous CN prepared from DCDA by using P123 template (d), prepared by using Triton X-100 (e, f), and by using BmimPF6 (g). Adapted with permission from ref.[107] Copyright 2010, Wiley-VCH.

Thus, by the self polymerization reaction of dicyandiamide using various soft templates, the Triton-(X-100) and the ionic liquids were found best templates to obtain CN with highly developed porous texture and large specific surface area.

5. Design and Fabrication of CN-based Heterostructures

The design of CN-based heterojunctions is engineered by employing both of the CN and the coupled semiconductors under solar light. In CN heterojunctions, the VB and CB edges of some typical semiconductors versus NHE at pH=7.0 are depicted in Figure 9.[108]

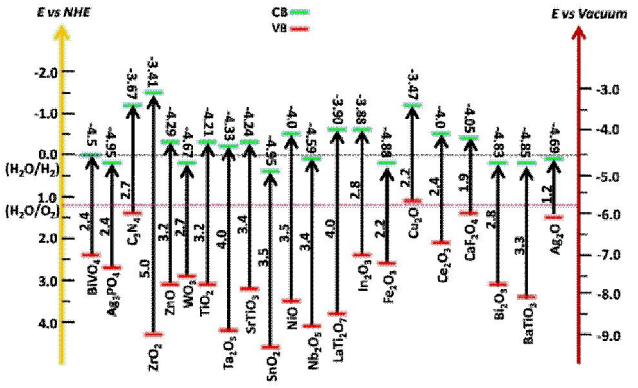

Figure 9. Some typical semiconductors band gaps with proper VB and CB edges versus the NHE at pH=7.

As CN is coupled with semiconductors having different electronic and band structures, a new electronic structure is formed due to band bending, which results from potential difference in the heterojunction. Simultaneously, a built-in electric-field at the interface is produced, that spatially separate and migrate the charge carriers.[109] Based on the VB and CB potentials, the CN-based hetero-junctions could be categorized into three major kinds, such as Type I, Type II, and the Z-scheme, as depicted in Figure 10.[110] In such types of heterojunctions, CN could be taken as semiconductor number 1 or 2, relative to the band levels of the coupled semiconductors. In Type I heterojunctions (Figure 10(a)), the CB edge of semiconductor-1 would be higher than the CB level of semiconductor-2, and its VB level would be lower than the VB level of semiconductor-2. Therefore, under solar irradiation with energy of photons equal or greater than the semiconductor band gap, electron and hole pairs are generated and both would transfer to the semiconductor-2, due to its band edge levels. While, both the electron and holes are collected in semiconductor-2, and as a whole there is no apparent improvement of photogenerated charge carrier's separation that results in the low photo-redox efficiency. In Type II heterojunctions (Figure 10(b)), the CB edge of semiconductor-1 would be higher than the CB level of semiconductor-2. Similarly, its VB level would be higher than the VB edge of semiconductor-2. Under solar irradiation, band bending are formed at interface junction and the charge carrier's moves in opposite directions.[111] Type II heterojunctions are more advantageous due to efficient electron-hole pairs separation in them. Further, the redox reactions took place in two dissimilar semiconductors. In Z-scheme heterojunctions (Figure 10(c)), the CB edge of semiconductor-1 is located above CB of the semiconductor-2 and VB level of the semiconductor-1 is close to the CB band level of semiconductor-2.[112] Thus, selecting a suitable semiconductor photocatalyst for coupling with CN is of great importance for improving interfacial charge transport and separation and solar energy utilization more efficiently.

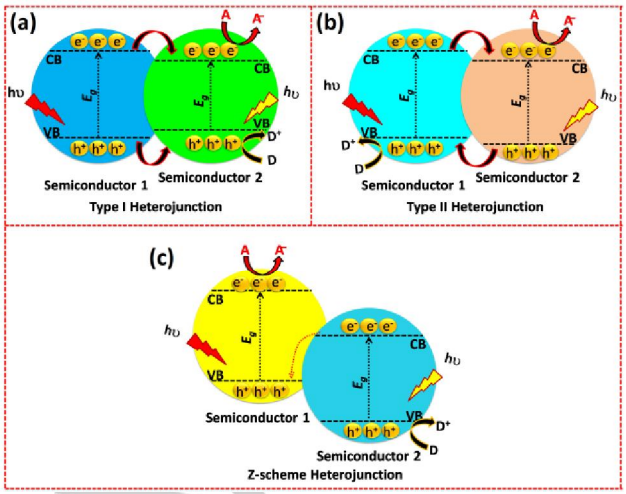

Figure 10. Schematic of the band alignments of the three various kinds of heterojunctions: Type I (a), Type II (b), and Z-scheme (c). In the fig, "A" represent electrons acceptor and "D" represent electrons donor.

Summary of some latest publications on CN based heterojunctions and the evaluated photocatalytic reactions are shown in Table 2. Although, an effective charge carrier's separation can be accomplished in Type II heterojunctions, however, the main shortfall of this system is that the redox powers of photogenerated charges are decreased during charge transfer. This is because of the slightly positive VB level of the semiconductor 1 and slightly negative CB level of the semiconductor 2.[113] Thus, to achieve strong redox ability of Type II heterojunctions is a great challenge for researchers.

Table 2. Typical examples of type-I, -II, and the Z-scheme heterojunctions.

CN based heterojunctions	Types	Photocatalytic reactions	Reference (Year)
Ag_2CO_3–CN	Type(II)	Methyl Orange (MO) & Rhodamine B (RhB) degradation	(2015)[9d]
AgCl–Ag_3PO_4@CN	Type(II)	Sulfamethoxazole degradation	(2017)[114]
Ag_3PO_4–CN	Type(II)	RhB degradation	(2014)[115]
Ag_3PO_4–CN	Type(II)	Diclofenac degradation	(2018)[116]

Ag_2O–CN	Type(I)	MO degradation	(2013)[117]
Ag–Ag_2O@CN	Type(I)	MO degradation	(2016)[118]
Ag_3PO_4–CN	Semicond−cond−semicond Z-scheme	CO_2 conversion to CO, CH_4, CH_3OH, & C_2H_5OH	(2015)[119]
AgBr–CN	Type(II)	MO & 4-chlorophenol degradation	(2013)[120]
$AgIO_3$–CN	Type(II)	MO & RhB degradation	(2015)[121]
$AgVO_3$–CN	Type(II)	Fuchsin & bisphenol A degradation	(2015)[122]
Ag_2WO_4–CN	Semicond−semicond Z-scheme	MO degradation	(2017)[123]
Bi_2WO_6–CN	Semicond−semicond Z-scheme	RhB degradation	(2015)[124]
BiOBr–CN	Type(II)	RhB degradation	(2013)[125]
BiOCl–CN	Type(II)	MO& phenol degradation	(2015)[126]
BiOCl–CN	Type(II)	4-chlorophenol degradation	(2018)[127]
BiOCl–CN	Type(II)	None	(2017)[128]
$Bi_4Ti_3O_{12}$–CN	Type(II)	RhB degradation	(2018)[129]
$BiVO_4$–Pyridine-Doped CN	Semicond−semicond Z-scheme	Phenol& MO degradation	(2017)[130]
$BiVO_4$–CN	Semicond−semicondZ-scheme	RhB & tetracycline degradation	(2019)[131]
$BiVO_4$–CN	Semicond−semicond Z-scheme	Methylene blue (MB) degradation	(2018)[132]
$BiVO_4$–CN	Type(II)	Benzyl alcohol, benzyl amine & aniline oxidation	(2017)[133]
$BiVO_4$–CN	Semicond−semicond Z-scheme	Tetracycline, oxytetracycline & ciprofloxacin degradation	(2016)[134]
$CaIn_2S_4$–CN	Type(I)	H_2 evolution & MO degradation	(2015)[135]
CdS–CN	Type(II)	H_2 evolution	(2013)[136]
CdS–CN	Type(II)	Azo dye & MO degradation	(2017)[137]
CdS QD–CN	Type(II)	H_2 evolution	(2015)[138]
CdSe QD–CN	Type(II)	H_2 evolution	(2018)[139]
$Cd_{0.5}Zn_{0.5}S$–CN	Semicond−semicondZ-scheme	H_2 evolution	(2018)[140]
CeO_2–CN	Type(II)	CO_2 reduction to CO & CH_4	(2016)[141]
CeO_2–CN	Type(II)	2,4-dichlorophenol	(2019)[142]
CeO_2–CN	Type(II)	H_2 evolution	(2018)[143]
Pd-CeO_2–CN	Type(II)	Detoxification of toxic Cr(VI)	(2017)[144]
CeO_2–attapulgite–CN	Type(II)	Desulfurization	(2017)[145]
N-CeOx–CN	Type(II)	H_2 evolution	(2015)[146]
$CoTiO_3$–CN	Semicond−semicondZ-scheme	H_2 evolution	(2016)[147]

Cu_2O–CN	Type(II)	H_2 evolution	(2014)[148]
Cu_2O–CN	Type(II)	MB & MO degradation	(2017)[149]
Cu_2O–CN	Type(II)	H_2 evolution	(2017)[150]
Fe_2O_3–CN	Type(II)	RhB degradation	(2015)[151]
$FeSe_2$–CN	Type(II)	H_2 evolution	(2020)[152]
CN–CN	Type(II)	NO removal	(2013)[153]
In_2O_3–CN	Type(II)	H_2 evolution & CO_2 conversion to CH_4	(2014)[154]
$InVO_4$–CN	Type(II)	H_2 evolution	(2015)[155]
$LaFeO_3$–gC_3N_4	Semicond−semicondZ-scheme	H_2 evolution & MB degradation	(2017)[156]
$MgIn_2S_4$–CN	Type(II)	4-nitroaniline (4-NA) reduction and MO degradation	(2019)[157]
MnO_2–CN	Semicond−semicondZ-scheme	RhB & phenol degradation	(2017)[158]
MoS_2–CN	Type(II)	MO degradation	(2017)[159]
MoS_2–CN	Type(II)	H_2 evolution	(2016)[160]
MoS_2–CN	Semicond−semicondZ-scheme	CO_2 conversion	(2017)[161]
MoS_2–CN	Semicond−semicondZ-scheme	CO_2 conversion	(2018)[161]
0D(MoS_2) –2D(CN)	Semicond−semicondZ-scheme	H_2 evolution	(2018)[162]
N-$SrTiO_3$–CN	Semicond−semicondZ-scheme	RhB degradation	(2014)[163]
NiO–CN	Type(II)	MB degradation	(2014)[164]
Polypyrrole–CN	Type(II)	RhB degradation	(2015)[165]
Red phosphor–CN	Type(II)	H_2 evolution & CO_2 conversion to CH_4	(2013)[166]
$SmVO_4$–CN	Type(II)	RhB degradation	(2013)[167]
SnO_2–CN	Type(II)	H_2 evolution & MO degradation	(2014)[168]
SnO_2–CN	Type(II)	MO degradation	(2018)[169]
SnO_2–B-P codoped CN	Type(II)	CO_2 conversion	(2017)[170]
SnS_2–CN	Type(II)	RhB, MO & 4-nitrophenol degradation	(2015)[171]
SnS_2–CN	Type(II)	MO degradation	(2016)[172]
TiO_2–CN	Type(II)	H_2 evolution & ciprofloxacin degradation	(2016)[173]
TiO_2–CN	Type(II),Semicond−semicond Z-scheme	N_2O decomposition	(2018)[174]
TiO_2–CN	Type(II)	H_2 evolution	(2016)[44e]
Au-TiO_2–gC_3N_4	Type(II)	H_2 evolution	(2018)[175]
B-TiO_2–CN	Type(II)	H_2 evolution	(2015)[176]

C-TiO_2–CN	Type(II)	MO degradation	(2017)[177]
N-TiO_2–CN	Type(II)	NO removal	(2018)[178]
N-TiO_2–CN	Type(II)	H_2 evolution & RhB degradation	(2015)[32d]
N-TiO_2–CN	Type(II)	CO_2 conversion to CO & CH_4	(2014)[179]
Ti^{3+}-TiO_2–O-CN	Type(II)	RhB degradation	(2017)[180]
UiO-66–CN	Semicond−semicond Z-scheme	H_2 evolution	(2015)[181]
UiO-66–CN	Semicond−semicond Z-scheme	Cr(VI) reduction	(2019)[182]
V_2O_5–CN	Semicond−semicond Z-scheme	RhB & tetracycline degradation	(2016)[183]
WO_3–CN	Type(II)	RhB degradation	(2014)[184]
WO_3–CN	Semicond−semicond Z-scheme	MB degradation	(2017)[185]
WO_3–CN	Semicond−semicond Z-scheme	H_2 evolution	(2017)[186]
WO_3@CN	Semicond−semicond Z-scheme	RhB degradation	(2019)[187]
WO_3@CN	Semicond−semicond Z-scheme	CO_2 conversion to CH_3OH	(2014)[188]
$ZnFe_2O_4$@CN	Type(I)	H_2 generation	(2014)[189]
$ZnIn_2S_4$@CN	Type(II)	H_2 generation, MO & phenol degradation	(2015)[190]
$ZnIn_2S_4$@CN	Type(II)	2,4-dichloro-phenoxyacetic acid decomposition	(2016)[191]
$ZnIn_2S_4$–NC@CN	Semicond−cond−semicond Z-scheme	H_2 evolution	(2015)[192]
ZnO@CN	Type(II)	MB & MO degradation	(2017)[193]

5.1. CN-based Type-II Heterojunctions

The fabrication of CN-based Type II hetero-junctions is beneficial for photoinduced charge carrier's separation owing to the stagger band structure of the coupled semiconductors. An appropriate band configuration is the key deliberation to choose the 2nd catalyst for fabricating CN-based Type II heterojunctions. Li *et al*.[194] fabricated composites of CN/TiO_2 (Figure 11(a)), that exhibit super-imposed XRD patterns of TiO_2 and CN, demonstrating the heterojunction formation. The samples exhibited better visible-light catalytic performance for degradation of methyl orange (MO) as compared to the bare CN (Figure 11(b)). The activity of the optimized nanocomposite was also examined under UV–vis irradiations. Compared to the individual CN and TiO_2, the nanocomposite displayed drastically improved photoactivity for methyl orange (MO) degradation. This was ascribed to the superior charge carrier's separation by electrons transfer from the CB of CN to the CB of TiO_2 (Figure 11(c, d)).

He *et al*.[195] reported ZnO/CN nanocomposites for CO_2 conversion under UV-vis irradiation. Figure 11(e) clearly indicates that the XRD patterns of both the components exist in ZnO/CN composites. The formation of ZnO/CN heterojunctions significantly promoted charge carriers separation and considerably improved its activity for photo-catalytic CO_2 conversion. The optimized ZnO/CN nanocomposite exhibited CO_2 reduction rate of 45.6 $\mu molh^{-1}$ $gcat^{-1}$ (Figure 11(f)), about 4.9 and 6.4-time enhanced compared to the individual CN and P25 photocatalysts, respectively. The charge separation and transport mechanism is depicted in Figure 11(g).

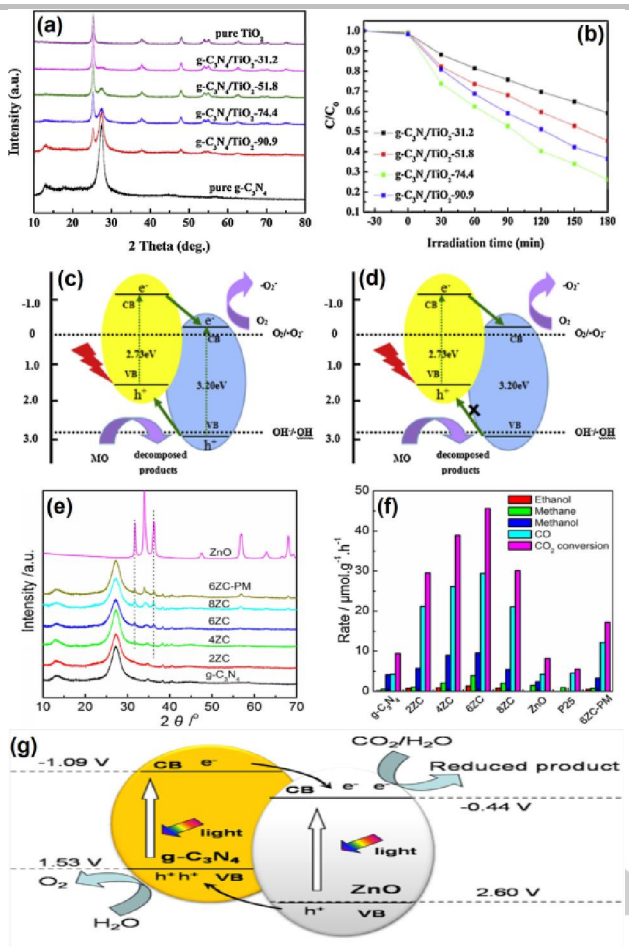

Figure 11.XRD patterns (a), photocatalytic activities for methyl orange degradation (b), and charge carriers separation and transport mechanism (c, d) of CN/TiO_2 composites. Reproduced from ref.[194] with permission. Copyright 2016, Elsevier. XRD patterns (e), photocatalytic CO_2 conversion activities (f), and charge carriers separation and transfer mechanism (g) of ZnO/CN heterojunctions. Reproduced from ref.[195] with permission. Copyright 2015, Elsevier.

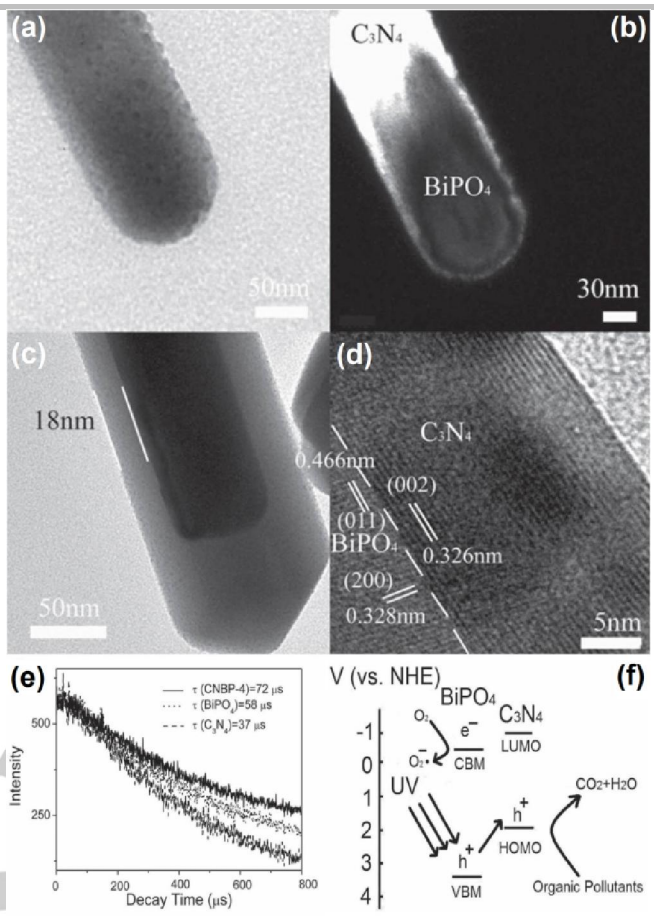

Figure 12. Bright-field TEM micrograph (a), dark-field TEM micrograph (b), TEM micrograph (c), and HRTEM micrograph (d) of the CN-$BiPO_4$ (CNBP-10) nanocomposite. Photo-luminescence decay curves of the CN/$BiPO_4$ (CNBP-4), $BiPO_4$, and CN samples measured at excitation wavelength of 254 nm, and emission wavelength of 550 nm (e), Charge carrier's separation and transport mechanism in $BiPO_4$/CN nanocomposite (f). Adapted with permission from ref.[197]. Copyright 2012, Wiley-VCH.

It is noteworthy, that CN could be simply exfoliated into thin nanosheets structures with high flexibility. Thus, the exfoliated CN sheets facilitate the synthesis of CN-based core/shell heterostructures, in which the highly flexible CN sheets cover the coupled semiconductors [195-196]. The construction of core-shell heterostructures prevent the nanosheets aggregation and efficiently consume the absorption capability of the CN shell. Pan *et al.*[197] reported the synthesis $BiPO_4$@CN core-shell nanocomposites via electrostatic self-assembly technique. They observed a flat CN coating layer with thickness of approximately 18 nm onto $BiPO_4$ surface as shown in Figure 12(a-d).

The $BiPO_4$@CN core/shell nanocomposite exhibited improved UV-vis and visible light activity for photodegradation of MB, which was accredited to the enhanced charge carriers separation by the photo-induced electron-hole transfer at the interfacial junction of $BiPO_4$ and the CN. The promoted charge carrier separation of $BiPO_4$@CN core-shell composites was confirmed by electrochemical impedance spectra photocurrent results. Further, the photoluminescence (PL) decay results (Figure 12(e)) revealed that the charge carriers recombination is drastically inhibited. As depicted in Figure 12(f), the energy band levels between the CN and $BiPO_4$ components well match for Type II heterojunction. Thus, the photo-induced charge carrier's could be extensively separated by transferring the CN excited electrons to the more positive CB of $BiPO_4$ and holes of the $BiPO_4$ to more negative VB of CN.

Notably, an appropriate semiconductor with narrow band gap not only performs as the Type II band alignment complement in CN-based heterojunctions for improvement of charge carrier's separation, but also improves the optical absorption behavior of the composites. Liu *et al.*[198] reported the construction of Ag_3PO_4@CN core-shell nanocomposites by an ultrasonication-chemisorption

technique. The TEM images (Figure 13(a, b)) demonstrated that CN wrapped the Ag_3PO_4 nanoparticles and performed as shell. The HRTEM image (Figure 13(c)) revealed that a close interface contact exists between Ag_3PO_4 and the CN components, and the lattice-fringes with d-spacing of 0.27 nm (2 1 0, planes) were attributed to the Ag_3PO_4 nanoparticles. As shown in Figure 13(d), the Ag_3PO_4@CN core@shell nanocomposite exhibited exceptional visible-light activity (97 %) for methylene blue degradation in only 30 min irradiation period. The improved charge separation in the Ag_3PO_4@CN nanocomposite was established via the photocurrent response and electrochemical impedance spectra (EIS) results. The charge transfer mechanism and the MB degradation over the Ag_3PO_4@CN nanocomposite was proposed as shown in Figure 13(e). They demonstrated that the CN VB and CB levels are located at 1.3 and -1.4 eV, respectively. While, the VB and CB levels of Ag_3PO_4 are at 2.9 and 0.45 eV position, respectively. The CN CB level is negative compared to CB level of the Ag_3PO_4. Thus, electrons excited to the CB of CN were transferred to the Ag_3PO_4 CB through the well-established interface junction. The electrons then diffused to the surface of catalyst and reacted with molecular oxygen and the produced •OH through a series of reactions. The generated •OH finally decomposed the methylene blue dye. In contrast, the photo-excited holes of Ag_3PO_4 were transferred to the CN VB and performed as the main active oxidants for methylene blue degradation. Thus, the charge recombination was greatly inhibited and the visible-light activity was significantly enhanced.

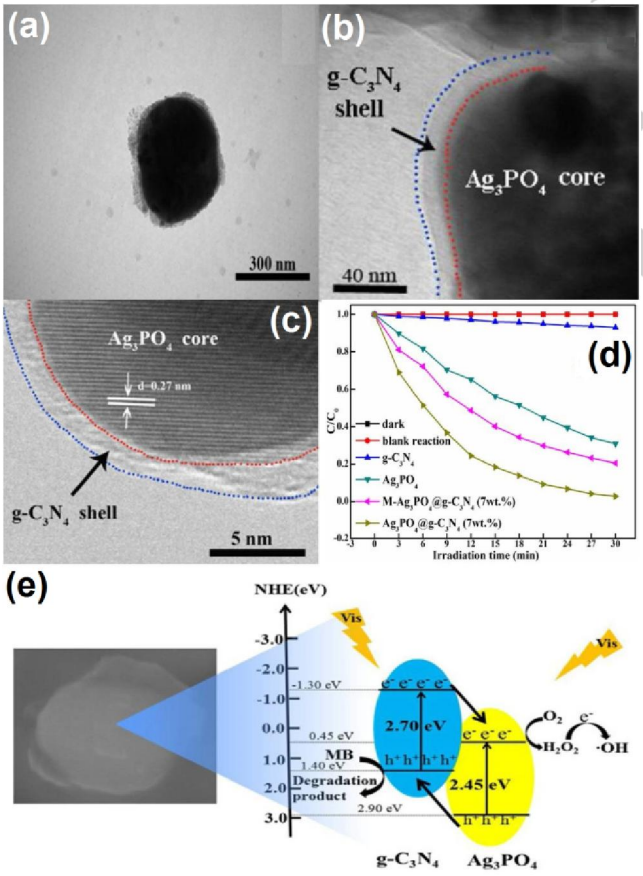

Figure 13.TEM images (a, b), HRTEM image (c), photocatalytic degradation of methylene blue (d), and charge transfer mechanism and photocatalytic processes (e) of Ag_3PO_4@CN core@shell nanocomposites. Reproduced from ref.[198] with permission. Copyright 2016, Elsevier.

In Type II heterojunction, the multi-component or ternary system can significantly enhance the charge separation by a synergistic effect. Jiang *et al*.[199] reported the construction of CN/TiO_2/ZnO ternary heterojunctions for p-Toluenesulfonic acid (p-TSA) degradation under visible-light irradiation. The TEM micrograph of CN/TiO_2/ZnO nanohybrid (CP3) is provided in Figure 14(a). It is clear that the TiO_2 and ZnO particles are dispersed on the unique graphitic-like CN structure. From HRTEM image Figure 14(b), it was confirmed that the TiO_2 (101) facets (0.35 nm) and ZnO (002) facets (0.26 nm) were stacked on nanosheets of CN, and in the ternary hybrid CN acted as a layer. The fabricated CN/TiO_2/ZnO nanohybrid exhibited superior photo-catalytic efficiency for p-TSA degradation (Figure 14(c)). Schematic mechanism of charge separation and transport in the facet coupled nanocomposite is shown in Figure 14(d).

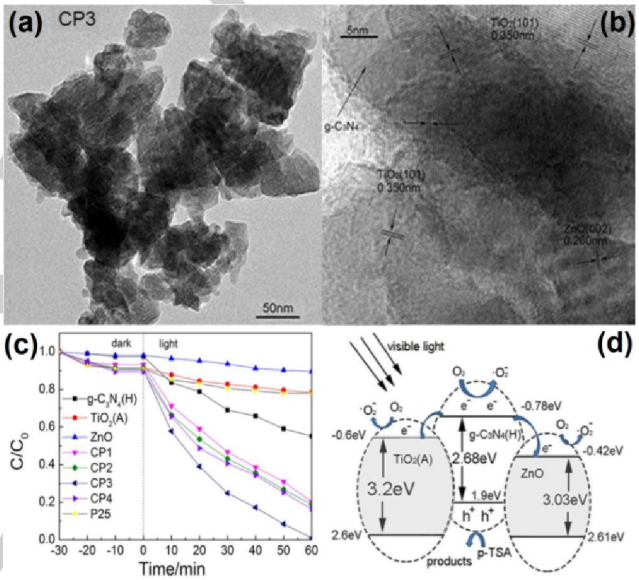

Figure 14.TEM image (a), HRTEM image (b), of CN/TiO_2/ZnO (CP3) nanohybrid. Adsorption/photocatalytic degradation curves of p-TSA (c), of TiO_2, ZnO, CN, P25, and various CN/TiO_2/ZnO nanocomposites. Proposed charge separation mechanism for the facet coupled ternary nanocomposites (d). Reproduced from ref.[199] with permission. Copyright 2017, Elsevier.

They demonstrated that charge carrier's were induced only from the CN component under visible light, because TiO_2 and ZnO cannot be excited under visible-light. Thus, the excited electrons of CN were transferred to the CB's of TiO_2 and ZnO where they easily reduced molecular oxygen to $\bullet O_2^-$. Simultaneously, the VB holes of CN directly oxidized p-TSA pollutant into inorganic minerals. Similar synergistic effects were also observed in other multicomponent or ternary system, like CN/Fe_3O_4/AgI,[200] CN/ZnO/AgCl,[201] CN/Fe_3O_4/Ag_2CrO_4,[200] and CN/Fe_3O_4/BiOI.[202]

The layered structured MnO_2 could also be utilized to fabricate CN-based 2D/2D composites.[203] Li *et al*.[204] fabricated 2D/2D CN/MoS_2 nanocomposite via the self assembly of MoS_2 and nanosheet CN. As revealed in Figure 15(a), the 2D CN and 2D MoS_2 were achieved by exfoliation of their bulks using ultrasonication. From TEM

micrographs of 2D CN/MoS_2 heterojunctions (Figure 15(b, c)), the presence of CN and MoS_2 sheets were confirmed. As clear from Figure 15(d), the mechanism of charge carrier's transfer of the fabricated 2D MoS_2/CN heterojunctions could be allocated to the Type II heterojunctions. When the 2D MoS_2/CN nanocomposites were irradiated under visible-light, the photogenerated electrons of CN were transferred to the CB of MoS_2 and holes in the VB of MoS_2 were transferred to the CN VB. The photo-induced holes collected in the VB of CN oxidized dye molecule into inorganic compounds, like CO_2 and H_2O.

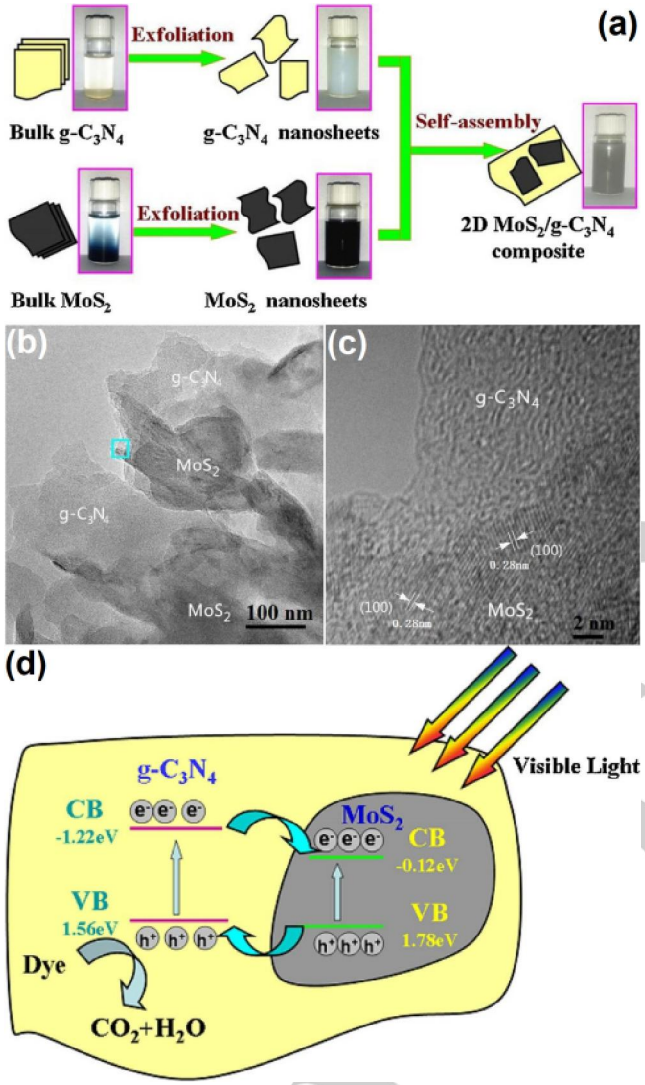

Figure 15. The synthesis scheme (a), TEM image (b), HRTEM image (c), and charge carrier's transfer mechanism (d) of MoS_2/CN 2D/2D composites. Reproduced from ref.[204] with permission. Copyright 2016, Elsevier.

Based on the above discussion, it is established that Type II heterojunctions are much favorable for improved charge separation and remarkably improved photocatalytic activities. It is noteworthy, that the efficient solar energy utilization, large surface area, more surface active sites, and effective interface junction in Type II heterojunction is much crucial for the significantly improved photocatalytic activities.

5.2. CN-based Z-scheme Heterojunctions

Very recently, an innovative type of Z-scheme-heterojunction distinct to the Type II heterojunction has been reported which overcome the weak redox ability.[205]All-solid-state Z-scheme mechanisms (with solidstate electron mediators) and Direct Z-scheme (without electron mediators) are highly investigateddue to their capability of remarkably promoting space charge isolation. Distinct from the typeII heterojunctions,Z-scheme systems involve spatialmigration of electrons causing enhanced charge carriers separation leading to the occurrence of reduction and oxidation reactions at different components of the heterojunctions.[206] There exist two types of CN based Z-scheme heterojunctions: (1) semiconductor−CN/semiconductor Z-scheme heterojunctions (Figure 16a), and (2) semiconductor/CN/conductor (electron-mediator)-semiconductor Z-scheme heterojunction (Figure 16(b)).[207] A lot of publications have been reported on the fabrication of CN-based Z-scheme heterojunctions including TiO_2/CN,[208] Ag_2CO_3/CN,[209] Ag_3PO_4/CN,[210] AgBr/CN,[211] $CoTiO_3$/CN,[147] Bi_2WO_6/CN,[212] $BiVO_4$/CN,[213] CdS/CN,[214] α-Fe_2O_3/CN,[215] $NiTiO_3$/CN,[216] MoO_3/CN,[217] WO_3/CN,[218] ZnO/CN,[219] etc. Thus, the wonderful Z-scheme heterojunction display dual function role in photocatalysis such as high charge separation and the strong redox ability due to the reasonably negative CB level and very positive VB level.[220] In semiconductor-semiconductor Z-scheme composites, the photo-induced electrons of the semiconductor 2 with less negative CB will combine with holes of the semiconductor 1 with less positive VB level, leaving the electron in comparatively negative CB of semiconductor 1 and holes in comparatively positive VB of semiconductor 2. In the semiconductor/conductor/semiconductor Z-scheme system, a conductor is employed as a bridge between two semiconductors to transport electrons from semiconductor 2 to semiconductor 1. Zheng *et al*.[221] fabricated CdS−Au/CN heterojunctions that showed enhanced photoactivity for H_2 production and CO_2 conversion. Similarly, Yang *et al*.[222] reported the synthesis of AgBr/Ag/CN composites for methyl orange degradation. Thus, the conductors such as nanocarbon, Cu, Au and Ag etc. serve as electrons mediator between semiconductors to effectively improve the photo-induced charge transfer.

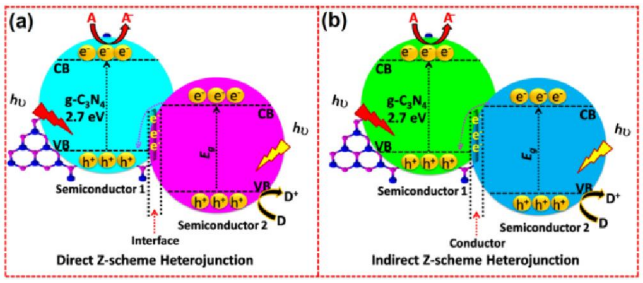

Figure 16. Schematic for the photo-induced charge separation phenomenon in different kinds of heterojunctions: (a) Semiconductor-semiconductor Z-scheme, (b) semiconductor/conductor/ semiconductor Z-scheme. Here, "A" represents electron acceptor and "D" represents electron donor.

Although, there have been a lot of reports on CN based Z-scheme heterojunctions, but only a few of them provided charge transfer mechanisms with clear experimental evidences. Ohno *et al*.[188] used a double-beam photo-

acoustic spectroscopy to investigate charge carrier transfer phenomenon in WO_3/CN hybrid under visible-light illumination. Intensity of the double-beam photo-acoustic was obtained from partial-reduction of W^{6+} to the W^{5+} via the photo-induced electron of nanosized WO_3. The CB of CN is comparatively energetic than that of the WO_3, thus, the excited CN electrons would transfer to WO_3 leading to the high concentration of W^{5+}. It is noteworthy that if the charge transfers follow the mechanism of Type II heterojunctions, then a high intensity in photo-acoustic spectrum would be achieved. But instead, a low photo-acoustic intensity was obtained along with enhanced photoactivities by the comparison of WO_3/CN with un-modified WO_3. Thus, it was confirmed that charge separation proceed in a Z-scheme approach, the photo-induced electrons of WO_3 recombined with the VB holes of CN. Kumar *et al*.[223] reported the fabrication of N doped ZnO coupled CN Z-scheme heterojunction thorough an efficient chemical-probe to explore charge transfer phenomenon. The CN has a more negative CB level compared to the N-ZnO. According to the Type(II) mechanism, the reduction and oxidation potentials of such heterojunction would be decided by the slightly negative CB level of N-ZnO nanoparticles and slightly positive VB level of the CN. Worth noting, the less negative CB of N-ZnO is energetically inadequate to reduce O_2 to the corresponding $\bullet O_2^-$, meanwhile, the CN VB is insufficient to generate •OH from H_2O. They performed EPR analysis to measure the $\bullet O_2^-$ trapped by the 5,5-dimethyl-1-pyrroline N-oxide (DMPO). Simultaneously, they used terephthalic-acid as a probe molecule to explore the production of •OH. They found that both the $\bullet O_2^-$ and •OH were present in reaction system. This proved that this system do not follow Type(II) heterojunction, but instead follow Z-scheme system. The CN based nanocomposites are still governed by the heterojunction Type II and due to the strong redox capacity of Z-scheme heterojunctions, it is highly desired to fabricate CN-based Z-scheme heterojunctions for potential photocatalysis.

Recently, Hong *et al*.[183] fabricated V_2O_5/CN Z-scheme composites via the in-situ growth technique (Figure 17(a)). As clear from Figure 17(b), the XRD characteristic patterns of both the components exist in the heterojunctions. The visible-light activities of the composites for rhodamine B and tetracycline degradation were significantly enhanced in comparison to the bare V_2O_5 and CN. Obviously, the catalytic efficiency of the amount optimized composite (VC1.0 %) for rhodamine B degradation was 7.3 and 13.0-time enhanced compared to the bare CN and V_2O_5 (Figure 17(c)). Similarly, the photo-degradation performance of the amount optimized composite (VC1.0 %) for tetracycline was 75.7 % (Figure 17(d)). From radical trapping and the electron-spin resonance (ESR) results, solid-state Z-scheme heterojunction phenomenon was predicted as shown in Figure 17(e). They demonstrated that the system not only improved the separation of photogenerated charges but also exhibited strong redox ability for pollutants degradation.

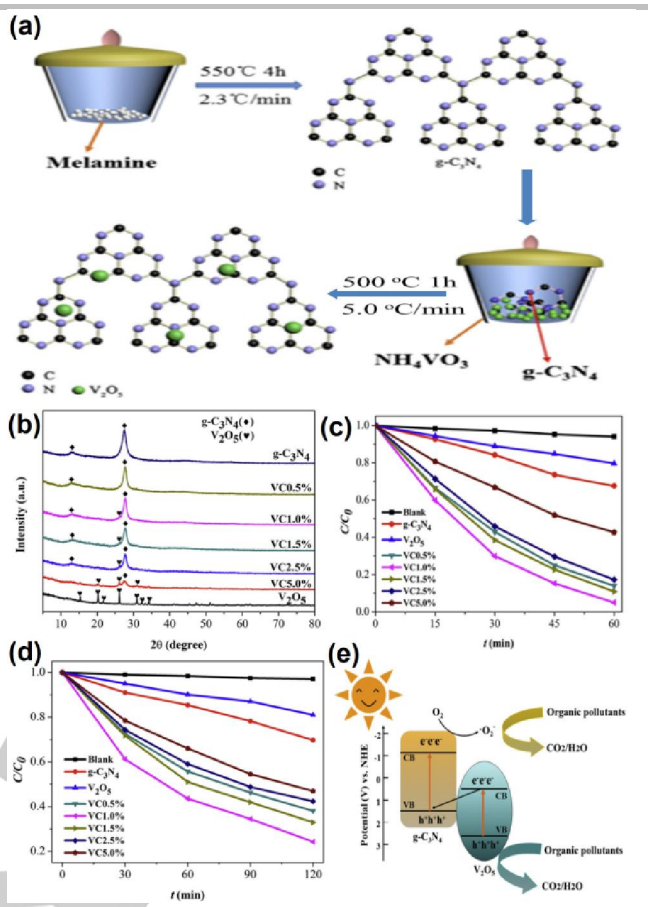

Figure 17. Schematic illustration of in-situ growth strategy of V_2O_5/CN nanocomposites (a), XRD patterns (b), photoactivity for rhodamine B degradation (c), and photocatalytic activity for tetracycline (d), of V_2O_5, CN, and V_2O_5/CN. Proposed charge transfer phenomenon and the catalytic processes over V_2O_5/CN nanocomposites (e). Reproduced from ref.[183] with permission. Copyright 2016, Elsevier.

It is important to note that in Z-scheme systems, electron mediators can also be employed for effective charge separation in two semiconductor components.[224] The applications of electrons mediated Z-scheme heterojunctions are restricted to the liquid-phase only. Thus, it is highly advantageous to design all-solid-state Z-scheme heterojunctions utilizing the conductive-solid materials as the electrons mediator.[225] The all-solid-state Z-scheme heterojunctions could be utilized in both of the liquid-solid and solid-gas systems. Usually, the nanometric sized metal with excellent electrical conductivity is employed as charge mediators for fabricating Z-scheme heterojunctions. Li *et al*.[226] fabricated g-CNS/Au/CdS Z-scheme heterojunctions via two steps self-assembly technique. From TEM image (Figure 18(a)), it is clear that the surface of g-CNS was covered with many dark color Au nanoparticles and each nanoparticle of Au was covered with bright color layered CdS. Further, HRTEM image (Figure 18(b)), revealed that lattice fringe with d-spacing of 0.34 nm (1 1 1) crystal plane were attributed to the Cds. The g-CNS/Au/CdS nanocomposite exhibited significant visible-light catalytic activity for H_2 production in aqueous solution of lactic acid scavenger (Figure 18(c)). Thus, a Z-scheme charge transfer phenomenon was proposed for g-CNS/Au/CdS nanocomposite as shown in Figure 18(d). In this system, Au played the role of electron mediator between the g-CNS and CdS components. As under visible-light irradiations, the

weak reductive photo-excited electrons of CdS would quickly transfer to the Au. Meanwhile, the weak oxidative photo-excited holes of g-CNS would quikly transfer to the Au. Thus, the photogenerated charge carriers would annihilate at Au. Hence, the photogenerated highly reductive electrons in the CB of g-CNS would take part in H_2O reduction to evolve H_2. Similarly, the highly oxidizing holes left in the VB of Cds would participate in the lactic acid oxidation. In this way, the redox ability of the charge carrier's would be significantly enhanced.

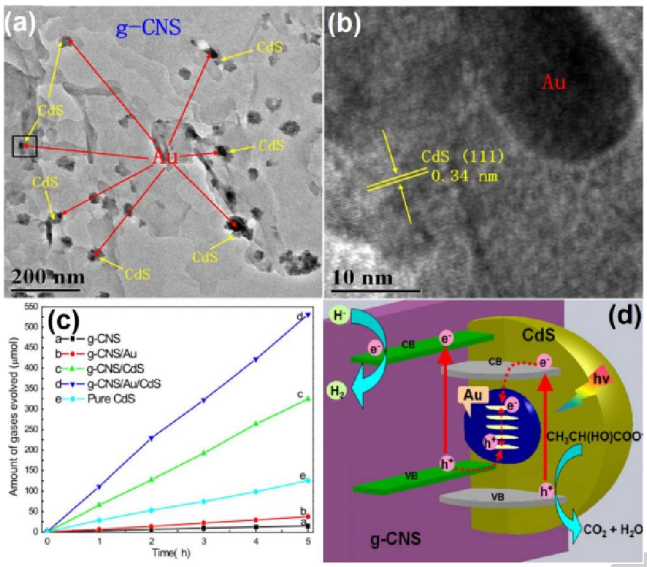

Figure 18. TEM micrograph (a) and HRTEM micrograph (b) of g-CNS@Au-CdS composites. Photocatalytic H_2 evolution activity (c) of g-CNS, g-CNS/Au, g-CNS/CdS, g-CNS/Au/CdS and the CdS samples in the lactic acid aqueous solution. Schematic of Z-scheme charge transport mechanism in the g-CNS@Au-CdS nanocomposite (d). Reproduced from ref.[226] with permission. Copyright 2015, Elsevier.

5.2.1 Quantum dots/CN Z-scheme Heterojunctions

Recently, the quantum dots are widely employed in photocatalysis owing to inhibition of the charge recombination as a result of the short average diffusion distance from core to the surface.[227] For example, Fu *et al*.[228] reported MoS_2 quantum dot/CN0D/2D composites by a combine hydrothermal and microemulsion technique. The visible-light catalytic activity of the composites was appraised for rhodamine B degradation. The modification of CN with MoS_2 QDs significantly improved its photocatalytic activity. As clear from Figure 19(a), the photocatalytic degradation rate of the optimized 7 % MoS_2 QD/CN composite for rhodamine B degradation was 8.8 times high compared to the bare CN. Further, the nanocomposites exhibited enhanced photocurrent density response and low charge transfer resistance compared to the bare CN and MoS_2 QDs. Further, it was confirmed through active species trapping measurements that the $\bullet O_2^-$, h^+ and •OH are the main reactive species. Hence, Z-scheme charge transfer phenomenon was proposed as depicted in Figure 19(b).

In brief, the charge transfer phenomenon in various composite systems depends on the component catalysts, their ratio, synthesis conditions, and the close interface contact. To clarify the charge transfer mechanisms, various techniques such as electron paramagnetic resonance, photoluminescence spectroscopy, surface photovoltage spectroscopy and reactive species trapping experiments are highly efficient tools.

5.2.2 CN/Metal Schottky Junction

The construction of semiconductor-metal heterojunction is extensively employed to generate a space-charge region called the Schottky barrier. In semiconductor-metal heterojunction, the interface junction between the two components allow transferring of electrons from one module to the other by the Fermi-energy levels alignment, leading to the improved charge separation and photocatalytic activities.[229]Beside various types of heterojunctions, the CN modification with noble metal cocatalysts like Au, Ag, Pt, and Pd, the transition metal co-catalysts like Fe, Cu and Ni, and hydroxides and sulfides of transition metal is another approach to improve its photocatalytic performance. The function of the co-catalyst is to increase the surface catalysis by acting as the active reaction sites and also enhances charge carriers separation of CN. When CN is modified with metal co-catalysts, a Schottky-barrier and the space charge region is formed at interfacial contact due to the difference in their Fermi energy levels and work functions. Simultaneously, an electric-field is produced because of the relocation of charges between CN and metal co-catalysts.[230] In fact, CN has low Fermi energy and CB levels in comparison to the Fermi energy levels of the metal co-catalysts as depicted in Figure 19(c).

Thus, electrons in the CB of CN would be captured by the co-catalysts leaving the positive holes in VB of the CN. This will lead to the enhanced charge separation and visible-light catalytic activities. Hence, due to the Schottky barrier, electrons appears in metal and holes in the CN.

5.3. CN/Noble Metal Heterojunctions

Except for the role of electron mediator, the noble metal nanoparticles such as Au, Ag etc. also reveal the localized surface-plasmon resonance (SPR) consequence under solar irradiation.[231] When the incident photons frequency matches the free valence electrons frequency on the metal particles, swing against the restoring force of positive nuclei. Noteworthy, this frequency of resonance photons differ from that of the noble metals. Thus, highly energetic-electrons are generated at the surface of noble-metal particles due to the localized SPR excitation, which then transfer to the CN CB and participate in various reduction reactions as depicted in Figure 19(d).

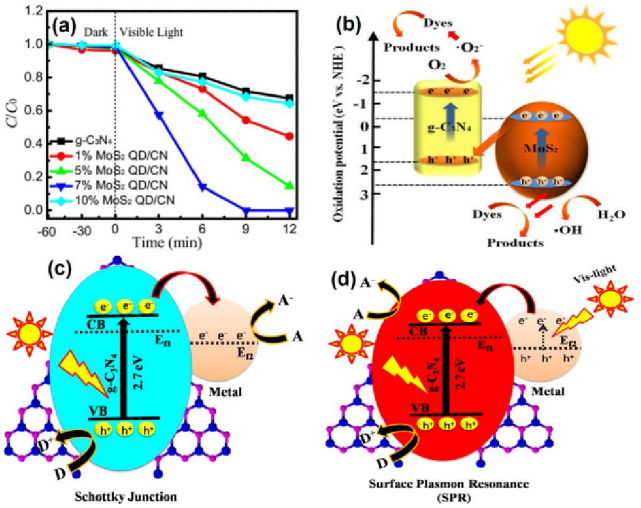

Figure 19. The activity of CN and MoS_2 QD/CN composites for rhodamine B photo-degradation (a), and Schematic for charge separation and transfer and the photocatalytic processes over MoS_2 QD/CN composites (b). Reproduced from ref.[228] with permission. Copyright 2017, Elsevier. The Schematic for charge separation and transfer in Schottky junction of the metal/CN nano-hybrids (c), schematic for the photo-induced charge transfer and separation in noble-metal/CN nano-hybrids (d). Here, "A" represents electron acceptor, "D" represents electron donor, and "Ef" represents the Fermi energy level.

Bi *et al*.[232] fabricated Ni/CN heterojunction via a facile solvo-thermal approach using acetyl-acetone nickel and melamine precursors. They demonstrated that the Ni particles with average size of ~30 nm (d-spacing = 0.209 nm) were dispersed onto the CN nanosheets surface. Consequently, the charge carrier's separation efficiency was greatly enhanced. It is important to note that by coupling a metal with CN, a Schottky barrier is formed that facilitate electron hole pair's separation owing to the electrons transfer among the metal nanoparticles and CN. Recently, Fan *et al*.[233] fabricated Cu/CN catalysts via a facile technique. From TEM image (Figure 20(a)), it can be seen that Cu particles with average diameter of 30 nm were uniformly dispersed on the surface of CN. Further, HRTEM image (Figure 20(b)) revealed that lattice fringe with d-spacing of 0.255 nm were attributed to the (111) plane of Cu phase in Cu/CN heterojunction. The Cu/CN composites displayed excellent cocatalyst-free visible-light catalytic activity for H_2 generation. This demonstrates that the loaded Cu could effectively trap photo-induced electrons of CN and perform as a co-catalyst. Thus, a possible photocatalytic mechanism for H_2O reduction to evolve H_2 over Cu/CN heterojunction was proposed as provided in Figure 20(c). Under visible-light irradiation, the photoexcited electrons of CN transfer to the Cu nanoparticles, because the Fermi energy level of Cu nanoparticles is lower than CB level of the CN. Moreover, the super electrical conductivity of Cu and the strong contact between Cu and CN will form a Schottky barrier, which facilitates the electrons transport from CN to Cu. The electrons in Cu would be trapped by H_2O to evolve H_2 and the holes in VB of CN would be utilized by methanol as a sacrificial agent. Thus, the Cu act as a cocatalyst to speed up photocatalysis and the enriched electrons on Cu would promote the reduction of H^+ to generate H_2.

The SPR behavior in noble metal nanoparticles can improve the utilization of visible-light photons and exhibit extraordinary sound effects with semiconductors.[231b, 234] Thus, to enhance the photocatalytic efficiency of CN, coupling of noble-metals is highly desirable.[235] The SPR effect of noble-metal nanoparticles cause intense localized electromagnetic fields, which accelerates the generation of charge carrier's in CN.[236] Further, the suitable Fermi energy level of noble-metal particles facilitate the charge carrier's separation, that results in the improvement of CN quantum efficiency, because of the intimate contact between noble-metal nanoparticles and CN in the fabricated heterojunctions.[237] Additionally, the electron transfer further shift the Fermi energy level to highly negative potential and enhances the electrons reduction ability in vicinity of the Fermi level close to CB of the semiconductor CN.[237c, 238] Worth noting, the noble metal/CN nanocomposites could display enhanced photo-activities.

For instance, Cheng *et al*.[239] fabricated Au loaded CN (AuNPs/CN) nanocomposites by ultrasonic assisted liquid-exfoliation of CN via the photo-reduction of Au(III) under solar irradiation. From TEM image (Fig. 20(d)), it can be seen that Au nannoparticles with diameters of 5-20 nm are dispersed on the CN surface. The resultant nanocomposites showed exceptional visible-light catalytic activities for methyl orange degradation. The enhanced activities were accredited to the improved charge carrier's separation and the SPR effect of the AuNPs. The mechanism of methyl orange photo-degradation over AuNP/CN nanocomposite is shown in Figure 20(e). They demonstrated that charge carriers are generated in CN upon visible-light irradiations. The AuNP traps the photo-induced electrons of CN and facilitate electron-hole pair's separation by interfacial electron transfer mechanism. Simultanuously, the AuNPs plasmon excitation resulted in the production of additional charge carriers on its surface. The electrons in CB of the CN and AuNPs would react with the O_2 species to generate super oxide radicals ($\bullet O_2^-$). The photo-induced holes left in VB of the CN and AuNPs would efficiently degrade methyl orange.

Similarly, noble-metal Ag has been regarded as excellent co-catalyst in fabricating CN-based heterojunctions.[240] For example, Ma *et al*.[241] fabricated Ag/CN nanocomposite via the thermal polymerization of the melamine combined with the photo-assisted reduction process. The visible light activity of the composites was appraised for the Escherichia coli (E. coli) inactivation. The nanocomposites showed remarkably improved photocatalytic disinfection efficiency in comparison to the bare CN. The superior photocatalytic bactericidal effect of the composites was attributed to the synergestic effect of both Ag and CN, as a result of the extended optical absorption and promoted charge carriers separation. They demonstrated that the photoinduced electrons on the Ag surface in Ag/CN nanocomposites would react with surface adsorbed O_2 species to generate $\bullet O_2^-$ and H_2O_2. Subsequently, the highly reactive species including h^+ and $\bullet O_2^-$ would directly attack the E. coli, oxidize and split the semi-permeable membrane of its cell wall, causing leakage of cell organelles, finally leading to its death.

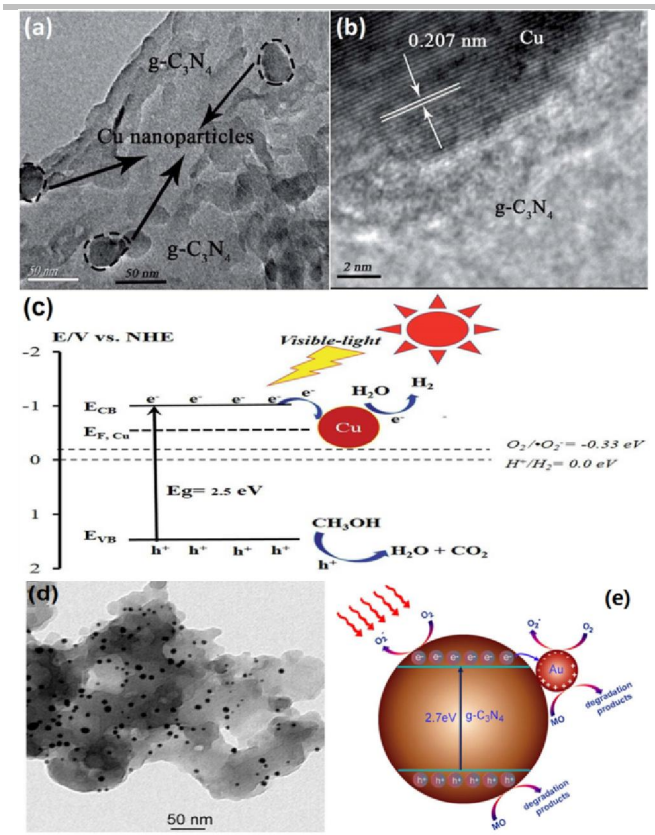

Figure 20.TEM micrograph (a), HRTEM micrograph (b), and charge transfer mechanism and the photo-catalytic processes in Cu/CN (c). Reproduced from ref.[233] with permission. Copyright 2016, The Royal Chemical Society. TEM micrograph of AuNP/CN nanocomposites (d), Schematic of the charge transport and visible-light catalytic processes for methyl orange degradation over AuNPs/CN nanocomposites (e), Reproduced from ref.[239] with permission. Copyright 2013, The American Chemical Society.

Yang *et al.*[242] fabricated Ag/CN composite via a polymerization photo-deposition technique. The Ag/CN composite displayed enhanced visible-light photocatyalytic activities for MO and p-nitrophenol degradation compared to the bare CN. The superior performance was accredited to the extended optical absorption via the SPR effect of Ag metal and to the promoted charge carriers separation and transportation. Bai *et al.*[243] reported the core–shell plasmonic Ag@CN nanocomposites via a reflux treating method that exhibited exceptional photoactivity for methylene blue degradation and H_2 evolution. Thus, due to the SPR effect of noble-metal nanoparticles, solar energy can be utilized more efficiently and the materials will show exceptional photocatalytic performance.

5.4. CN/Graphene Heterojunctions

Graphene has been considered as a promising material for coupling with semiconductors owing to its numerous properties such as, acting as electrons acceptor and transport channels, supporting materials, cocatalysts and photocatalysts.[244] In addition, graphene promotes the adsorption and surface active sites. Graphene has been categorized as a zero band gap semiconductor with exceptional thermal, mechanical and optical characteristics that ensure the electron transport and high mobility.[245] The VB orbitals of sp^2 hybridized C-atoms in graphene are made of three planar δ orbitals separated by an angle of 120° and a 2p orbital which lies perpendicular to the plane of graphene. Thus, the graphene with interconnected hexagons of C-atoms has been considered as the thinnest material in the world.[246] The unique characteristics of graphene motivated researchers to fabricate graphene/CN 2D-2D heterojunctions via hybridization. In such heterojunctions, the close contact between two semiconductors facilitate effective charge transfer across the interface junction and inhibits the charge carrier's recombination, because graphene sheet works as the conductive channels.[247] For instance, Xiang *et al.*[248] synthesized graphene@CN heterojunctions via an impregnation chemically reduction method. TEM images (Figure 21(a, b)) show that CN is successfully modified with graphene. This exceptional stacking structure was favorable for transfer of electron from CN to the graphene. Hence, the resultant nanocomposites exhibited exceptional photoactivity for H_2 production. Further, the surface area of graphene/CN nanocomposites was greatly enlarged with the increase in amount of graphene coupled. The graphene acted as a support for the CN photocatalyst. When pt was loaded on the nanocomposites, and under visible-light irradiations, the excited electrons of CN were migrated to the graphene, which then collected on the cocatalyst Pt and reduced the H^+ to evolve H_2 as shown in Figure 21(c). Thus, the photoactivity for H_2 evolution was much significant compared to the graphene/CN composite and pure CN. This work signified an important strategy for enhancing the photoactivity of CN by employing graphene as a support material and pt as a co-catalyst.

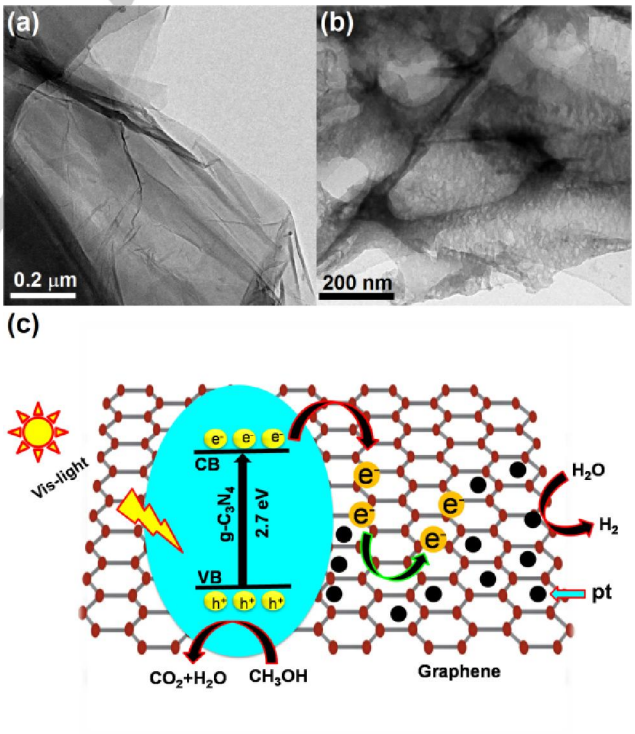

Figure 21.TEM micrographs (a) of graphene, and (b) of graphene/CN nanocomposite. Schematic for charge carrier's transport in graphene/CN nanocomposites (c). Reproduced from ref.[248] with permission. Copyright 2011, The American Chemical Society.

Beside the graphene/CN binary hybrids, graphene/CN based ternary hybrids also received much attention. For

example, Liu *et al*.[249] incorporated Fe(III) into graphene and the CN composite. The introduction of Fe(III) into graphene made Fe(III) smaller in size with uniform distribution, that was accredited to the synergistic effect between graphene and the Fe(III). The amount optimized Fe(III)/graphene/CNnanocomposite showed exceptional visible-light absorption, and enhanced charge carrier's separation owing to the presence of graphene as an electron transport channel. Further, the ternary nanocomposites exhibited significant photoactivity for degradation of methyl orange (Figure 22(a)) compared to the bare CN. The schematic mechanism (Figure 22(b)) revealed that the visible-light induced electrons of CN would transfer to graphene and react with the adsorbed O_2 to generate $\bullet O_2^-$ radicals.

Notably, the electrons in CB of CN (−1.23 V) cannot energetically transfer to Fe(III) (0.77V), because of the large difference in their energy levels. Further, the excited VB electrons of CN are thermodynamically favorable to be transferred to the Fe(III) and form Fe(II). The photoinduced VB holes would participate in pollutants degradation. Above all, important achievements can pave the approach for fabricating CN-based heterojunctions as highly proficient photocatalysts. The visible-light absorption and charge carrier's separation can be improved by effectively tailoring the structure of the photocatalysts.

5.5. CN/CNTs Heterojunctions

Recently, marvelous attention has been given to the coupling of carbonaceous nanomaterials such as graphene and carbon nanotubes (CNTs) with CN (Figure 22(c, d)) due to their superior electrical conductivity, light-harvesting properties, high specific surface areas, high electron storage capacity, and excellent reduction ability [250]. Coupling of graphene and CNTs prolongs the life time of photoinduced charge carrier's of the CN by accepting the photo-induced electrons of CN and acts as cocatalysts for reduction reactions.

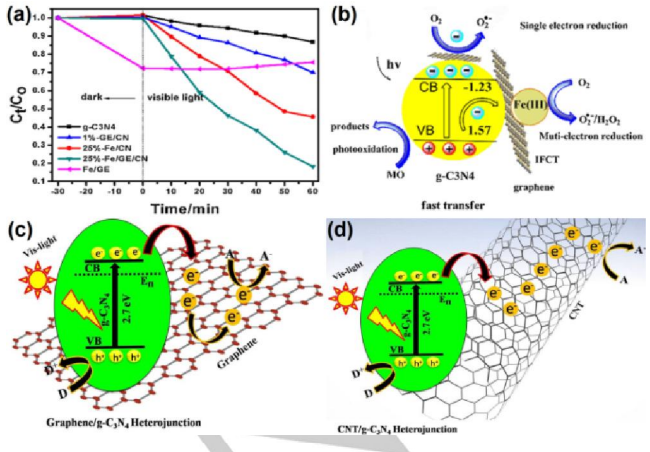

Figure 22. Visible-light catalytic performance for degradation of methyl orange (a), Schematic for charge transport and the photocatalytic processes over the Fe(III) incorporated graphene−CN ternary composites (b). Reproduced from ref.[249] with permission. Copyright 2016, Elsevier. Schematic of Graphene/CN composites (c) and CNT/CN heterojunctions (d).

To synthesize CN-based based highly capable photocatalysts, several important principles should be fulfilled: (1) enhancing charge separation and transfer to hinder the rate of recombination, (2) enhancing solar energy utilization, and (3) improving the photocatalysts stability for long term reactions. In general, the construction of heterostructures offers diverse promising virtues: (1) visible-light utilization can be enhanced, (2) redox overpotential at active sites can be lowered by employing cocatalysts and the stability can be improved through proper surface passivation. Generally, under solar irradiation, the electrons excited to the CN CB would relax to the VB in extremely short time losing energy as heat. Consequently, the fast charge recombination is enormously adverse for photocatalytic reactions. However, when a suitable band gap semiconductor is coupled with CN, the enhanced charge carrier's separation can be achieved through systematic charge transfer at interfacial contact of heterojunctions. As, CN exhibits energy band gap of about 2.7 eV, with its CB level placed at −1.3 eV and VB level at +1.4 eV, versus the NHE at pH 0.[70] Thus, CN can be utilized in efficient photocatalytic reactions. A variety of CN-based heterojunctions are discussed below.

The fabrication of the carbon nanodot/CN nanocomposites not only improved the catalytic H_2 production ability of CN but also exhibited a double-electron H_2 generation mechanism due to the catalytic H_2O_2 splitting [251]. Ma *et al*.[252] synthesized CNT/CN nanosheet 3D porous composites for O_2 evolution reactions. The resultant nanocomposites displayed enhanced catalytic O_2 evolution activity and strong durability which was the best among all the reported non-metal catalysts. Song *et al*.[253] reported the CNT/CN composites for highly stable water splitting to evolve H_2. The TEM image of CNT/CN composite (Figure 23(a)) revealed that CN existed as well separated layered structures rather than the overlapped ones. The HRTEM image (Figure 23(b)) showed that electrostatic contact between the CN conjugated plane and the π bonded electrons of CNTs tightly adsorbed CNTs onto the CN surface. The amorphicism of CNT@CN heterojunction was further investigated by the measurement of selected area electron diffraction patterns (Figure 23(c)). The resultant nanocomposites exhibited significant photoactivity for H_2 production, which was accredited to the synergistic-effect between CNTs and CN. The maximum H_2 yield (6548.4 μmol g^{-1}) by the 12-mg/L CNT/CN (CG12) photocatalyst was 138.7-time greater compared to the bare CN (47.2 μmol g^{-1}) under visible-light irradiations for 10 h. Notably, the apparent quantum efficiency of the CG12 heterojunction for H_2 production after visible-light irradiations for 50 h was up to 37.9%, indicating high stability for H_2O splitting. It was confirmed that H_2O_2 is the major intermediate involved in the photo-catalytic H_2 generation reactions as shown in Figure 23(d). The CNTs strongly attracted the excited electrons of CNdue to its excellent conductibility, and then quickly transferred to the surface for catalytic reactions. Consequently, charge separation and the reduction ability of photo-excited electrons were greatly improved.

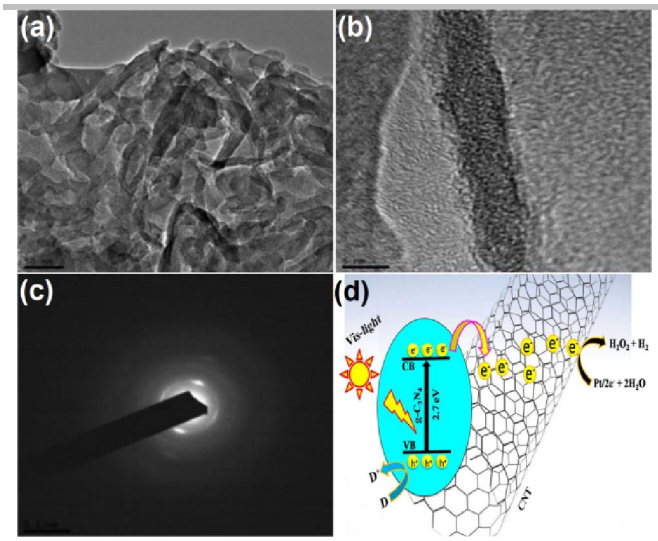

Figure 23.TEM micrograph (a), HRTEM micrograph (b), and the selected area electron diffraction patterns (c), of 12-mg/L CNT/CN (CG12) photocatalyst. Schematic for photo-catalytic H_2 generation over CNTs/CN nanocomposites (d). Reproduced from ref.[253] with permission. Copyright 2018, Wiley-VCH.

Recently, the multi-walled carbon nanotubes (MWNTs) have received tremendous attention owing to their smart structural and electrical properties. Further, MWNTs exhibits superior electron conducting capacity. Thus, they have prospective applications in environmental photocatalysis.[254] For instance; Ge *et al.*[255] synthesized multi-walled carbon nanotubes (MWNTs)/CN composites by a facile heating technique for H_2 production from methanol aqueous solution with the aid of cocatalyst Pt. The TEM micrograph of MWNTs/CN nanocomposite (Figure 24(a)) revealed that the MWNTs with different lengths and diameters were bound with the CN, which confirmed the formation of interface junctions between the CN and carbon nanotubes. The TEM image of MWNTs/CN composite (Figure 24(b)) after photocatalytic reaction clearly showed Pt particles dispersed on the MWNTs surface. Hence, it was confirmed that the CN excited electrons were transferred to the MWNTs surface which then reduced Pt species. The amount optimized MWNTs/CN heterojunction exhibited greatly improved photoactivity for H_2 production with a rate of 7.58 µmol h^{-1} (Figure 24(c)), about 3.7-fold enhanced compared to the amount evolved by CN upon visible-light irradiations. The H_2 evolution mechanism over the MWNTs/CN composites (Figure 24(d)) revealed that the MWNTs plays an important role in the enhancement of charge separation and the photo-activity for H_2 production.

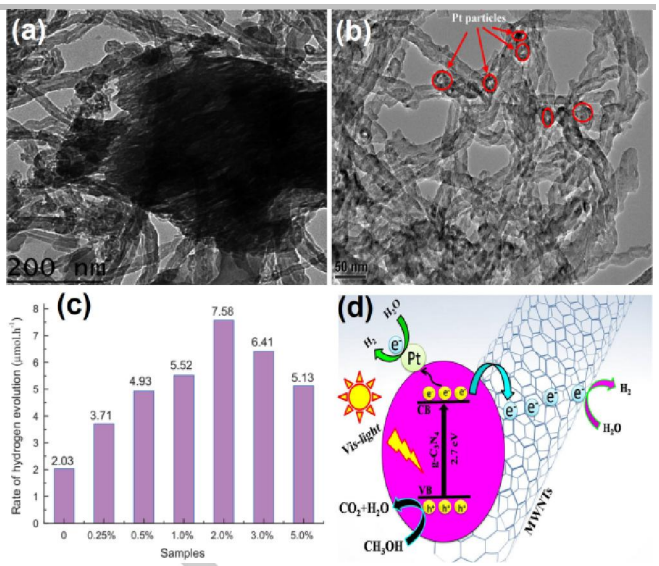

Figure 24. TEM micrographs of MWNTs/CN composite (a) before photocatalytic reaction, and (b) after photocatalytic reaction. Photo-catalytic H_2 generation over CN and MWNTs/CN heterojunctions (c), Schematic for charge transfer mechanism and the photocatalytic processes in MWNTs/CN composites (d). Reproduced from ref.[255] with permission. Copyright 2012, Elsevier.

Above all, it is confirmed that the MWCNTs/CN all-organic metal free composites could greatly improve the visible-light photocatalytic H_2 production with or without the addition of cocatalysts.

5.6. CN/MOFs Heterojunctions

Metal organic framework (MOF) is a new class of highly porous inorganic-organic complex hybrid semiconductor, in which the metal-oxide clusters or metal ions are connected with organic linkers and comprise a three dimensional structural motif. The function of organic linker's is to serve as receivers for harvesting solar light and trigger the metal ions/metal-oxide clusters to behave like semiconductors. Usually, MOFs possesses good stability, tunable metrics, and potentially small band gaps. Distinct from other semiconductors, MOFs exhibit huge specific surface areas, controllable size of the pores and tunable light harvesting properties. Among various MOFs, MIL a crystalline titanium dicarboxylate MOF exhibit high porosity, thermal stability and photochemical properties, due to the huge specific surface area and accessible pore diameters. In MIL type, high density immobilized Ti sites are present within the porous structure. By incorporating various organic ligands, its photocatalytic performance could be greatly improved. In recent years, considerable attention has been paid to couple MOFs with CN due to their unique structures, species diversities, controllable pore size, and huge specific surface areas.[256] For example, Wang *et al.*[181] fabricated a novel UiO-66/CN composite photocatalyst via the hybridization of Zr-MOF (UiO-66) and CN using a thermal calcination technique. The resultant composite exhibited enhanced photocatalytic hydrogen evolution activity with an optimal production rate of 14110 µmol $h^{-1}g^{-1}$, which was about 17-fold compared to that of the bare CN (800 µmol $h^{-1}g^{-1}$). This enhancement in the photocatalytic performance was due to the efficient interfacial migration of photo-excited charge from CN to the UiO-66 MOF. In addition, the high amount of CN directed the UiO-66/CN composite with a quasi-polymeric nature. In another report, Du *et al.*[257] fabricated

MIL-100(Fe)/CN composite via ball-milling technique by mixing the MIL-100(Fe) and CN components, followed by annealing at 300 ^{o}C for 2 h. XRD patterns (Figure25(a)) clearly shows the characteristic peaks of MIL-100(Fe) in the composite confirming the formation heterojunction. The TEM micrograph of the composite (Figure25(b)) revealed that the CN nanosheets were closely adhered onto the MIL-100(Fe). The visible light absorption characteristic of the composite was remarkably enhanced as could be observed from Figure25(c). The photocatalytic Cr(VI) reduction activity under visible light irradiations with increasing the MIL-100(Fe) amount was drastically improved (Figure25(d)). This enhancement in the Cr(VI) reduction ability was attributed to the promoted charge separation and extended visible light absorption. They demonstrated that under visible light irradiations, the excited electrons in the CB of CN (-1.12 V) were transferred to the CB of MIL-100(Fe) (-0.11 V), and hence electrons in the CB of MIL-100(Fe) facilitated the Cr(VI) reduction to Cr(III) as illustrated in schematic (Figure25(f)). The holes generated in the VB of CN (1.84 V) and MIL-100(Fe) (2.52 V) were utilized by the scavenger species like oxalic acid, citric acid and diclofenac sodium. Meanwhile, the accelerated electron-hole pairs separation lead to the highly efficient reduction of Cr(VI) (Figure25(e)). Thus, based on the abundant characteristics of MOF, it could be regarded as an ideal material for combining with CN so as to achieve high photocatalytic performance under visible light.

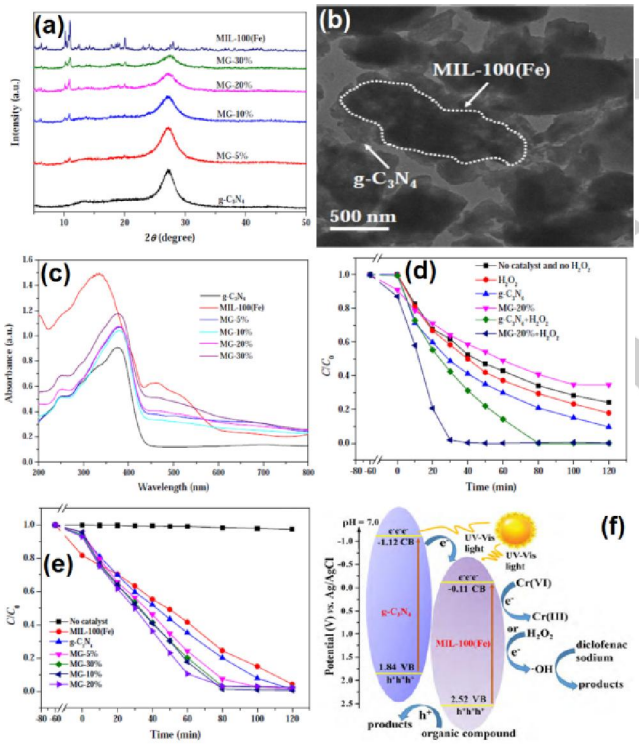

Figure25.(a) XRD patterns of CN, MIL-100(Fe) and MG-x composites (where, M represent MOF and G represent CN and x shows 5, 10, 20, and 30 %age composition of MIL-100(Fe) in the composites), (b) TEM image of MG-20% composite, (c) UV-vis absorption spectra of CN, MIL-100(Fe) and MG-x composites, (d) photocatalytic activity for Cr(VI) reduction and (e) photocatalytic degradation of diclofenac sodium under different control conditions over the CN, MIL-100(Fe) and MG-x composites, (f) charge transfer and the photocatalytic reduction mechanism of Cr(VI) and diclofenac sodium degradation over MG-20% composite. Adapted with permission from reference [257] copyright (2018) Elsevier.

5.7. CN/LDHs Heterojunctions

Layered double hydroxides (LDHs) (or hydrotalcite-like compounds) are a class of two-dimensional (2D) compounds comprised of the positively charged brucite-like layers containing charge compensating anions and solvation molecules within the interlayer region. These compounds are generally represented by the formula $[M_{1-x}^{2+}\ Mx^{3+}\ (OH)_2(A^{n-})_{x/n}]^{x+}.mH_2O$.[258] The LDHs include fractions of divalent metal cations like Zn^{2+}, Ni^{2+}, Mg^{2+} and Cu^{2+}, which are octahedrally coordinated via hydroxyl groups and have been substituted isomorphously by the trivalent metal cations like Fe^{3+}, Ga^{3+} and Al^{3+} producing positively charged layers. The value of "*x*" generally falls in the range of 0.20-0.33, and represents the mole fraction (M^{2+}) in the metallic ions. The "A^{n-}" denotes interlayer balcony anions such as Cl^-, SO_4^{2-}, CO_3^{2-}, NO^{3-}. LDHs have been regarded as the promising materials for a broad range of applications in energy conversion and environmental remediation.[259] It has been discovered that due to some useful physicochemical properties such as large specific surface areas, compositional flexibilities and positive surface charges, LDHs have been favorable for CO_2 adsorption. So far, the CN photocatalyst exhibit small surface area and limited number of active sites, owing to its stacked structure, it hinders the adsorption of CO_2. Thus, to improve its surface adsorption ability, an important strategy is to construct heterojunctions of LDHs and CN. For example, Tonda et al.[260] fabricated CN/NiAl-LDH 2D/2D heterojunctions via one-step in situ hydrothermal route (Figure 26(a)).

The XRD patterns of CN/NiAl-LDH composite (Figure26(b)) revealed the diffraction peaks of both the components and the intensity of NiAl-LDH peaks gradually enhanced with the increase in its content. A blue shift in the absorption spectra of CN/NiAl-LDH composite (Figure26(c)) was observed compared to the bare CN, which was due to the strong interaction between the two components. The TEM image (Figure26(d)) revealed that during in situ growth, both the CN and NiAl-LDH nanosheets strongly interacted with each other owing to the opposite surface charges and lead to avoid the restacking of NiAl-LDH in the composites. The HR-TEM micrograph (Figure26(e)) revealed lattice fringes of both CN (002) and NiAl-LDH (012) with inter planar distance of 0.32 and 0.26 nm, respectively. This composite showed outstanding performance for visible-light catalytic CO_2 conversion to CO (Figure26(f)) compared to that of the bare CN and NiAl-LDH components. The significant activity was attributed to the exceptional interfacial contact between the two components that remarkably suppressed the charge recombination. Figure 26(g) revealed that under visible light irradiations, both the components were excited to produce electron-hole pairs. The excited electrons in the CB of CN were transferred to the CB of NiAl-LDH, and the holes produced in the VB of NiAl-LDH transferred to the VB of CN due to the proper bands alignment. Hence, CO2 reduction was promoted on the surface of NiAl-LDH due to the significant charge separation. Thus, the construction of LDHs/CN heterojunctions is an important strategy to promote the charge carriers separation, thereby improving the redox reactions on the photocatalyst surfaces.

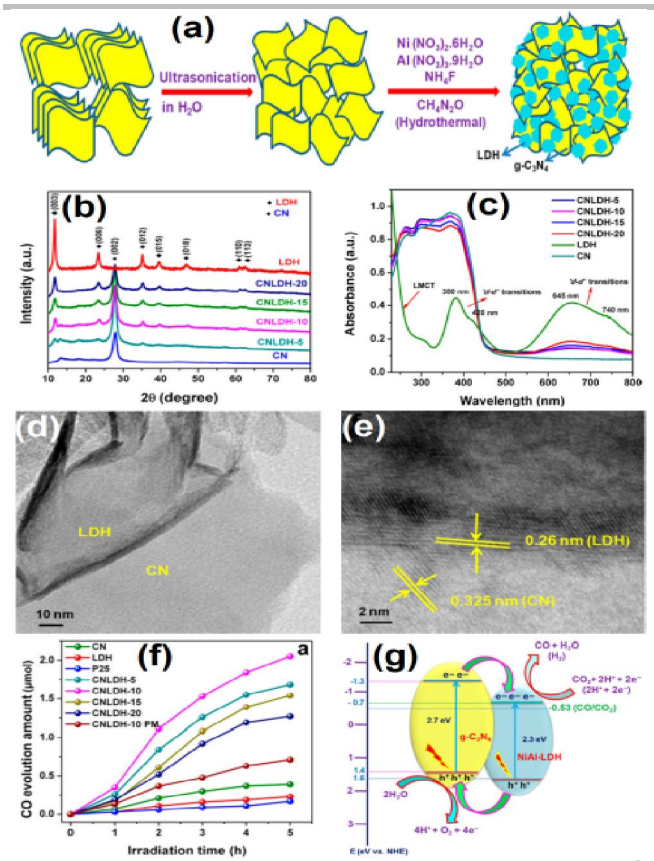

Figure 26. Schematic of the preparation of CN/NiAl-LDH composites (a), XRD patterns (b) and UV-vis absorption spectra (c) of CN, NiAl-LDH, and CN/NiAl-LDH composites, TEM image (d) and HRTEM image (e) of CN/NiAl-LDH composite, photocatalytic CO_2 conversion to CO over the CN, NiAl-LDH, and CN/NiAl-LDH composites (f), and proposed charge transfer mechanism and photo-reduction of CO_2 over the CN/NiAl-LDH composite (g). Adapted with permission from reference[260] Copyright 2018, ACS.

6.Applications of CN-based Heterojunctions

In recent few years, CN-based heterojunctions have been widely utilized in H_2O splitting, CO_2 reduction, and pollutants oxidation reactions. In this section, applications of the CN-based heterojunctions in photocatalysis are briefly summarized.

6.1 Photocatalytic CO_2 Conversion

The increase in atmospheric CO_2 concentration due to the rapid collapse of fossil energy fuels such as the coal, petroleum, and natural gas raised serious alarms about the continuous dependence on the exploit of these fossil fuels for energy production and various chemicals [261]. Mimicking the natural photosynthesis phenomenon by transforming the solar energy into chemical fuels is a prospective method for solving both of the energy crisis and greenhouse effect [262]. In this phenomenon, the photocatalysts (semiconductors) convert CO_2 into the hydrocarbon fuels via the solar energy utilization[252, 263] as described in Figure 27.

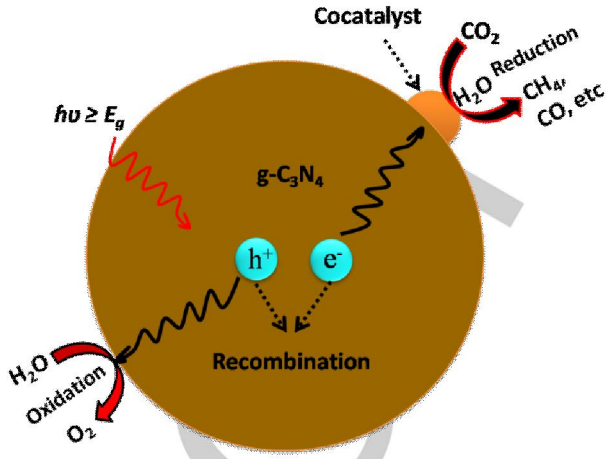

Figure 27. The photo-catalytically conversion of CO_2 on semiconductor CN.

The CO_2 photo-reduction involve multi-electrons transfer reactions and the redox potential values for various products like, HCOOH, CO, HCHO, CH_3COOH, and CH_4 versus the reversible H_2 electrode (RHE) are provided below [264].

$CO_2 + 2H^+ + 2e^- \rightarrow$ HCOOH (E_{redox} = -0.20V) (1)

$CO_2 + 2H^+ + 2e^- \rightarrow$ CO + H_2O (E_{redox} = -0.12V) (2)

$CO_2 + 4H^+ + 4e^- \rightarrow$ HCHO + H_2O (E_{redox} = -0.07V) (3)

$CO_2 + 6H^+ + 6e^- \rightarrow$ CH_3OH + H_2O (E_{redox} = +0.03V) (4)

$CO_2 + 8H^+ + 8e^- \rightarrow$ CH_4 + $2H_2O$ (E_{redox} = +0.17V) (5)

Owing to the highly stable chemical structure of CO_2, it's very tough to reduce it at room temperature. Because of this attribute, the photo-conversion of CO_2 into chemical fuels is an immense challenge for research communities. Several other features that influence the photo-conversion of CO_2 includes efficient charge separation, band gap alignment, kinetics of the electrons transferring to the CO_2, basicity of the catalysts, and adsorption of CO_2 molecules [265]. Nanostructured CN photo-catalysts had been extensively used for CO_2 conversion owing to their high stability, proper CB position and narrow band gap. However, their photocatalytic efficiency was extremely low. Thus, many approaches were developed to improve the photo-catalytic efficiency of CN for efficient CO_2 conversion.[119, 266] Lang *et al.*[267] reported Pd/CN photocatalysts for CO_2 reduction to CO and CH_4. The CO_2 conversion over Pd/CN photocatalysts was 61.4%, with CO productivity (4.3 μmol g^{-1} h^{-1}), and CH_4 (0.45 μmol g^{-1} h^{-1}) confirming the existence of highly reactive adsorption and activation sites of CO_2. Yu *et al.*[268] synthesized Pt/CN photocatalysts for CO_2 conversion to hydrocarbons fuel. The photocatalysts showed high activity for CO_2 conversion and more importantly, selectivity of the reactions product was effected

by the modified Pt. Han *et al*.[269] reported CeO_2/CN heterojunctions that displayed high photo-catalytic activity for selective CO_2 conversion to CH_4 with production of 4.79 mmol g^{-1} h^{-1}. The CO_2 molecules adsorption on the catalysts surfaces is also a vital step in CO_2 photo-reduction. Hence, to improve the surface adsorption capability of CN for CO_2, various approaches have been accomplished. Huang *et al*.[270] modified the CN material with amine-groups. Consequently, the CO_2 adsorption capability for CN was significantly improved, which lead to the superior photocatalytic CO_2 conversion activity.

6.2 Photocatalytic Water Splitting

The photocatalytic H_2O splitting to evolve H_2 over semiconductor photocatalysts with the aid of solar energy is a great challenge for researchers to produce zero emission fuel. H_2 has been regarded as a promising chemical fuel alternative to fossil fuels, owing to its high energy density (i.e. 140 MJ kg^{-1}) on the gravimetric base in comparison to that of the hydrocarbon fuels which approximately falls in the range of 40-50 MJ kg^{-1}.[271] Thermodynamically, for efficient H_2 evolution, the CB potential of the semiconductors would be highly negative than the standard reduction potential value of H_2O (i.e. 0V versus NHE). Similarly, for efficient O_2 evolution, the VB potential of semiconductors would be highly positive than the standard oxidation potential value of H_2O (i.e. 1.23V versus NHE) [272]. The redox potentials for overall H_2O splitting reaction at pH = 7, gives an overall ΔG = +237.2 KJ/mol[273] and the mechanism is depicted in Figure 28.

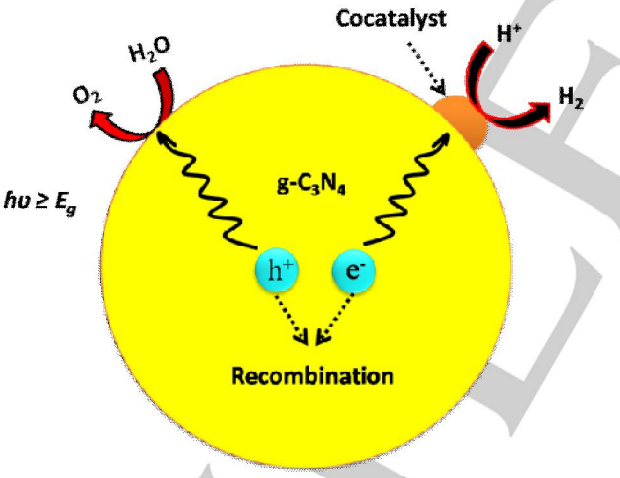

Figure 28. The photocatalytic reactions for overall H_2O splitting on CN.

$$2H^+ + 2e^- \rightarrow H_2 \quad (1)$$

$$H_2O + 2(h^+) \rightarrow 1/2O_2 + 2H^+ \quad (2)$$

$$H_2O \rightarrow 1/2O_2 + H_2 \quad (\Delta G = +237.2\ kJ/mol)$$

The single component CN displays weak visible-light catalytic activity for H_2O reduction to produce H_2. However, the modification of CN with metal cocatalysts, non-metals, holes (h^+) scavenger and semiconductors could greatly improve its performance for photocatalytic H_2 production. The CN based numerous photocatalysts have been constructed for enhance photocatalytic H_2O splitting to evolve H_2.[268, 274] Ran *et al*.[275] reported P-doped CN that exhibited exceptional visible light activity for H_2 evolution with amount of 1596 mmol g^{-1} h^{-1} (QE = 3.56 %) at wavelength 420 nm. The superior performance of P-doped CN was accredited to the macroporous analogues raised from the empty mid gap states (i.e. -0.16V versus NHE) that significantly extended its optical absorption up to 557 nm. The phosphorus doping also improved the CN surface-area to 123 m^2 g^{-1} and further reduced the surface charge migration length to 8 nm. Zhang *et al*.[105] reported Pt loaded hierarchical CN nanospheres that exhibited enhanced photo-activity for H_2 generation with quantum efficiency of 9.6% at 420 nm, that was superior compared to that of the bare CN nanosheets (3.75%). Shen *et al*.[276] reported TiO_2/CN nanocomposites that displayed superior visible-light activity for H_2 production (556 µmol g^{-1}) in comparison to the bare CN (108 µmol g^{-1}). Hou *et al*.[277] reported MoS_2/CN composites via the thermal deposition method that showed high photo-catalytic performance for H_2 generation with quantum efficiency of 2.1% at 420 nm. Recently, Xiang *et al*.[248] reported the graphene@CN composites that showed enhanced catalytic activity for H_2 evolution (451 µmol h^{-1} g^{-1}), about 3-time higher compared to that of the bare CN. In such composite, graphene performed as the electron acceptor and efficiently suppressed charge carrier's recombination.

6.3 Photocatalytic Degradation of Pollutants

Due to the rapid growth of industrialization and human population, a variety of hazardous pollutants are released into the surroundings which not only raised the serious environmental problems but also posed a threat to the sustainable development of human race. Even low concentration of environmental pollutants posed serious threats to human beings and the animals health, and their degradation is a great challenge for scientific researchers. Among various techniques, semiconductor photocatalysis has been proved to be a promising technique due to the low cost and high efficiency.[278] Polymeric CN photocatalyst showed promising applications in photocatalysis for pollutant degradation. Due the suitable valence and CB levels of CN, the photo-induced holes display reasonably high oxidation capability and directly convert organic pollutants to intermediate products. Similarly, the excited electrons of CN could reduce the O_2 molecules to generate the $\bullet O_2^-$ radicals which on reaction with electrons and H^+ can also generate the •OH as depicted in Figure 29.

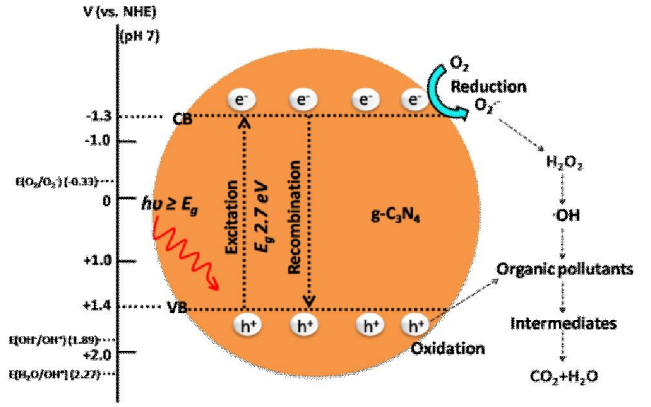

Figure 29. The produced highly reactive radicals during photocatalytic degradation of pollutants on CN.

$$h^+_{VB} + Org \rightarrow Org^+ \quad (1)$$

$$O_2 + e^-_{CB} \rightarrow \bullet O_2^- \quad (2)$$

$$2e^- + 2H^+ + \bullet O_2^- \rightarrow \bullet OH + OH^- \quad (3)$$

The highly reactive species such as h^+, •OH, and $\bullet O_2^-$ produced over CN can oxidize a variety of pollutants into inorganic minerals (CO_2 and H_2O).[279] Though, the photo-catalytic activity of single component CN is still inadequate for practical applications. Various approaches have been developed for modification of the CN photocatalyst so as to promote its catalytic performance for efficient pollutant degradation. For instance, Bu *et al*.[280] reported Ag modified mesoporous CN photocatalysts that showed superior visible-light activity for rhodamine B dye degradation compared to the bare CN. The CN adsorption capacity was also enhanced by modification with Ag. Jiang *et al*.[281] reported the CN/CdS nanocomposites that exhibited significantly improved visible-light catalytic activity for methylene blue degradation compared to the bare CN and CdS. The improved activity of the nanocomposites was accredited to the synergistic effect between the CN and CdS components, which greatly enhanced the photogenerated charge carrier's separation efficiency, and effectively inhibited the photo-corrosion. In another work, Li *et al*.[282] reported the synthesis of CN/rGO composite photocatalysts that exhibited exceptional visible-light catalytic activities for RhB and 4-nitrophenol degradation. The visible-light photoactivities of the CN/rGO composites were strongly influenced by varying the amount of rGO. The amount optimized composite exhibited 3.0 and 2.7 times enhanced photoactivity for RhB and 4-nitrophenol degradation respectively, in comparison to the bare CN. This was accredited to the extended visible-light response, improved electron transportation and electronic conductivity. You *et al*.[283] reported the synthesis of S and O co-doped CN for visible-light photo-degradation of RhB. The degradation rate of S and O co-doped CN was 6-fold improved in comparison to the bare CN. The co-doping of S and O in CN resulted in a strongly delocalized HOMO and LOMO, which obviously improved the active sites and enhanced charge separation. Thus, the enhanced charge separation of CN is the key factor for proficient photocatalytic degradation of pollutants.

7. Conclusions and perspectives

The metal-free polymeric CN photocatalyst offer unique optical, electronic, and textural properties which can be altered for tailoring the solar energy utilization to produce chemical fuel and for environmental remediation. However, compared to the inorganic semiconductors, polymeric CN exhibits several shortfalls such as small surface area, limited solar energy utilization, high exciton binding energy, and fastcharge recombination rate. Further, the low crystallinity and surface defects greatly limit its practical applications in photocatalysis. Thus, it is highly urgent to develop diverse synthetic strategies to improve the crystal-structure, nano-structure, electronicstructure, and hetero-structure of CN with enhanced solar energy harvesting, high quantum yield, better charge carrier's separation and transportation, high stability and excellent photocatalytic efficiency. A variety of CN nanostructure materials have been synthesized via soft and hard template methods that exhibited excellent photocatlytic activityin comparison to the bulk CN due to their surface rich properties, improved charge carrier's separation, optimal electronic structure, and promoted mass diffusion during photocatalytic processes. Further, to enhance charge separation and the visible-light photoactivities of CN, fabricating heterojunctions with other semiconductors having energetically matched energy band structures or metals as cocatalysts are more beneficial. In this review, we have categorized CN-based heterojunction into several classes, including Type-II, Z-scheme, metal/CN Schottky junctions, noble metal/CN, graphene/CN, carbon nanotubes (CNTs)/CN, metal-organic frameworks (MOFs)/CN, layered double hydroxides **(**LDH)/CN heterojunctions. Among the aforementioned heterojunctions, CN-based Type-II and Z-scheme heterojunctions have been proved to have excellent applications in photocatalysis for H_2O splitting, CO_2 conversion and pollutants degradation. Hence, the applications of CN in photocatalysis could be extensively enriched by rational design of the CN-based heterostructures. Although, tremendous efforts have been dedicated to modify the CN photocatalyst in order to optimize its photocatalytic performance, but further developments are notably required to utilize the CN in efficient photocatalysis. Since, the CN-based materials designed in those works still suffered from drawbacks such as low stability and apparaent quantum efficiency, and are faraway from industrial requirements. Until now, several main challenges facing CN in efficient photocatalysis should be resolved by making it practical for commercial scale use in the future. (1) To develop new approaches for fabrication of CN nanoarchitectures with exceptional specific surface areas and more active sites, (2) to improve the solar energy utilization capability of CN to mimic the natural photosynthesis in plants, (3) to significantly enhance the charge separation and photo-redox properties of CN to attain high quantum efficiency by designing CN-based rational heterostructures. Additionally, the photocatalytic reaction mechanisms of CO_2 conversion, water splitting and pollutant degradation for CN-based photocatalysts should be clearly affirmed. There has been unlimited scope of

opportunities and challenges facing the CN-based research in the sustainable field of photocatalysis for solar fuel generation and environmental purification in future, which will require huge efforts from worldwide scientific researchers. We hope this review would serve as a roadmap for the future challenges in the rational design of CN-based photocatalysts.

Conflicts of interest

There are no conflicts to declare.

Acknowledgments The work was financially supported by the Ministry of Science and Technology of China (Grant No. 2018YFA0702100), the National Natural Science Foundation of China (Grant No. 11874169).

Keywords: CN • fundamentals • nanostructures design • heterojunctions • applications

References

[1] a) D. Kim, K. K. Sakimoto, D. Hong, P. Yang, *Angew. Chem., Int. Ed.* **2015**, *54*, 3259-3266;b) J. Safaei, N. A. Mohamed, M. F. Mohamad Noh, M. F. Soh, N. A. Ludin, M. A. Ibrahim, W. N. Roslam Wan Isahak, M. A. Mat Teridi, *J. Mater. Chem. A* **2018**, *6*, 22346-22380;c) J. Safaei, H. Ullah, N. A. Mohamed, M. F. Mohamad Noh, M. F. Soh, A. A. Tahir, N. Ahmad Ludin, M. A. Ibrahim, W. N. R. Wan Isahak, M. A. Mat Teridi, *Appl. Catal. B* **2018**, *234*, 296-310.

[2] Y. Gong, J. Wang, Z. Wei, P. Zhang, H. Li, Y. Wang, *ChemSusChem* **2014**, *7*, 2303-2309.

[3] C. George, M. Ammann, B. D'Anna, D. J. Donaldson, S. A. Nizkorodov, *Chem. Rev.* **2015**, *115*, 4218-4258.

[4] a) A. Fujishima, K. Honda, *Nature* **1972**, *238*, 37-38;b) H. Zhang, G. Liu, L. Shi, H. Liu, T. Wang, J. Ye, *Nano Energy* **2016**, *22*, 149-168;c) X. Y. Meng, D. Y. Liu, G. W. Qin, *Energy Environ. Sci.* **2018**, *11*, 692-701;d) M. G. Kibria, Z. Mi, *J. Mater. Chem. A* **2016**, *4*, 2801-2820;e) S. Liu, Z.-R. Tang, Y. Sun, J. C. Colmenares, Y.-J. Xu, *Chem. Soc. Rev.* **2015**, *44*, 5053-5075.

[5] a) K. Maeda, K. Teramura, D. Lu, T. Takata, N. Saito, Y. Inoue, K. Domen, *Nature* **2006**, *440*, 295-295;b) J. Willkomm, K. L. Orchard, A. Reynal, E. Pastor, J. R. Durrant, E. Reisner, *Chem. Soc. Rev.* **2016**, *45*, 9-23;c) S. J. A. Moniz, S. A. Shevlin, D. J. Martin, Z.-X. Guo, J. Tang, *Energy Environ. Sci.* **2015**, *8*, 731-759.

[6] a) J. L. White, M. F. Baruch, J. E. Pander, Y. Hu, I. C. Fortmeyer, J. E. Park, T. Zhang, K. Liao, J. Gu, Y. Yan, T. W. Shaw, E. Abelev, A. B. Bocarsly, *Chem. Rev.* **2015**, *115*, 12888-12935;b) H.-Q. Xu, J. Hu, D. Wang, Z. Li, Q. Zhang, Y. Luo, S.-H. Yu, H.-L. Jiang, *J. Am. Chem. Soc.* **2015**, *137*, 13440-13443;c) H. Takeda, K. Ohashi, A. Sekine, O. Ishitani, *J. Am. Chem. Soc.* **2016**, *138*, 4354-4357.

[7] A. Fujishima, K. Honda, *Bull. Chem. Soc. Jpn.* **1971**, *44*, 1148-1150.

[8] T. Inoue, A. Fujishima, S. Konishi, K. Honda, *Nature* **1979**, *277*, 637-638.

[9] a) T. Zhang, W. Lin, *Chem. Soc. Rev.* **2014**, *43*, 5982-5993;b) L. Wang, T. Sasaki, *Chem. Rev.* **2014**, *114*, 9455-9486;c) S. Bai, J. Jiang, Q. Zhang, Y. Xiong, *Chem. Soc. Rev.* **2015**, *44*, 2893-2939;d) D. J. Martin, G. Liu, S. J. A. Moniz, Y. Bi, A. M. Beale, J. Ye, J. Tang, *Chem. Soc. Rev.* **2015**, *44*, 7808-7828;e) H. Wang, L. Zhang, Z. Chen, J. Hu, S. Li, Z. Wang, J. Liu, X. Wang, *Chem. Soc. Rev.* **2014**, *43*, 5234-5244;f) C. An, S. Wang, Y. Sun, Q. Zhang, J. Zhang, C. Wang, J. Fang, *J. Mater. Chem. A* **2016**, *4*, 4336-4352.

[10] a) J. Yu, J. Low, W. Xiao, P. Zhou, M. Jaroniec, *J. Am. Chem. Soc.* **2014**, *136*, 8839-8842;b) Y. Ma, X. Wang, Y. Jia, X. Chen, H. Han, C. Li, *Chem. Rev.* **2014**, *114*, 9987-10043;c) G. Liu, H. G. Yang, J. Pan, Y. Q. Yang, G. Q. Lu, H.-M. Cheng, *Chem. Rev.* **2014**, *114*, 9559-9612.

[11] a) S. Wu, H. Cao, S. Yin, X. Liu, X. Zhang, *J. Phys. Chem. C* **2009**, *113*, 17893-17898;b) S. Liu, G. Huang, J. Yu, T. W. Ng, H. Y. Yip, P. K. Wong, *ACS Appl. Mater. Interfaces* **2014**, *6*, 2407-2414.

[12] Z. Li, Y. Qu, K. Hu, M. Humayun, S. Chen, L. Jing, *Appl. Catal. B* **2017**, *203*, 355-362.

[13] a) X. Bai, L. Wang, R. Zong, Y. Lv, Y. Sun, Y. Zhu, *Langmuir* **2013**, *29*, 3097-3105;b) X. Wang, M. Liao, Y. Zhong, J. Y. Zheng, W. Tian, T. Zhai, C. Zhi, Y. Ma, J. Yao, Y. Bando, D. Golberg, *Adv. Mater.* **2012**, *24*, 3421-3425.

[14] a) B. Kiss, T. D. Manning, D. Hesp, C. Didier, A. Taylor, D. M. Pickup, A. V. Chadwick, H. E. Allison, V. R. Dhanak, J. B. Claridge, J. R. Darwent, M. J. Rosseinsky, *Appl. Catal. B* **2017**, *206*, 547-555;b) X. Wu, X. Wang, J. Li, G. Zhang, *J. Mater. Chem. A* **2017**, *5*, 23822-23830;c) M. Humayun, L. Xu, L. Zhou, Z. Zheng, Q. Fu, W. Luo, *Nano Res.* **2018**, *11*, 6391-6404;d) J. Shan, F. Raziq, M. Humayun, W. Zhou, Y. Qu, G. Wang, Y. Li, *Appl. Catal. B* **2017**, *219*, 10-17.

[15] a) L. Cheng, Q. Xiang, Y. Liao, H. Zhang, *Energy Environ. Sci.* **2018**, *11*, 1362-1391;b) H. Zhang, X. Zuo, H. Tang, G. Li, Z. Zhou, *Phys. Chem. Chem. Phys.* **2015**, *17*, 6280-6288.

[16] H. Ullah, A. A. Tahir, T. K. Mallick, *Appl. Catal. B* **2018**, *224*, 895-903.

[17] a) X. Zhou, Q. Xu, W. Lei, T. Zhang, X. Qi, G. Liu, K. Deng, J. Yu, *Small* **2014**, *10*, 674-679;b) S. Han, L. Hu, Z. Liang, S. Wageh, A. A. Al-Ghamdi, Y. Chen, X. Fang, *Adv. Funct. Mater.* **2014**, *24*, 5719-5727;c) M. F. M. Noh, H. Ullah, N. A. Arzaee, A. Ab Halim, M. A. F. A. Rahim, N. A. Mohamed, J. Safaei, S. N. F. M. Nasir, G. Wang, M. A. M. Teridi, *Dalton Trans.* **2020**, *49*, 12037-12048.

[18] a) F. Raziq, Y. Qu, X. Zhang, M. Humayun, J. Wu, A. Zada, H. Yu, X. Sun, L. Jing, *J. Phys. Chem. C* **2016**, *120*, 98-107;b) M. Humayun, Z. Li, L. Sun, X. Zhang, F. Raziq, A. Zada, Y. Qu, L. Jing, *Nanomaterials* **2016**, *6*.

[19] a) A. Zhu, Q. Zhao, X. Li, Y. Shi, *ACS Appl. Mater. Interfaces* **2014**, *6*, 671-679;b) T. Choi, S. Lee, Y. J. Choi, V. Kiryukhin, S. W. Cheong, *Science* **2009**, *324*, 63;c) M. Humayun, A. Zada, Z. Li, M. Xie, X. Zhang, Y. Qu, F. Raziq, L. Jing, *Appl. Catal. B* **2016**, *180*, 219-226.

[20] a) G. Wang, Y. Ling, H. Wang, X. Yang, C. Wang, J. Z. Zhang, Y. Li, *Energy Environ. Sci.* **2012**, *5*, 6180-6187;b) J. Su, X. Feng, J. D. Sloppy, L. Guo, C. A. Grimes, *Nano Lett.* **2011**, *11*, 203-208;c) J. Kim, C. W. Lee, W. Choi, *Environ. Sci. Technol.* **2010**, *44*, 6849-6854;d) K. R. Reyes-Gil, C. Wiggenhorn, B. S. Brunschwig, N. S. Lewis, *J. Phys. Chem. C* **2013**, *117*, 14947-14957.

[21] a) C. Li, G. Chen, J. Sun, J. Rao, Z. Han, Y. Hu, Y. Zhou, *ACS Appl. Mater. Interfaces* **2015**, *7*, 25716-25724;b) C. Ye, J.-X. Li, Z.-J. Li, X.-B. Li, X.-B. Fan, L.-P. Zhang, B. Chen, C.-H. Tung, L.-Z. Wu, *ACS Catal.* **2015**, *5*, 6973-6979;c) X. Ding, K. Zhao, L. Zhang, *Environ. Sci. Technol.* **2014**, *48*, 5823-5831.

[22] a) H. Sakamoto, T. Ohara, N. Yasumoto, Y. Shiraishi, S. Ichikawa, S. Tanaka, T. Hirai, *J. Am. Chem. Soc.* **2015**, *137*, 9324-9332;b) A. V. Akimov, R. Asahi, R. Jinnouchi, O. V. Prezhdo, *J. Am. Chem. Soc.* **2015**, *137*, 11517-11525.

[23] H. Ullah, A. A. Tahir, S. Bibi, T. K. Mallick, S. Z. Karazhanov, *Appl. Catal. B* **2018**, *229*, 24-31.

[24] a) W.-C. Huang, L.-M. Lyu, Y.-C. Yang, M. H. Huang, *J. Am. Chem. Soc.* **2012**, *134*, 1261-1267;b) C. W. Li, M. W. Kanan, *J. Am. Chem. Soc.* **2012**, *134*, 7231-7234.

[25] a) S. Chen, S. Shen, G. Liu, Y. Qi, F. Zhang, C. Li, *Angew. Chem., Int. Ed.* **2015**, *54*, 3047-3051;b) Y. Li, T. Takata, D. Cha, K. Takanabe, T. Minegishi, J. Kubota, K. Domen, *Adv. Mater.* **2013**, *25*, 125-131.

[26] a) B. Wang, Y. Wang, Y. Lei, N. Wu, Y. Gou, C. Han, S. Xie, D. Fang, *Nano Res.* **2016**, *9*, 886-898;b) Y. Sun, H. Cheng, S. Gao, Z. Sun, Q. Liu, Q. Liu, F. Lei, T. Yao, J. He, S. Wei, Y. Xie, *Angew. Chem., Int. Ed.* **2012**, *51*, 8727-8731.

[27] a) R. Asahi, T. Morikawa, H. Irie, T. Ohwaki, *Chem. Rev.* **2014**, *114*, 9824-9852;b) L.-L. Tan, W.-J. Ong, S.-P. Chai, B. T. Goh, A. R. Mohamed, *Appl. Catal. B* **2015**, *179*, 160-170.

[28] N. A. Mohamed, J. Safaei, A. F. Ismail, M. F. A. M. Jailani, M. N. Khalid, M. F. M. Noh, A. Aadenan, S. N. S. Nasir, J. S. Sagu, M. A. M. Teridi, *Appl. Surf. Sci.* **2019**, *489*, 92-100.

[29] a) F. Goettmann, A. Fischer, M. Antonietti, A. Thomas, *Angew. Chem., Int. Ed.* **2006**, *45*, 4467-4471;b) X. Wang, K. Maeda, A. Thomas, K. Takanabe, G. Xin, J. M. Carlsson, K. Domen, M. Antonietti, *Nat. Mater.* **2009**, *8*, 76-80.

[30] a) A. Zada, M. Humayun, F. Raziq, X. Zhang, Y. Qu, L. Bai, C. Qin, L. Jing, H. Fu, *Adv. Energy Mater.* **2016**, *6*, 1601190;b) F. Raziq, L. Sun, Y. Wang, X. Zhang, M. Humayun, S. Ali, L. Bai, Y. Qu, H. Yu, L. Jing, *Adv. Energy Mater.* **2018**, *8*, 1701580.

[31] a) M. Humayun, Q. Fu, Z. Zheng, H. Li, W. Luo, *Appl. Catal. A* **2018**, *568*, 139-147;b) G. Dong, Y. Zhang, Q. Pan, J. Qiu, *J. Photochem. Photobiol., A* **2014**, *20*, 33-50.

[32] a) L. Shi, T. Wang, H. Zhang, K. Chang, J. Ye, *Adv. Funct. Mater.* **2015**, *25*, 5360-5367;b) G. Dong, W. Ho, Y. Li, L. Zhang, *Appl. Catal. B* **2015**, *174-175*, 477-485;c) G. Li, Z. Lian, W. Wang, D. Zhang, H. Li, *Nano Energy* **2016**, *19*, 446-454;d) J. Bian, Q. Li, C. Huang, J. Li, Y. Guo, M. Zaw, R.-Q. Zhang, *Nano Energy* **2015**, *15*, 353-361.

[33] a) J. Liu, H. Wang, Z. P. Chen, H. Moehwald, S. Fiechter, R. van de Krol, L. Wen, L. Jiang, M. Antonietti, *Adv. Mater.* **2015**, *27*, 712-718;b) Y. Shiraishi, Y. Kofuji, H. Sakamoto, S. Tanaka, S. Ichikawa, T. Hirai, *ACS Catal.* **2015**, *5*, 3058-3066.

[34] a) F. Raziq, Y. Qu, M. Humayun, A. Zada, H. Yu, L. Jing, *Appl. Catal. B* **2017**, *201*, 486-494;b) G. Liu, T. Wang, H. Zhang, X. Meng, D. Hao, K. Chang, P. Li, T. Kako, J. Ye, *Angew. Chem., Int. Ed.* **2015**, *54*, 13561-13565.

[35] a) X. Song, Y. Hu, M. Zheng, C. Wei, *Appl. Catal. B* **2016**, *182*, 587-597;b) J. Zhang, A. Wang, W. Zhao, C. Li, X. Chen, Y. Wang, W. Zhu, Q. Zhong, *Dyes Pigm.* **2018**, *153*, 241-247;c) J. Liu, W. Li, L. Duan, X. Li, L. Ji, Z. Geng, K. Huang, L. Lu, L. Zhou, Z. Liu, W. Chen, L. Liu, S. Feng, Y. Zhang, *Nano Lett.* **2015**, *15*, 5137-5142.

[36] a) K. Wang, Q. Li, B. Liu, B. Cheng, W. Ho, J. Yu, *Appl. Catal. B* **2015**, *176-177*, 44-52;b) J. Xiao, Y. Xie, F. Nawaz, Y. Wang, P. Du, H. Cao, *Appl. Catal. B* **2016**, *183*, 417-425.

[37] Y. Cui, G. Zhang, Z. Lin, X. Wang, *Appl. Catal. B* **2016**, *181*, 413-419.

[38] D. M. Teter, R. J. Hemley, *Science* **1996**, *271*, 53.

[39] a) Y. Zhao, J. Zhang, L. Qu, *ChemNanoMat* **2015**, *1*, 298-318;b) A. Zambon, J. M. Mouesca, C. Gheorghiu, P. A. Bayle, J. Pécaut, M. Claeys-Bruno, S. Gambarelli, L. Dubois, *Chem. Sci.* **2016**, *7*, 945-950.

[40] Y. Zheng, L. Lin, B. Wang, X. Wang, *Angew. Chem., Int. Ed.* **2015**, *54*, 12868-12884.

[41] M. Humayun, H. Ullah, J. Cao, W. Pi, Y. Yuan, S. Ali, A. A. Tahir, P. Yue, A. Khan, Z. Zheng, Q. Fu, W. Luo, *Nano-Micro Lett.* **2019**, *12*, 7.

[42] K. Maeda, X. Wang, Y. Nishihara, D. Lu, M. Antonietti, K. Domen, *J. Phys. Chem. C* **2009**, *113*, 4940-4947.

[43] Z. Zhao, Y. Sun, F. Dong, *Nanoscale* **2015**, *7*, 15-37.

[44] a) Y. Zheng, L. Lin, X. Ye, F. Guo, X. Wang, *Angew. Chem., Int. Ed.* **2014**, *53*, 11926-11930;b) S. Ali, M. Humayun, W. Pi, Y. Yuan, M. Wang, A. Khan, P. Yue, L. Shu, Z. Zheng, Q. Fu, W. Luo, *J. Hazard. Mater.* **2020**, *397*, 122708;c) F. Raziq, M. Humayun, A. Ali, T. Wang, A. Khan, Q. Fu, W. Luo, H. Zeng, Z. Zheng, B. Khan, H. Shen, X. Zu, S. Li, L. Qiao, *Appl. Catal. B* **2018**, *237*, 1082-1090;d) D. Neena, M. Humayun, W. Zuo, C. S. Liu, W. Gao, D. J. Fu, *Appl. Surf. Sci.* **2020**, *506*, 145017;e) X. Wei, C. Shao, X. Li, N. Lu, K. Wang, Z. Zhang, Y. Liu, *Nanoscale* **2016**, *8*, 11034-11043;f) X. Yang, Z. Chen, J. Xu, H. Tang, K. Chen, Y. Jiang, *ACS Appl. Mater. Interfaces* **2015**, *7*, 15285-15293;g) Y. Bai, L. Ye, L. Wang, X. Shi, P. Wang, W. Bai, P. K. Wong, *Appl. Catal. B* **2016**, *194*, 98-104;h) Y. Wang, R. Shi, J. Lin, Y. Zhu, *Energy Environ. Sci.* **2011**, *4*, 2922-2929;i) S. Sharma, V. Dutta, P. Raizada, A. Hosseini-Bandegharaei, P. Singh, V.-H. Nguyen, *Environ. Chem. Lett.* **2020**, 1-36;j) P. Raizada, V. Soni, A. Kumar, P. Singh, A. A. P. Khan, A. M. Asiri, V. K. Thakur, V.-H. Nguyen, *J. Materiomics* **2020**;k) A. Kumar, P. Raizada, A. Hosseini-Bandegharaei, V. K. Thakur, V.-H. Nguyen, P. Singh, *J. Mater. Chem. A* **2021**.

[45] a) Z. Zhang, M. Xu, W. Ho, X. Zhang, Z. Yang, X. Wang, *Appl. Catal. B* **2016**, *184*, 174-181;b) N. D, M. Humayun, D. Bhattacharyya, D. Fu, *J. Photochem. Photobiol., A* **2020**, *396*, 112515.

[46] a) J. Liu, H. Wang, M. Antonietti, *Chem. Soc. Rev.* **2016**, *45*, 2308-2326;b) J. Xu, L. Zhang, R. Shi, Y. Zhu, *J. Mater. Chem. A* **2013**, *1*, 14766-14772;c) S. Ye, R. Wang, M.-Z. Wu, Y.-P. Yuan, *Appl. Surf. Sci.* **2015**, *358*, 15-27.

[47] J. Liebig, *Annalen der Pharmacie* **1834**, *10*, 1-47.

[48] E. C. Franklin, *J. Am. Chem. Soc.* **1922**, *44*, 486-509.

[49] L. Pauling, J. H. Sturdivant, *Proceedings of the National Academy of Sciences of the United States of America* **1937**, *23*, 615-620.

[50] C. E. Redemann, H. J. Lucas, *J. Am. Chem. Soc.* **1940**, *62*, 842-846.

[51] a) A. Y. Liu, M. L. Cohen, *Science* **1989**, *245*, 841;b) M. L. Cohen, *Phys. Rev. B* **1985**, *32*, 7988-7991;c) A. Snis, S. F. Matar, *Phys. Rev. B* **1999**, *60*, 10855-10863.

[52] a) C. Niu, Y. Z. Lu, C. M. Lieber, *Science* **1993**, *261*, 334;b) Z.-M. Ren, Y.-C. Du, Y. Qiu, J.-D. Wu, Z.-F. Ying, X.-X. Xiong, F.-M. Li, *Phys. Rev. B* **1995**, *51*, 5274-5277;c) L. Maya, D. R. Cole, E. W. Hagaman, *J. Am. Ceramic Soc.* **1991**, *74*, 1686-1688;d) K. M. Yu, M. L. Cohen, E. E. Haller, W. L. Hansen, A. Y. Liu, I. C. Wu, *Phys. Rev. B* **1994**, *49*, 5034-5037.

[53] D. C. Nesting, J. V. Badding, *Chem. Mater.* **1996**, *8*, 1535-1539.

[54] a) J. Ortega, O. F. Sankey, *Physical Review B* **1995**, *51*, 2624-2627;b) J. E. Lowther, *Phys. Rev. B* **1999**, *59*, 11683-11686.

[55] a) H. Huang, S. Yang, R. Vajtai, X. Wang, P. M. Ajayan, *Advanced Materials* **2014**, *26*, 5160-5165;b) Z. Zhang, K. Leinenweber, M. Bauer, L. A. J. Garvie, P. F. McMillan, G. H. Wolf, *J. Am. Chem. Soc.* **2001**, *123*, 7788-7796;c) J. L. Zimmerman, R. Williams, V. N. Khabashesku, J. L. Margrave, *Nano Lett.* **2001**, *1*, 731-734;d) Y. Zhang, H. Sun, C. Chen, *Phys. Rev. B* **2006**, *73*, 144115.

[56] a) Y. Zheng, J. Liu, J. Liang, M. Jaroniec, S. Z. Qiao, *Energy Environ. Sci.* **2012**, *5*, 6717-6731;b) J. Liebig, *Justus Liebigs Ann. Chem.* **1850**, *73*, 125-128;c) J. Sehnert, K. Baerwinkel, J. Senker, *J. Phys. Chem. B* **2007**, *111*, 10671-10680;d) E. Kroke, M. Schwarz, E. Horath-Bordon, P. Kroll, B. Noll, A. D. Norman, *New J. Chem.* **2002**, *26*, 508-512.

[57] a) E. Horvath-Bordon, E. Kroke, I. Svoboda, H. Fuess, R. Riedel, *New J. Chem.* **2005**, *29*, 693-699;b) A. Sattler, S. Pagano, M. Zeuner, A. Zurawski, D. Gunzelmann, J. Senker, K. Müller-Buschbaum, W. Schnick, *Chem. A Eur. J.* **2009**, *15*, 13161-13170;c) S. Chu, C. Wang, J. Feng, Y. Wang, Z. Zou, *Inter. J. Hydrogen Energy* **2014**, *39*, 13519-13526;d) B. V. Lotsch, W. Schnick, *Chem. Mater.* **2006**, *18*, 1891-1900.

[58] a) T. Komatsu, *J. Mater. Chem.* **2001**, *11*, 799-801;b) T. Komatsu, *J. Mater. Chem.* **2001**, *11*, 802-803.

[59] a) A. Sattler, W. Schnick, *Zeitschrift für anorganische und allgemeine Chemie* **2006**, *632*, 238-242;b) B. V. Lotsch, W. Schnick, *Chem. A Eur. J.* **2007**, *13*, 4956-4968.

[60] E. Horvath-Bordon, R. Riedel, P. F. McMillan, P. Kroll, G. Miehe, P. A. van Aken, A. Zerr, P. Hoppe, O. Shebanova, I. McLaren, S. Lauterbach, E. Kroke, R. Boehler, *Angewandte Chemie International Edition* **2007**, *46*, 1476-1480.

[61] M. J. Bojdys, J.-O. Müller, M. Antonietti, A. Thomas, *Chem. A Eur. J.* **2008**, *14*, 8177-8182.

[62] Y. Wang, B. Gao, Q. Yue, Z. Wang, *Journal of Materials Chemistry A* **2020**, *8*, 19133-19155.

[63] G. Liao, Y. Gong, L. Zhang, H. Gao, G.-J. Yang, B. Fang, *Energy & Environmental Science* **2019**, *12*, 2080-2147.

[64] a) N. Tian, H. Huang, X. Du, F. Dong, Y. Zhang, *Journal of Materials Chemistry A* **2019**, *7*, 11584-11612;b) Q. Cao, B.

Kumru, M. Antonietti, B. V. K. J. Schmidt, *Materials Horizons* **2020**, *7*, 762-786.
[65] a) P. Raizada, A. Sudhaik, P. Singh, P. Shandilya, V. K. Gupta, A. Hosseini-Bandegharaei, S. Agrawal, *J. Photochem. Photobiol., A* **2019**, *374*, 22-35;b) A. Kumar, P. Raizada, P. Singh, R. V. Saini, A. K. Saini, A. Hosseini-Bandegharaei, *Chem. Eng. J.* **2019**, 123496.
[66] P. Singh, P. Shandilya, P. Raizada, A. Sudhaik, A. Rahmani-Sani, A. Hosseini-Bandegharaei, *Arabian J. Chem.* **2020**, *13*, 3498-3520.
[67] a) P. Raizada, A. Sudhaik, P. Singh, A. Hosseini-Bandegharaei, P. Thakur, *Sep. Purif. Technol.* **2019**, *227*, 115692;b) V. Hasija, A. Sudhaik, P. Raizada, A. Hosseini-Bandegharaei, P. Singh, *. Environ. Chem. Eng.* **2019**, *7*, 103272.
[68] V. Dutta, S. Sharma, P. Raizada, A. Hosseini-Bandegharaei, V. K. Gupta, P. Singh, *J. Saudi Chem. Soc.* **2019**, *23*, 1119-1136.
[69] J. Zhang, X. Chen , K. Takanabe, K. Maeda, K. Domen, J. D. Epping, X. Fu, M. Antonietti, X. Wang *Angewandte Chemie International Edition* **2010**, *49*, 441-444.
[70] F. Raziq, C. Li, M. Humayun, Y. Qu, A. Zada, H. Yu, L. Jing, *Mater. Res. Bull.* **2015**, *70*, 494-499.
[71] S. Fang, K. Lv, Q. Li, H. Ye, D. Du, M. Li, *Appl. Surf. Sci.* **2015**, *358*, 336-342.
[72] a) S. G. Kumar, L. G. Devi, *J. Phys. Chem. A* **2011**, *115*, 13211-13241;b) M. F. R. Samsudin, H. Ullah, R. Bashiri, N. M. Mohamed, S. Sufian, Y. H. Ng, *ACS Sustainable Chem. Eng.* **2020**, *8*, 9393-9403.
[73] a) X. Li, J. Yu, M. Jaroniec, *Chem. Soc. Rev.* **2016**, *45*, 2603-2636;b) P. M. Wood, *Chem. Eng. J.* **1988**, *253*, 287-289.
[74] a) H. Narayanan, B. Viswanathan, S. Yesodharan, *Curr. Catal.* **2016**, *5*, 79-107;b) X. Li, J. Yu, J. Low, Y. Fang, J. Xiao, X. Chen, *J. Mater. Chem. A* **2015**, *3*, 2485-2534.
[75] F. Raziq, L. Sun, Y. Wang, X. Zhang, M. Humayun, S. Ali, L. Bai, Y. Qu, H. Yu, L. Jing, *Advanced Energy Materials* **2018**, *8*, 1701580.
[76] J. Wen, J. Xie, X. Chen, X. Li, *Appl. Surf. Sci.* **2017**, *391*, 72-123.
[77] Y. Gong, M. Li, Y. Wang, *ChemSusChem* **2015**, *8*, 931-946.
[78] a) B. Zhu, L. Zhang, B. Cheng, J. Yu, *Applied Catalysis B: Environmental* **2018**, *224*, 983-999;b) A. Thomas, A. Fischer, F. Goettmann, M. Antonietti, J.-O. Müller, R. Schlögl, J. M. Carlsson, *J. Mater. Chem.* **2008**, *18*, 4893-4908;c) Y. Ren, D. Zeng, W.-J. Ong, *Chin. J. Catal.* **2019**, *40*, 289-319.
[79] a) L. Xu, J. Xia, H. Xu, S. Yin, K. Wang, L. Huang, L. Wang, H. Li, *J. Power Sources* **2014**, *245*, 866-874;b) J. Di, J. Xia, S. Yin, H. Xu, L. Xu, Y. Xu, M. He, H. Li, *J. Mater. Chem. A* **2014**, *2*, 5340-5351.
[80] a) Y.-S. Jun, E. Z. Lee, X. Wang, W. H. Hong, G. D. Stucky, A. Thomas, *Advanced Functional Materials* **2013**, *23*, 3661-3667;b) Y. Ishida, L. Chabanne, M. Antonietti, M. Shalom, *Langmuir* **2014**, *30*, 447-451;c) M. Shalom, S. Gimenez, F. Schipper, I. Herraiz-Cardona, J. Bisquert, M. Antonietti, *Angewandte Chemie International Edition* **2014**, *53*, 3654-3658.
[81] a) H. Gao, S. Yan, J. Wang, Y. A. Huang, P. Wang, Z. Li, Z. Zou, *Phys. Chem. Chem. Phys.* **2013**, *15*, 18077-18084;b) H. Zou, X. Yan, J. Ren, X. Wu, Y. Dai, D. Sha, J. Pan, J. Liu, *J. Materiomics* **2015**, *1*, 340-347;c) K. Schwinghammer, M. B. Mesch, V. Duppel, C. Ziegler, J. Senker, B. V. Lotsch, *J. Am. Chem. Soc.* **2014**, *136*, 1730-1733.
[82] a) L. Lin, P. Ye, C. Cao, Q. Jin, G.-S. Xu, Y.-H. Shen, Y.-P. Yuan, *J. Mater. Chem. A* **2015**, *3*, 10205-10208;b) Y.-P. Yuan, L.-S. Yin, S.-W. Cao, L.-N. Gu, G.-S. Xu, P. Du, H. Chai, Y.-S. Liao, C. Xue, *Green Chem.* **2014**, *16*, 4663-4668.
[83] a) J. Zhang, J. Sun, K. Maeda, K. Domen, P. Liu, M. Antonietti, X. Fu, X. Wang, *Energy Environ. Sci.* **2011**, *4*, 675-678;b) S. Yin, J. Han, T. Zhou, R. Xu, *Catal. Sci. Technol.* **2015**, *5*, 5048-5061.
[84] a) F. Su, S. C. Mathew, G. Lipner, X. Fu, M. Antonietti, S. Blechert, X. Wang, *J. Am. Chem. Soc.* **2010**, *132*, 16299-16301;b) H. Tong, S. Ouyang, Y. Bi, N. Umezawa, M. Oshikiri, J. Ye, *Advanced Materials* **2012**, *24*, 229-251.
[85] J. Gao, Y. Wang, S. Zhou, W. Lin, Y. Kong, *ChemCatChem* **2017**, *9*, 1708-1715.
[86] a) J. Low, S. Cao, J. Yu, S. Wageh, *Chem. Commun.* **2014**, *50*, 10768-10777;b) J. Tong, L. Zhang, F. Li, M. Li, S. Cao, *Phys. Chem. Chem. Phys.* **2015**, *17*, 23532-23537.
[87] Y.-J. Yuan, Z. Shen, S. Wu, Y. Su, L. Pei, Z. Ji, M. Ding, W. Bai, Y. Chen, Z.-T. Yu, Z. Zou, *Applied Catalysis B: Environmental* **2019**, *246*, 120-128.
[88] a) H. Zhao, H. Yu, X. Quan, S. Chen, Y. Zhang, H. Zhao, H. Wang, *Applied Catalysis B: Environmental* **2014**, *152-153*, 46-50;b) S. Yang, Y. Gong, J. Zhang, L. Zhan, L. Ma, Z. Fang, R. Vajtai, X. Wang, P. M. Ajayan, *Advanced Materials* **2013**, *25*, 2452-2456.
[89] X. She, H. Xu, Y. Xu, J. Yan, J. Xia, L. Xu, Y. Song, Y. Jiang, Q. Zhang, H. Li, *J. Mater. Chem. A* **2014**, *2*, 2563-2570.
[90] S. Bai, X. Wang, C. Hu, M. Xie, J. Jiang, Y. Xiong, *Chem. Commun.* **2014**, *50*, 6094-6097.
[91] J. Safaei, N. A. Mohamed, M. F. M. Noh, M. F. Soh, M. A. Riza, N. S. M. Mustakim, N. A. Ludin, M. A. Ibrahim, W. N. R. W. Isahak, M. A. M. Teridi, *J. Alloys Compd.* **2018**, *769*, 130-135.
[92] Q. Lin, L. Li, S. Liang, M. Liu, J. Bi, L. Wu, *Applied Catalysis B: Environmental* **2015**, *163*, 135-142.
[93] X. Zhang, X. Xie, H. Wang, J. Zhang, B. Pan, Y. Xie, *J. Am. Chem. Soc.* **2013**, *135*, 18-21.
[94] H. Zhao, H. Yu, X. Quan, S. Chen, H. Zhao, H. Wang, *RSC Adv.* **2014**, *4*, 624-628.
[95] Y. Yin, J. Han, X. Zhang, Y. Zhang, J. Zhou, D. Muir, R. Sutarto, Z. Zhang, S. Liu, B. Song, *RSC Adv.* **2014**, *4*, 32690-32697.
[96] P. Niu, L. Zhang, G. Liu, H.-M. Cheng, *Advanced Functional Materials* **2012**, *22*, 4763-4770.
[97] W.-J. Ong, L.-L. Tan, Y. H. Ng, S.-T. Yong, S.-P. Chai, *Chem. Rev.* **2016**, *116*, 7159-7329.
[98] aX. Zhuang, Y. Mai, D. Wu, F. Zhang, X. Feng, *Advanced Materials* **2015**, *27*, 403-427;bW. Yang, X. Zhang, Y. Xie, *Nano Today* **2016**, *11*, 793-816.
[99] S. Han, D. Wu, S. Li, F. Zhang, X. Feng, *Advanced Materials* **2014**, *26*, 849-864.
[100] a) A. Thomas, F. Goettmann, M. Antonietti, *Chem. Mater.* **2008**, *20*, 738-755;b) K. Kailasam, J. D. Epping, A. Thomas, S. Losse, H. Junge, *Energy Environ. Sci.* **2011**, *4*, 4668-4674.
[101] Y.-S. Jun, W. H. Hong, M. Antonietti, A. Thomas, *Advanced Materials* **2009**, *21*, 4270-4274.
[102] Y. Shi, Y. Wan, D. Zhao, *Chem. Soc. Rev.* **2011**, *40*, 3854-3878.
[103] A. Vinu, *Advanced Functional Materials* **2008**, *18*, 816-827.
[104] X. Wang, K. Maeda, X. Chen, K. Takanabe, K. Domen, Y. Hou, X. Fu, M. Antonietti, *J. Am. Chem. Soc.* **2009**, *131*, 1680-1681.
[105] J. Zhang, M. Zhang, C. Yang, X. Wang, *Advanced Materials* **2014**, *26*, 4121-4126.
[106] H. Yan, *Chem. Commun.* **2012**, *48*, 3430-3432.
[107] Y. Wang, X. Wang, M. Antonietti, Y. Zhang, *ChemSusChem* **2010**, *3*, 435-439.
[108] Y. Xu, M. A. A. Schoonen, *American Mineralogist* **2000**, *85*, 543-556.
[109] Y. Wang, Q. Wang, X. Zhan, F. Wang, M. Safdar, J. He, *Nanoscale* **2013**, *5*, 8326-8339.
[110] J. Zhang, M. Zhang, R.-Q. Sun, X. Wang, *Angewandte Chemie International Edition* **2012**, *51*, 10145-10149.
[111] R. Marschall, *Advanced Functional Materials* **2014**, *24*, 2421-2440.
[112] M. Humayun, F. Raziq, A. Khan, W. Luo, *Green Chem. Lett. Rev.* **2018**, *11*, 86-102.
[113] K. Maeda, *ACS Catalysis* **2013**, *3*, 1486-1503.
[114] L. Zhou, W. Zhang, L. Chen, H. Deng, J. Wan, *Catal. Commun.* **2017**, *100*, 191-195.
[115] D. Jiang, J. Zhu, M. Chen, J. Xie, *J. Colloid Interface Sci.* **2014**, *417*, 115-120.
[116] W. Zhang, L. Zhou, J. Shi, H. Deng, *Catalysts* **2018**, *8*.

[117] M. Xu, L. Han, S. Dong, *ACS Applied Materials & Interfaces* **2013**, *5*, 12533-12540.
[118] X. Wang, J. Yan, H. Ji, Z. Chen, Y. Xu, L. Huang, Q. Zhang, Y. Song, H. Xu, H. Li, *SpringerPlus* **2016**, *5*, 369.
[119] Y. He, L. Zhang, B. Teng, M. Fan, *Environ. Sci. Technol.* **2015**, *49*, 649-656.
[120] H. Xu, J. Yan, Y. Xu, Y. Song, H. Li, J. Xia, C. Huang, H. Wan, *Applied Catalysis B: Environmental* **2013**, *129*, 182-193.
[121] Y. Li, K. Li, Y. Yang, L. Li, Y. Xing, S. Song, R. Jin, M. Li, *Chem. A Eur. J.* **2015**, *21*, 17739-17747.
[122] W. Zhao, Z. Wei, H. He, J. Xu, J. Li, S. Yang, C. Sun, *Applied Catalysis A: General* **2015**, *501*, 74-82.
[123] B. Zhu, P. Xia, Y. Li, W. Ho, J. Yu, *Appl. Surf. Sci.* **2017**, *391*, 175-183.
[124] C. Zhang, R. Li, Y. Zhao, M. Wang, *Aust. J. Chem.* **2017**, *70*, 889-895.
[125] L. Ye, J. Liu, Z. Jiang, T. Peng, L. Zan, *Applied Catalysis B: Environmental* **2013**, *142-143*, 1-7.
[126] Q. Li, X. Zhao, J. Yang, C.-J. Jia, Z. Jin, W. Fan, *Nanoscale* **2015**, *7*, 18971-18983.
[127] Q. Wang, W. Wang, L. Zhong, D. Liu, X. Cao, F. Cui, *Applied Catalysis B: Environmental* **2018**, *220*, 290-302.
[128] Z. Chen, Q. Zhang, Y. Luo, *ChemPhotoChem* **2017**, *1*, 350-354.
[129] Z. Cui, H. Yang, X. Zhao, *Mater. Sci. Eng: B* **2018**, *229*, 160-172.
[130] Q. Meng, H. Lv, M. Yuan, Z. Chen, Z. Chen, X. Wang, *ACS Omega* **2017**, *2*, 2728-2739.
[131] C. Li, H. Che, C. Liu, G. Che, P. A. Charpentier, W. Z. Xu, X. Wang, L. Liu, *J. Taiwan Inst. Chem. Eng.* **2019**, *95*, 669-681.
[132] Z. Wang, J. Lv, J. Zhang, K. Dai, C. Liang, *Appl. Surf. Sci.* **2018**, *430*, 595-602.
[133] S. Samanta, S. Khilari, D. Pradhan, R. Srivastava, *ACS Sustainable Chemistry & Engineering* **2017**, *5*, 2562-2577.
[134] M. Yan, F. Zhu, W. Gu, L. Sun, W. Shi, Y. Hua, *RSC Adv.* **2016**, *6*, 61162-61174.
[135] D. Jiang, J. Li, C. Xing, Z. Zhang, S. Meng, M. Chen, *ACS Applied Materials & Interfaces* **2015**, *7*, 19234-19242.
[136] J. Zhang, Y. Wang, J. Jin, J. Zhang, Z. Lin, F. Huang, J. Yu, *ACS Applied Materials & Interfaces* **2013**, *5*, 10317-10324.
[137] W. L. Xu Huanyan, Jin Liguo,Wu Kejia, *J. Mater. Sci. Technol.* **2017**, *33*, 30-38.
[138] S.-W. Cao, Y.-P. Yuan, J. Fang, M. M. Shahjamali, F. Y. C. Boey, J. Barber, S. C. Joachim Loo, C. Xue, *Inter. J. Hydrogen Energy* **2013**, *38*, 1258-1266.
[139] Y. Zhong, W. Chen, S. Yu, Z. Xie, S. Wei, Y. Zhou, *ACS Omega* **2018**, *3*, 17762-17769.
[140] W. Xue, X. Hu, E. Liu, J. Fan, *Appl. Surf. Sci.* **2018**, *447*, 783-794.
[141] M. Li, L. Zhang, M. Wu, Y. Du, X. Fan, M. Wang, L. Zhang, Q. Kong, J. Shi, *Nano Energy* **2016**, *19*, 145-155.
[142] M. Humayun, Z. Hu, A. Khan, W. Cheng, Y. Yuan, Z. Zheng, Q. Fu, W. Luo, *J. Hazard. Mater.* **2019**, *364*, 635-644.
[143] W. Zou, B. Deng, X. Hu, Y. Zhou, Y. Pu, S. Yu, K. Ma, J. Sun, H. Wan, L. Dong, *Applied Catalysis B: Environmental* **2018**, *238*, 111-118.
[144] K. Saravanakumar, R. Karthik, S.-M. Chen, J. Vinoth Kumar, K. Prakash, V. Muthuraj, *J. Colloid Interface Sci.* **2017**, *504*, 514-526.
[145] X. Li, W. Zhu, X. Lu, S. Zuo, C. Yao, C. Ni, *Chem. Eng. J.* **2017**, *326*, 87-98.
[146] J. Chen, S. Shen, P. Wu, L. Guo, *Green Chem.* **2015**, *17*, 509-517.
[147] R. Ye, H. Fang, Y.-Z. Zheng, N. Li, Y. Wang, X. Tao, *ACS Applied Materials & Interfaces* **2016**, *8*, 13879-13889.
[148] J. Chen, S. Shen, P. Guo, M. Wang, P. Wu, X. Wang, L. Guo, *Applied Catalysis B: Environmental* **2014**, *152-153*, 335-341.
[149] X. Yan, R. Xu, J. Guo, X. Cai, D. Chen, L. Huang, Y. Xiong, S. Tan, *Mater. Res. Bull.* **2017**, *96*, 18-27.
[150] S. Anandan, J. J. Wu, D. Bahnemann, A. Emeline, M. Ashokkumar, *Colloids Surf., A* **2017**, *527*, 34-41.
[151] X. Liu, A. Jin, Y. Jia, J. Jiang, N. Hu, X. Chen, *RSC Adv.* **2015**, *5*, 92033-92041.
[152] J. Jia, W. Sun, Q. Zhang, X. Zhang, X. Hu, E. Liu, J. Fan, *Applied Catalysis B: Environmental* **2020**, *261*, 118249.
[153] F. Dong, Z. Zhao, T. Xiong, Z. Ni, W. Zhang, Y. Sun, W.-K. Ho, *ACS Applied Materials & Interfaces* **2013**, *5*, 11392-11401.
[154] S.-W. Cao, X.-F. Liu, Y.-P. Yuan, Z.-Y. Zhang, Y.-S. Liao, J. Fang, S. C. J. Loo, T. C. Sum, C. Xue, *Applied Catalysis B: Environmental* **2014**, *147*, 940-946.
[155] B. Hu, F. Cai, T. Chen, M. Fan, C. Song, X. Yan, W. Shi, *ACS Applied Materials & Interfaces* **2015**, *7*, 18247-18256.
[156] K. Xu, J. Feng, *RSC Adv.* **2017**, *7*, 45369-45376.
[157] W. Chen, Y.-X. Hua, Y. Wang, T. Huang, T.-Y. Liu, X.-H. Liu, *J. Catal.* **2017**, *349*, 8-18.
[158] P. Xia, B. Zhu, B. Cheng, J. Yu, J. Xu, *ACS Sustainable Chemistry & Engineering* **2018**, *6*, 965-973.
[159] Y. Cao, Q. Li, W. Wang, *RSC Adv.* **2017**, *7*, 6131-6139.
[160] Y. Cui, C. Yang, S. Tang, Y. Zhao, F. Chen, *J. Wuhan University of Technology-Mater. Sci. Ed.* **2019**, *34*, 23-29.
[161] H. Qin, R.-T. Guo, X.-Y. Liu, W.-G. Pan, Z.-Y. Wang, X. Shi, J.-Y. Tang, C.-Y. Huang, *Dalton Trans.* **2018**, *47*, 15155-15163.
[162] Y. Liu, H. Zhang, J. Ke, J. Zhang, W. Tian, X. Xu, X. Duan, H. Sun, M. O Tade, S. Wang, *Applied Catalysis B: Environmental* **2018**, *228*, 64-74.
[163] S. Kumar, S. Tonda, A. Baruah, B. Kumar, V. Shanker, *Dalton Trans.* **2014**, *43*, 16105-16114.
[164] H.-Y. Chen, L.-G. Qiu, J.-D. Xiao, S. Ye, X. Jiang, Y.-P. Yuan, *RSC Adv.* **2014**, *4*, 22491-22496.
[165] S. Hu, L. Ma, H. Wang, L. Zhang, Y. Zhao, G. Wu, *RSC Adv.* **2015**, *5*, 31947-31953.
[166] Y.-P. Yuan, S.-W. Cao, Y.-S. Liao, L.-S. Yin, C. Xue, *Applied Catalysis B: Environmental* **2013**, *140-141*, 164-168.
[167] T. Li, L. Zhao, Y. He, J. Cai, M. Luo, J. Lin, *Applied Catalysis B: Environmental* **2013**, *129*, 255-263.
[168] Y. Zang, L. Li, X. Li, R. Lin, G. Li, *Chem. Eng. J.* **2014**, *246*, 277-286.
[169] B. Babu, M. Cho, C. Byon, J. Shim, *Mater. Lett.* **2018**, *212*, 327-331.
[170] F. Raziq, Y. Qu, M. Humayun, A. Zada, H. Yu, L. Jing, *Applied Catalysis B: Environmental* **2017**, *201*, 486-494.
[171] Z. Zhang, J. Huang, M. Zhang, Q. Yuan, B. Dong, *Applied Catalysis B: Environmental* **2015**, *163*, 298-305.
[172] L. Chen, M. Chen, D. Jiang, J. Xie, *J. Mol. Catal. A* **2016**, *425*, 174-182.
[173] Z. Jiang, C. Zhu, W. Wan, K. Qian, J. Xie, *J. Mater. Chem. A* **2016**, *4*, 1806-1818.
[174] I. Troppová, M. Šihor, M. Reli, M. Ritz, P. Praus, K. Kočí, *Appl. Surf. Sci.* **2018**, *430*, 335-347.
[175] C. Marchal, T. Cottineau, M. G. Méndez-Medrano, C. Colbeau-Justin, V. Caps, V. Keller, *Advanced Energy Materials* **2018**, *8*, 1702142.
[176] H. Chen, Y. Xie, X. Sun, M. Lv, F. Wu, L. Zhang, L. Li, X. Xu, *Dalton Trans.* **2015**, *44*, 13030-13039.
[177] Z. Lu, L. Zeng, W. Song, Z. Qin, D. Zeng, C. Xie, *Applied Catalysis B: Environmental* **2017**, *202*, 489-499.
[178] G. Jiang, J. Cao, M. Chen, X. Zhang, F. Dong, *Appl. Surf. Sci.* **2018**, *458*, 77-85.
[179] S. Zhou, Y. Liu, J. Li, Y. Wang, G. Jiang, Z. Zhao, D. Wang, A. Duan, J. Liu, Y. Wei, *Applied Catalysis B: Environmental* **2014**, *158-159*, 20-29.
[180] K. Li, Z. Huang, X. Zeng, B. Huang, S. Gao, J. Lu, *ACS Applied Materials & Interfaces* **2017**, *9*, 11577-11586.
[181] R. Wang, L. Gu, J. Zhou, X. Liu, F. Teng, C. Li, Y. Shen, Y. Yuan, *Advanced Materials Interfaces* **2015**, *2*, 1500037.
[182] X.-H. Yi, S.-Q. Ma, X.-D. Du, C. Zhao, H. Fu, P. Wang, C.-C. Wang, *Chem. Eng. J.* **2019**, *375*, 121944.
[183] Y. Hong, Y. Jiang, C. Li, W. Fan, X. Yan, M. Yan, W. Shi, *Applied Catalysis B: Environmental* **2016**, *180*, 663-673.
[184] I. Aslam, C. Cao, M. Tanveer, W. S. Khan, M. Tahir, M. Abid, F. Idrees, F. K. Butt, Z. Ali, N. Mahmood, *New J. Chem.* **2014**, *38*, 5462-5469.
[185] L. Cui, X. Ding, Y. Wang, H. Shi, L. Huang, Y. Zuo, S. Kang, *Appl. Surf. Sci.* **2017**, *391*, 202-210.

[186] W. Yu, J. Chen, T. Shang, L. Chen, L. Gu, T. Peng, *Applied Catalysis B: Environmental* **2017**, *219*, 693-704.

[187] S. Deng, Z. Yang, G. Lv, Y. Zhu, H. Li, F. Wang, X. Zhang, *Applied Physics A* **2019**, *125*, 44.

[188] T. Ohno, N. Murakami, T. Koyanagi, Y. Yang, *J. CO2 Utilization* **2014**, *6*, 17-25.

[189] J. Chen, S. Shen, P. Guo, P. Wu, L. Guo, *J. Mater. Chem. A* **2014**, *2*, 4605-4612.

[190] H. Liu, Z. Jin, Z. Xu, Z. Zhang, D. Ao, *RSC Adv.* **2015**, *5*, 97951-97961.

[191] P. Qiu, J. Yao, H. Chen, F. Jiang, X. Xie, *J. Hazard. Mater.* **2016**, *317*, 158-168.

[192] F. Shi, L. Chen, M. Chen, D. Jiang, *Chem. Commun.* **2015**, *51*, 17144-17147.

[193] J. Qin, C. Yang, M. Cao, X. Zhang, S. Rajendran, S. Limpanart, M. Ma, R. Liu, *Mater. Lett.* **2017**, *189*, 156-159.

[194] J. Li, Y. Liu, H. Li, C. Chen, *J. Photochem. Photobiol., A* **2016**, *317*, 151-160.

[195] L. Liu, Y. Qi, J. Yang, W. Cui, X. Li, Z. Zhang, *Appl. Surf. Sci.* **2015**, *358*, 319-327.

[196] L. Liu, Y. Qi, J. Hu, Y. Liang, W. Cui, *Appl. Surf. Sci.* **2015**, *351*, 1146-1154.

[197] C. Pan, J. Xu, Y. Wang, D. Li, Y. Zhu, *Advanced Functional Materials* **2012**, *22*, 1518-1524.

[198] L. Liu, Y. Qi, J. Lu, S. Lin, W. An, Y. Liang, W. Cui, *Applied Catalysis B: Environmental* **2016**, *183*, 133-141.

[199] D. Jiang, H. Yu, H. Yu, *Physica E: Low-dimensional Systems and Nanostructures* **2017**, *85*, 1-6.

[200] A. Habibi-Yangjeh, A. Akhundi, *J. Mol. Catal. A* **2016**, *415*, 122-130.

[201] A. Akhundi, A. Habibi-Yangjeh, *Applied Surface Science* **2015**, *358*, 261-269.

[202] M. Mousavi, A. Habibi-Yangjeh, *J. Colloid Interface Sci.* **2016**, *465*, 83-92.

[203] N. Li, J. Zhou, Z. Sheng, W. Xiao, *Appl. Surf. Sci.* **2018**, *430*, 218-224.

[204] J. Li, E. Liu, Y. Ma, X. Hu, J. Wan, L. Sun, J. Fan, *Appl. Surf. Sci.* **2016**, *364*, 694-702.

[205] a) P. Zhou, J. Yu, M. Jaroniec, *Advanced Materials* **2014**, *26*, 4920-4935;b) X. Ma, Q. Jiang, W. Guo, M. Zheng, W. Xu, F. Ma, B. Hou, *RSC Adv.* **2016**, *6*, 28263-28269.

[206] a) A. Sudhaik, P. Raizada, S. Thakur, R. V. Saini, A. K. Saini, P. Singh, V. K. Thakur, V.-H. Nguyen, A. A. P. Khan, A. M. Asiri, *J. Taiwan Inst. Chem. Eng.* **2020**, *113*, 142-154;b) A. Kumar, P. Raizada, V. K. Thakur, V. Saini, A. A. P. Khan, N. Singh, P. Singh, *Chem. Eng. Sci.* **2020**, 116219;c) A. Sudhaik, P. Raizada, P. Singh, A. Hosseini-Bandegharaei, V. K. Thakur, V.-H. Nguyen, *J. Environ. Chem. Eng.* **2020**, *8*, 104483.

[207] H. Li, H. Yu, X. Quan, S. Chen, Y. Zhang, *ACS Applied Materials & Interfaces* **2016**, *8*, 2111-2119.

[208] M. J. Muñoz-Batista, A. Kubacka, M. Fernández-García, *Catal. Sci. Technol.* **2014**, *4*, 2006-2015.

[209] J. Chen, J. Zhong, J. Li, S. Huang, W. Hu, M. Li, Q. Du, *Mol. Catal* **2017**, *435*, 91-98.

[210] L. Zhou, W. Zhang, L. Chen, H. Deng, *J. Colloid Interface Sci.* **2017**, *487*, 410-417.

[211] Y. Feng, J. Shen, Q. Cai, H. Yang, Q. Shen, *New J. Chem.* **2015**, *39*, 1132-1138.

[212] M. Li, L. Zhang, X. Fan, Y. Zhou, M. Wu, J. Shi, *J. Mater. Chem. A* **2015**, *3*, 5189-5196.

[213] a) N. Tian, H. Huang, Y. He, Y. Guo, T. Zhang, Y. Zhang, *Dalton Trans.* **2015**, *44*, 4297-4307;b) N. A. Mohamed, H. Ullah, J. Safaei, A. F. Ismail, M. F. Mohamad Noh, M. F. Soh, M. A. Ibrahim, N. A. Ludin, M. A. Mat Teridi, *J. Phys. Chem. C* **2019**, *123*, 9013-9026.

[214] X. Yang, W. Xin, X. Yin, X. Shao, *Chem. Phys. Lett.* **2016**, *651*, 127-132.

[215] X. She, J. Wu, H. Xu, J. Zhong, Y. Wang, Y. Song, K. Nie, Y. Liu, Y. Yang, M.-T. F. Rodrigues, R. Vajtai, J. Lou, D. Du, H. Li, P. M. Ajayan, *Advanced Energy Materials* **2017**, *7*, 1700025.

[216] Z. Huang, X. Zeng, K. Li, S. Gao, Q. Wang, J. Lu, *ACS Applied Materials & Interfaces* **2017**, *9*, 41120-41125.

[217] Y. He, L. Zhang, X. Wang, Y. Wu, H. Lin, L. Zhao, W. Weng, H. Wan, M. Fan, *RSC Adv.* **2014**, *4*, 13610-13619.

[218] K. Kailasam, A. Fischer, G. Zhang, J. Zhang, M. Schwarze, M. Schröder, X. Wang, R. Schomäcker, A. Thomas, *ChemSusChem* **2015**, *8*, 1404-1410.

[219] W. Yu, D. Xu, T. Peng, *J. Mater. Chem. A* **2015**, *3*, 19936-19947.

[220] H. Cheng, J. Hou, O. Takeda, X.-M. Guo, H. Zhu, *J. Mater. Chem. A* **2015**, *3*, 11006-11013.

[221] D. Zheng, C. Pang, X. Wang, *Chem. Commun.* **2015**, *51*, 17467-17470.

[222] Y. Yang, W. Guo, Y. Guo, Y. Zhao, X. Yuan, Y. Guo, *J. Hazard. Mater.* **2014**, *271*, 150-159.

[223] S. Kumar, A. Baruah, S. Tonda, B. Kumar, V. Shanker, B. Sreedhar, *Nanoscale* **2014**, *6*, 4830-4842.

[224] a) A. Iwase, Y. H. Ng, Y. Ishiguro, A. Kudo, R. Amal, *J. Am. Chem. Soc.* **2011**, *133*, 11054-11057;b) Y. Sasaki, A. Iwase, H. Kato, A. Kudo, *J. Catal.* **2008**, *259*, 133-137;c) Y. Bai, L. Ye, L. Wang, X. Shi, P. Wang, W. Bai, P. K. Wong, *Applied Catalysis B: Environmental* **2016**, *194*, 98-104;d) W. Zhao, L. Xie, M. Zhang, Z. Ai, H. Xi, Y. Li, Q. Shi, J. Chen, *Inter. J. Hydrogen Energy* **2016**, *41*, 6277-6287.

[225] a) H. Tada, T. Mitsui, T. Kiyonaga, T. Akita, K. Tanaka, *Nat. Mater.* **2006**, *5*, 782-786;b) F. Wu, X. Li, W. Liu, S. Zhang, *Appl. Surf. Sci.* **2017**, *405*, 60-70.

[226] W. Li, C. Feng, S. Dai, J. Yue, F. Hua, H. Hou, *Applied Catalysis B: Environmental* **2015**, *168-169*, 465-471.

[227] M. F. R. Samsudin, H. Ullah, A. A. Tahir, X. Li, Y. H. Ng, S. Sufian, *J. Colloid Interface Sci.* **2021**, *586*, 785-796.

[228] Y. Fu, Z. Li, Q. Liu, X. Yang, H. Tang, *Chin. J. Catal.* **2017**, *38*, 2160-2170.

[229] a) S. Bai, X. Li, Q. Kong, R. Long, C. Wang, J. Jiang, Y. Xiong, *Advanced Materials* **2015**, *27*, 3444-3452;b) T. Sun, H.-Y. Jiang, C.-C. Ma, F. Mao, B. Xue, *Catal. Commun.* **2016**, *79*, 45-48.

[230] a) J. Yu, S. Wang, B. Cheng, Z. Lin, F. Huang, *Catal. Sci. Technol.* **2013**, *3*, 1782-1789;b) Y. Lu, D. Chu, M. Zhu, Y. Du, P. Yang, *Phys. Chem. Chem. Phys.* **2015**, *17*, 17355-17361.

[231] a) S. Linic, P. Christopher, D. B. Ingram, *Nat. Mater.* **2011**, *10*, 911-921;b) S. Samanta, S. Martha, K. Parida, *ChemCatChem* **2014**, *6*, 1453-1462.

[232] L. Bi, D. Xu, L. Zhang, Y. Lin, D. Wang, T. Xie, *Phys. Chem. Chem. Phys.* **2015**, *17*, 29899-29905.

[233] M. Fan, C. Song, T. Chen, X. Yan, D. Xu, W. Gu, W. Shi, L. Xiao, *RSC Adv.* **2016**, *6*, 34633-34640.

[234] L.-L. Tan, W.-J. Ong, S.-P. Chai, A. R. Mohamed, *Applied Catalysis B: Environmental* **2015**, *166-167*, 251-259.

[235] a) J. Wang, J. Cong, H. Xu, J. Wang, H. Liu, M. Liang, J. Gao, Q. Ni, J. Yao, *ACS Sustainable Chemistry & Engineering* **2017**, *5*, 10633-10639;b) M. G. Méndez-Medrano, E. Kowalska, A. Lehoux, A. Herissan, B. Ohtani, S. Rau, C. Colbeau-Justin, J. L. Rodríguez-López, H. Remita, *J. Phys. Chem. C* **2016**, *120*, 25010-25022.

[236] a) J. S. Jang, H. G. Kim, J. S. Lee, *Catal. Today* **2012**, *185*, 270-277;b) N. Serpone, A. V. Emeline, *J. Phys. Chem. Lett.* **2012**, *3*, 673-677;c) S. Mubeen, J. Lee, N. Singh, S. Krämer, G. D. Stucky, M. Moskovits, *Nat. Nanotechnol.* **2013**, *8*, 247-251.

[237] a) D. B. Ingram, P. Christopher, J. L. Bauer, S. Linic, *ACS Catalysis* **2011**, *1*, 1441-1447;b) K. Lee, R. Hahn, M. Altomare, E. Selli, P. Schmuki, *Advanced Materials* **2013**, *25*, 6133-6137;c) S. N. Basahel, K. Lee, R. Hahn, P. Schmuki, S. M. Bawaked, S. A. Al-Thabaiti, *Chem. Commun.* **2014**, *50*, 6123-6125.

[238] H. Zhu, X. Chen, Z. Zheng, X. Ke, E. Jaatinen, J. Zhao, C. Guo, T. Xie, D. Wang, *Chem. Commun.* **2009**, 7524-7526.

[239] N. Cheng, J. Tian, Q. Liu, C. Ge, A. H. Qusti, A. M. Asiri, A. O. Al-Youbi, X. Sun, *ACS Applied Materials & Interfaces* **2013**, *5*, 6815-6819.

[240] a) M. J. Muñoz-Batista, O. Fontelles-Carceller, M. Ferrer, M. Fernández-García, A. Kubacka, *Applied Catalysis B: Environmental* **2016**, *183*, 86-95;b) J. Jin, Q. Liang, C. Ding, Z. Li, S. Xu, *J. Alloys Compd.* **2017**, *691*, 763-771.

[241] S. Ma, S. Zhan, Y. Jia, Q. Shi, Q. Zhou, *Applied Catalysis B: Environmental* **2016**, *186*, 77-87.

[242] Y. Yang, Y. Guo, F. Liu, X. Yuan, Y. Guo, S. Zhang, W. Guo, M. Huo, *Applied Catalysis B: Environmental* **2013**, *142-143*, 828-837.

[243] X. Bai, R. Zong, C. Li, D. Liu, Y. Liu, Y. Zhu, *Applied Catalysis B: Environmental* **2014**, *147*, 82-91.

[244] A. Ali Tahir, H. Ullah, P. Sudhagar, M. Asri Mat Teridi, A. Devadoss, S. Sundaram, *Chem. Record* **2016**, *16*, 1591-1634.

[245] a) S. Cao, J. Yu, *J. Photochem. Photobiol., A* **2016**, *27*, 72-99;b) G. Cheng, F. Xu, J. Xiong, F. Tian, J. Ding, F. J. Stadler, R. Chen, *Advanced Powder Technology* **2016**, *27*, 1949-1962;c) A. K. Geim, *Science* **2009**, *324*, 1530.

[246] a) K. S. Novoselov, V. I. Fal′ ko, L. Colombo, P. R. Gellert, M. G. Schwab, K. Kim, *Nature* **2012**, *490*, 192-200;b) M. J. Allen, V. C. Tung, R. B. Kaner, *Chem. Rev.* **2010**, *110*, 132-145.

[247] W.-J. Ong, L.-L. Tan, S.-P. Chai, S.-T. Yong, A. R. Mohamed, *Nano Energy* **2015**, *13*, 757-770.

[248] Q. Xiang, J. Yu, M. Jaroniec, *J. Phys. Chem. C* **2011**, *115*, 7355-7363.

[249] Q. Liu, Y. Guo, Z. Chen, Z. Zhang, X. Fang, *Applied Catalysis B: Environmental* **2016**, *183*, 231-241.

[250] a) S. Iijima, *Nature* **1991**, *354*, 56-58;b) K. S. Novoselov, A. K. Geim, S. V. Morozov, D. Jiang, Y. Zhang, S. V. Dubonos, I. V. Grigorieva, A. A. Firsov, *Science* **2004**, *306*, 666;c) X.-H. Li, J.-S. Chen, X. Wang, J. Sun, M. Antonietti, *J. Am. Chem. Soc.* **2011**, *133*, 8074-8077.

[251] J. Liu, Y. Liu, N. Liu, Y. Han, X. Zhang, H. Huang, Y. Lifshitz, S.-T. Lee, J. Zhong, Z. Kang, *Science* **2015**, *347*, 970.

[252] M.-Q. Yang, N. Zhang, M. Pagliaro, Y.-J. Xu, *Chem. Soc. Rev.* **2014**, *43*, 8240-8254.

[253] L. Song, X. Kang, S. Zhang, *Inter. J. Energy Res.* **2018**, *42*, 1649-1656.

[254] A. Suryawanshi, P. Dhanasekaran, D. Mhamane, S. Kelkar, S. Patil, N. Gupta, S. Ogale, *Inter. J. Hydrogen Energy* **2012**, *37*, 9584-9589.

[255] L. Ge, C. Han, *Applied Catalysis B: Environmental* **2012**, *117-118*, 268-274.

[256] M. Humayun, M. He, W. Feng, C. Jin, Z. Yao, Y. Wang, W. Pi, S. Ali, A. Khan, M. Wang, Z. Zheng, Q. Fu, H. Xia, W. Luo, *Solar Energy* **2021**, *215*, 121-130.

[257] X. Du, X. Yi, P. Wang, J. Deng, C.-c. Wang, *Chinese Journal of Catalysis* **2019**, *40*, 70-79.

[258] R. Liu, Z. Chen, Y. Yao, Y. Li, W. A. Cheema, D. Wang, S. Zhu, *RSC Advances* **2020**, *10*, 29408-29418.

[259] Z.-z. Yang, C. Zhang, G.-m. Zeng, X.-f. Tan, H. Wang, D.-l. Huang, K.-h. Yang, J.-j. Wei, C. Ma, K. Nie, *Journal of Materials Chemistry A* **2020**, *8*, 4141-4173.

[260] S. Tonda, S. Kumar, M. Bhardwaj, P. Yadav, S. Ogale, *ACS Applied Materials & Interfaces* **2018**, *10*, 2667-2678.

[261] a) P. V. Kamat, *J. Phys. Chem. C* **2007**, *111*, 2834-2860;bC. D. Windle, R. N. Perutz, *Coord. Chem. Rev.* **2012**, *256*, 2562-2570.

[262] a) T. Kothe, S. Pöller, F. Zhao, P. Fortgang, M. Rögner, W. Schuhmann, N. Plumeré, *Chem. A Eur. J.* **2014**, *20*, 11029-11034;b) J. Barber, *Chem. Soc. Rev.* **2009**, *38*, 185-196.

[263] K. Xie, N. Umezawa, N. Zhang, P. Reunchan, Y. Zhang, J. Ye, *Energy Environ. Sci.* **2011**, *4*, 4211-4219.

[264] a) J. Low, B. Cheng, J. Yu, *Appl. Surf. Sci.* **2017**, *392*, 658-686;b) J. Fu, J. Yu, C. Jiang, B. Cheng, *Advanced Energy Materials* **2018**, *8*, 1701503.

[265] a) G. Liu, N. Hoivik, K. Wang, H. Jakobsen, *Solar Energy Materials and Solar Cells* **2012**, *105*, 53-68;b) K. Li, X. An, K. H. Park, M. Khraisheh, J. Tang, *Catal. Today* **2014**, *224*, 3-12.

[266] a) K. Wang, Q. Li, B. Liu, B. Cheng, W. Ho, J. Yu, *Applied Catalysis B: Environmental* **2015**, *176-177*, 44-52;b) H. Shi, G. Chen, C. Zhang, Z. Zou, *ACS Catalysis* **2014**, *4*, 3637-3643;c) T. Di, B. Zhu, B. Cheng, J. Yu, J. Xu, *J. Catal.* **2017**, *352*, 532-541.

[267] Q. Lang, W. Hu, P. Zhou, T. Huang, S. Zhong, L. Yang, J. Chen, S. Bai, *Nanotechnology* **2017**, *28*, 484003.

[268] Y. Shiraishi, Y. Kofuji, S. Kanazawa, H. Sakamoto, S. Ichikawa, S. Tanaka, T. Hirai, *Chem. Commun.* **2014**, *50*, 15255-15258.

[269] Z. Han, Y. Yu, W. Zheng, Y. Cao, *New J. Chem.* **2017**, *41*, 9724-9730.

[270] Q. Huang, J. Yu, S. Cao, C. Cui, B. Cheng, *Appl. Surf. Sci.* **2015**, *358*, 350-355.

[271] a) Y. Li, X. Cheng, X. Ruan, H. Song, Z. Lou, Z. Ye, L. Zhu, *Nano Energy* **2015**, *12*, 775-784;b) G. Xie, K. Zhang, B. Guo, Q. Liu, L. Fang, J. R. Gong, *Advanced Materials* **2013**, *25*, 3820-3839.

[272] a) S. Cao, J. Yu, *J. Phys. Chem. Lett.* **2014**, *5*, 2101-2107;b) T. Jafari, E. Moharreri, S. A. Amin, R. Miao, W. Song, L. S. Suib, *Molecules* **2016**, *21*.

[273] M. G. Walter, E. L. Warren, J. R. McKone, S. W. Boettcher, Q. Mi, E. A. Santori, N. S. Lewis, *Chem. Rev.* **2010**, *110*, 6446-6473.

[274] a) G. Zhang, S. Zang, X. Wang, *ACS Catalysis* **2015**, *5*, 941-947;b) F. Dong, L. Wu, Y. Sun, M. Fu, Z. Wu, S. C. Lee, *J. Mater. Chem.* **2011**, *21*, 15171-15174;c) X. Fan, L. Zhang, R. Cheng, M. Wang, M. Li, Y. Zhou, J. Shi, *ACS Catalysis* **2015**, *5*, 5008-5015.

[275] J. Ran, T. Y. Ma, G. Gao, X.-W. Du, S. Z. Qiao, *Energy Environ. Sci.* **2015**, *8*, 3708-3717.

[276] L. Shen, Z. Xing, J. Zou, Z. Li, X. Wu, Y. Zhang, Q. Zhu, S. Yang, W. Zhou, *Scientific Reports* **2017**, *7*, 41978.

[277] Y. Hou, A. B. Laursen, J. Zhang, G. Zhang, Y. Zhu, X. Wang, S. Dahl, I. Chorkendorff, *Angewandte Chemie International Edition* **2013**, *52*, 3621-3625.

[278] a) M. Humayun, N. Sun, F. Raziq, X. Zhang, R. Yan, Z. Li, Y. Qu, L. Jing, *Applied Catalysis B: Environmental* **2018**, *231*, 23-33;b) X. Zhao, J. Zhang, B. Wang, A. Zada, M. Humayun, *Materials* **2015**, *8*.

[279] a) H. Ji, F. Chang, X. Hu, W. Qin, J. Shen, *Chem. Eng. J.* **2013**, *218*, 183-190;b) F. Liang, Y. Zhu, *Applied Catalysis B: Environmental* **2016**, *180*, 324-329.

[280] Y. Bu, Z. Chen, W. Li, *Applied Catalysis B: Environmental* **2014**, *144*, 622-630.

[281] F. Jiang, T. Yan, H. Chen, A. Sun, C. Xu, X. Wang, *Appl. Surf. Sci.* **2014**, *295*, 164-172.

[282] Y. Li, H. Zhang, P. Liu, D. Wang, Y. Li, H. Zhao, *Small* **2013**, *9*, 3336-3344.

[283] R. You, H. Dou, L. Chen, S. Zheng, Y. Zhang, *RSC Adv.* **2017**, *7*, 15842-15850.

RECORDREVIEW

Metal-free polymeric graphitic carbon nitride (g-C_3N_4) as a promising visible-light-responsive photocatalyst has broad applications in solar energy conversion and environmental remediation owing to its low cost, robust and environmental friendly nature. In this critical review,we highlight the recent development, fundamentals, nanostructures design, advantages and challenges of g-C_3N_4.Further, we highlightthe latest information on the improvement of

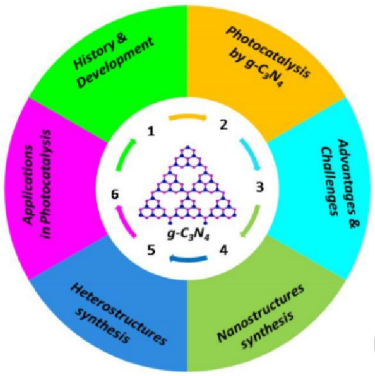

*M. Humayun, H. Ullah, A. A. Tahir, A. R.B. M. Yusoff,M. A. M. Teridi, M. K.Nazeeruddin, W. Luo**

1 – 32.

An Overview of the Recent Progress in Polymeric CarbonNitrideBased Photocatalysis